NASA

Technical Memorandum **79654**

Nuclear Gamma Rays from Energetic Particle Interactions

Reuven Ramaty, Benzion Kozlovsky and Richard E. Lingenfelter

September 1978

National Aeronautics and Space Administration

Goddard Space Flight Center
Greenbelt, Maryland 20771

NUCLEAR GAMMA RAYS FROM

ENERGETIC PARTICLE INTERACTIONS

Reuven Ramaty
Laboratory for High Energy Astrophysics
NASA/Goddard Space Flight Center
Greenbelt, Maryland

Benzion Kozlovsky
Physics Department, Tel-Aviv University, Ramat Aviv Israel, and
Physics Department, University of Maryland, College Park, Maryland

Richard E. Lingenfelter
Department of Astronomy and
Institute of Geophysics and Planetary Physics
University of California
Los Angeles, California

To appear in the Astrophysical Journal Supplement—

Subject Headings: Gamma ray lines, nuclear reactions, interstellar medium, galactic center

Abstract

Gamma ray line emission from nuclear deexcitation following energetic particle reactions is evaluated. The compiled nuclear data and the calculated gamma ray spectra and intensities can be used for the study of astrophysical sites which contain large fluxes of energetic protons and nuclei. A detailed evaluation of gamma ray line production in the interstellar medium is made in the present paper.

I. INTRODUCTION

The interaction of energetic particles with ambient matter produces nuclear gamma rays of energies ranging from tens of keV to about 20 MeV. These gamma rays exhibit a great wealth of spectral structure, ranging from very narrow lines to broad features, depending on the composition and energy spectrum of the energetic particles, and the composition and physical state of the ambient medium.

Observable gamma ray line emission is expected from many astrophysical sites, including solar flares, the interstellar medium, neutron stars and black holes, supernova remnants and nuclei of galaxies. Observations of such lines can reveal directly many astrophysical processes so far studied only indirectly. Studies of diffuse gamma-ray line emission may give information on the intensity, spatial distribution and perhaps even the sources of the otherwise unobservable low-energy component (less than about 100 MeV/nucleon) of the cosmic rays. Gamma-ray spectroscopy may also help determine the composition of the interstellar medium on a galactic scale, independent of the ionization and molecular state of the material. Furthermore, very narrow lines with a width of a few keV at energies of a few MeV permit the first direct measurements of the composition, size and spatial distribution of interstellar dust grains.

Nuclear gamma rays were, in fact, observed from the solar flares of 1972, August 4 and 7 (Chupp et al. 1973, 1975), and 1977, November 22 (Chambon et al. 1978), from the galactic center (Haymes et al. 1975, Leventhal, MacCallum and Stang, 1978a, b), from Centaurus A (Hall et al. 1976), and from a transient event of about 20-minute duration observed from the general direction of the galactic anticenter (Jacobson et al. 1978).

Energetic particle interactions with ambient matter can lead to gamma ray line emission in a variety of ways. These include the direct excitation

of nuclear levels, the production of excited secondary nuclei and radioactive species which decay into excited levels of other nuclei, and the production of neutrons and positrons. Many excited levels decay by photon emission, and these gamma rays are the topic of the present paper.

Gamma ray line emission from radiative capture of neutrons and annihilation of positrons produced in energetic particle interactions has already been discussed in detail (Ramaty, Kozlovsky and Lingenfelter 1975), and the positron annihilation line will be considered here for purposes of comparison only.

In the present paper we provide a detailed treatment of gamma ray production from nuclear deexcitation following energetic particle interactions. To this end we have surveyed in detail the most important nuclear reactions of protons and alpha particles with the abundant constituents of cosmic matter (He, C, N, O, Ne, Mg, Al, Si, S, Ca and Fe), and we give the cross sections relevant for gamma ray line astronomy in Section II.

The shapes of gamma ray lines contain valuable information on the physics of the emitting region, and they are important for considerations regarding the detectability of the lines above background. We treat gamma ray line shapes in Section III. Lines produced in the interstellar gas are broadened by the recoil velocity of the excited nucleus, but lines produced in the interstellar grains can be very narrow (Lingenfelter and Ramaty 1977) because some of the excited nuclei stop in solid materials before emitting gamma rays. We present several calculated gamma ray spectra, obtained by using a Monte Carlo simulation and the cross sections and line broadening effects. We also give the emissivities of the strong lines normalized to the energy density and the energy deposition rates of the energetic particles, and we compare the production rate of positrons with those of the strong nuclear lines. The positron production rates are based

on updated values of the cross sections given by Ramaty et al. (1975), which will be published in a separate paper.

The results of Sections II and III can be applied to the many astrophysical sources that were mentioned above. Such applications will become necessary with the expected launching in the near future of new gamma ray spectroscopy instruments on satellites such as the Solar Maximum Mission (SMM) and the third High Energy Astrophysical Observatory (HEAO-C). The general scope of gamma ray line astronomy, as well as a review of future missions, have been given recently (Lingenfelter and Ramaty 1978, Cline and Ramaty 1978).

In Section IV we apply our results to gamma ray line emission from the interstellar medium. Previous treatments of gamma ray line production by low energy cosmic ray interactions with the interstellar gas were given by Rygg and Fishman (1973), Meneguzzi and Reeves (1975) and Lingenfelter and Ramaty (1976, 1977), using much less detailed nuclear data and a more limited choice of energetic particle spectra and compositions, and ambient medium compositions. In the present paper, we calculate the fluxes of nuclear gamma ray lines from the interstellar medium by taking into account all the available nuclear data, and we consider a broad range of spectral parameters and compositions. In particular, we evaluate the effects on nuclear gamma ray production of the possible spatial gradients of the relative abundances of heavy elements in galaxies (Peimbert, Torres-Peimbert and Ray 1978, and references therein). We also compare the results of our calculations with observations of nuclear lines from the general direction of the galactic center.

We summarize our results in Section V.

II. NUCLEAR LINES AND CROSS SECTIONS

In this section we present the cross sections for the principal nuclear gamma ray lines resulting from interactions of energetic particles with ambient matter, assuming that both the particles and the matter have roughly solar composition. These lines include those produced both by direct excitation and by spallation reactions leading either to nuclei in excited states or to radionuclei which decay to excited states. The estimation of which lines may be important depends on the cross sections for excitation of a level and the assumed elemental and isotopic abundances. The relative line intensities, which also depend of course on the energy spectrum of the energetic particles, will be calculated in section III.

The lines which we have considered are listed by energy in Table I together with the emission mechanism, the principal production processes and the meanlife of either the excited state or the radioactive parent if it is longer. The meanlife can be important in determining the line width as we shall discuss in section IIIb below. For convenience the principal nuclei are also listed in Table 2 together with the relative solar abundance (Ross and Aller 1976), the direct deexcitation lines and the principal spallation product deexcitation lines. This is the order in which the gamma ray line cross sections will be discussed.

a. Lines from He Reactions

Nuclear interactions of α-particles with He produce several important gamma-ray lines. The strongest of these are at 0.431 MeV and 0.478 MeV resulting from deexcitations in ^{7}Be and ^{7}Li, respectively (Tables 1 and 2). The excited states of these isotopes (^{7}Li* and ^{7}Be*) can be populated by the reactions ^{4}He(α,n)^{7}Be*, ^{4}He(α,p)^{7}Li* and ^{4}He(α,n)^{7}Be(ε)^{7}Li*(10%), where the latter reaction includes production of ^{7}Be in both the ground state and its excited state. Since the mean life of ^{7}Be is 76 days, decaying by electron capture 10% of the time into ^{7}Li*, the 0.478-MeV line resulting from ^{7}Be(ε)^{7}Li* is delayed in comparison with prompt lines such as those resulting from the direct excitation of ^{7}Li* and ^{7}Be*. ^{7}Li and ^{7}Be can also be produced from C, N and O, but for compositions similar to solar abundances and steep energetic particle spectra these production modes are quite negligible in comparison with αα reactions.

The cross sections for αα reactions leading to total (ground state plus first excited state) ^{7}Be production and to ^{7}Li production in its first excited state are shown in Figure 1. The cross sections for the reactions ^{4}He(α,p)^{7}Li (total) and ^{4}He(α,n)^{7}Be(total) were measured by King et al. (1975) from 9.75 MeV/nucleon to 35 Mev/nucleon. The cross section for the reaction ^{4}He(α,p)^{7}Li* was measured from 9.75 to 12.5 MeV/nucleon by S. M. Austin (private communication, 1975). Above 12.5 MeV/nucleon we assumed that the ratio of this cross section to the total ^{7}Li production cross section is the same as at 12.5 MeV/nucleon. There are no direct measurements of the cross section for the reaction ^{4}He(α,n)^{7}Be*; we assume that above its threshold of 9.5 MeV/nucleon, the cross section for this reaction is the same as that for the mirror reaction ^{4}He(α,p)^{7}Li*. It should be noted that the cross sections for ^{7}Li (total) and ^{7}Be (total) are essentially equal (King et al. 1975). A more

detailed discussion of these cross sections and their comparison with previous estimates was given by Kozlovsky and Ramaty (1977).

The interactions of α-particles with He can also produce gamma rays at 3.562 MeV from ^{6}Li*. As discussed by Kozlovsky and Ramaty (1974b), because of isospin selection rules, this level can be populated only by the reaction ^{4}He(α,pn)^{6}Li*, and not by ^{4}He (α,d)^{6}Li*. For the former reaction we have adopted the cross section given by Mitler (1972), and we have assumed equal contributions for the production of ^{6}Li* and ^{6}Li (g.s.). According to these estimates, the cross section for the reaction ^{4}He(α, pn)^{6}Li* is assumed to be constant at about 1 mb above the threshold of about 15 MeV/nucleon.

Since in some astrophysical sites ^{3}He may have large abundances (e.g. solar flares, Garrard, Stone and Vogt 1973), we also considered the reaction ^{4}He (^{3}He, p)^{6}Li*. But since the cross section for this reaction, as measured by Harrison (1967), is not large (< 10 mb) we do not take this processes into account in our subsequent calculations.

As discussed by Kozlovsky and Ramaty (1974c), ^{4}He has no excited states that decay primarily by gamma ray emission. However, photon deexcitation of some excited states is possible, but only states with isotopic spin T = 1 are of interest. The reason for this is that only such states can deexcite by dipole radiation, and hence have a reasonable chance of competing with particle emission. The energies of these states lie above 25 MeV (Fiarman and Meyerhof 1973), but exact values extracted from data on the reactions ^{4}He(γ,p)^{3}H, ^{4}He(γ,n)^{3}He and ^{3}H(p,n)^{3}He and their in-

verses are quite model dependent (Gibson 1972). Two possible levels may lie at ~27 MeV and ~30 MeV. Kozlovsky and Ramaty (1974c) have estimated that the upper limits on the cross section for gamma-ray emission from these levels following (p,p') excitation is only about 10^{-3}mb. This value is quite low, and hence gamma-ray lines from (p,p') reactions on ^{4}He do not appear to have important astrophysical consequences.

b. Lines from C, N and O Reactions

The strongest deexcitation line in ^{12}C is at 4.438 MeV resulting from the deexcitation of its first excited state at 4.439 MeV. The various excitation modes of this level are given in Table 1. The cross section for the reaction $^{12}C(p,p')^{12}C^{*}4.439$ has been measured by Reich et al. (1956) between 5 and 5.7 MeV, by Barnard et al. (1966) between 6 and 11.5 MeV, by Conzett (1957) between 10 and 12 MeV, by Daehnick and Sherr (1964) between 14 and 19 MeV, by Dickens et al. (1963) between 18 and 30 MeV, by Stovall and Hintz (1964) at 40 MeV, by Fannon et al. (1967) at 49.5 MeV, by Horowitz and Bell (1970) at 100 MeV, by Emmerson et al. (1966) at 145 MeV, and by Tyren and Maris (1957) at 185 MeV. This cross section is shown by the solid curve in Figure 2. We have used the average cross section in the resonances near the maximum at 10 MeV. However, we have not averaged the cross section of the resonance at 5.35 MeV since it may have some effect on the calculations for very steep particle spectra.

The data points represented by the closed circles and squares are based on measurements of gamma rays at 4.44 MeV resulting from

the bombardment of C with protons (Zobel et al. 1968, Alard et al. 1974). The closed circle points were deduced by using the differential cross section at 135° given by Zobel et al. (1968) and their data on the angular distributions of gamma rays produced in proton bombardment of C. The data point of Alard et al. (1974) is already given in integral form. The difference between this gamma ray data (dashed curve) and the (p,p') data represented by the solid line is most likely due to the excitation of the 4.444 MeV level of ^{11}B by the reaction $^{12}C(p,2p)^{11}B^*$ which has an energy threshold of 22 MeV. Even though the 4.438 and 4.443 MeV lines cannot be resolved because kinematical Doppler broadening blends them into a single feature, in our calculations we have separated these lines by taking the cross section for producing the 4.443 MeV line from C equal to the difference between the dashed and solid curves in Figure 2.

The cross sections for reaction $^{12}C(\alpha,\alpha')^{12}C^{*4.439}$ are given by the dashed-dotted curve in this figure. This curve is based on measurements of Mitchel, Carter and Davis (1964) between 1.5 and 4.3 MeV/nucleon, of Corelli, Bleuler and Tendam (1959) at 4.6 MeV/nucleon, of Yavin and Farwell (1959) at 10 MeV/nucleon. The open circle at 13 MeV/nucleon (Zobel et al. 1968) is data based on gamma ray measurements; thus, as discussed above, it includes the contribution of the reaction $^{12}C(\alpha,\alpha')^{11}B^{*4.444}$. The dashed-crossed curve is our estimate for the sum of the cross sections of the reactions $^{12}C(\alpha,\alpha')^{12}C^{*4.439}$ and $^{12}C(\alpha,x)^{11}B^{*4.444}$. As in the case of proton induced interactions, we interpret the difference between the gamma ray data and the (α,α') data as due

to the contribution of ^{11}B. In our calculations, we use the dashed-dotted curve up to 5 MeV/nucleon and the dashed-crossed curve at higher energies. As above, we separate the 4.438 and 4.443 MeV lines by taking the difference between the dashed-dotted and dashed-crossed curves.

The 4.439 MeV level in ^{12}C can also be populated by spallation reactions on ^{16}O, and ^{14}N, as indicated in Table 1. The cross sections for reactions on ^{16}O were taken from Zobel et al. (1968) and Alard et al. (1974), and are shown by curve 1 in Figure 3 for proton induced reactions, and by curve 6 for α particle induced reactions. The shape of curve 1 below 25 MeV was obtained by normalizing the measurements of Zobel et al. (1968) to the preliminary data of Dyer and Bodansky (private communication 1977) for the reaction $^{24}Mg(p,x\gamma_{1.634})^{20}Ne$. Since both this and the $^{16}O(p,x)^{12}C^*$ reaction are $(p,p\alpha)$ processes, we expect them to have similar energy dependences. For the reaction $^{16}O(\alpha,x\gamma_{4.44})^{12}C$ we have only one measurement (Zobel et al. 1968) of ~110 mb at 13 MeV/nucleon, and curve 6 is our estimate of the energy dependence of the cross section for this reaction. For proton spallation of ^{14}N we use the measurement of Clegg et al. (1961) at 120 MeV, from which we estimate that the 4.438 MeV gamma ray cross section from ^{14}N is larger than that from ^{16}O by about a factor of 2.4. With solar abundances, N/O ~0.13, the 4.438 MeV yield from ^{14}N is about 30% of the yield from ^{16}O.

Excited states of ^{12}C above the 4.439 MeV level decay mostly by particle emission and hence they are not important sources of gamma ray lines. An exception is the 15.11 MeV level, which, be-

cause of conservation of isotopic spin, cannot decay by emitting α particles and hence deexcites only by gamma ray emission. The cross sections for exciting this level were compiled by Crannell, Ramaty and Crannell (1977) who found that the intensity of the 15.1 MeV line is at most about 2% of the 4.438 MeV line intensity.

Spallation reactions in ^{12}C can produce several gamma ray lines (Table 2). The first excited states of ^{11}C and ^{11}B at 1.995 MeV and 2.124 MeV can be populated by (p,pn) and (p,2p) reactions. Zobel et al. (1968) have measured the combined cross section for gamma-ray emission from these two levels and their data is shown in Figure 3 by open triangles. Curve 4 in this figure gives our estimate of this cross section, where we have used the fact that the thresholds of the above reactions are about 20 MeV. In our subsequent calculations, we take the cross sections of these two lines equal to each other. Zobel et al. (1968) have also observed a cluster of four lines between ~6.3. and 6.8 MeV at the energies indicated in Table 1, due to the deexcitation of higher levels in ^{11}C and ^{11}B. The cross section for this cluster, as given by Zobel et al. (1968) and Clegg et al. (1961), is on the average about 25% of the cross section (Figure 3) for the production of the ~5.2-MeV feature from ^{16}O by the same type of reactions. We use this ratio in our subsequent calculations and we assume equal cross sections for the four lines.

Two other strong spallation lines from ^{12}C are at 0.717 and 1.023 MeV resulting from deexcitation in $^{10*}B$. The cross sections for the production of these lines, measured by Clegg et al. (1961) at proton energies around 140 MeV, are, respectively, about 50%

and 20% of the cross section for producing the 4.44 MeV line from ^{16}O spallation at the same energy. Curve 3 in Figure 3 is our estimate of the cross section for 0.717 MeV photon production from ^{12}C, where we use the fact that the threshold for this process is about 20 MeV. For the 1.023 MeV photon production cross section we take 40% of the values represented by curve 3 in Figure 3.

The principal lines from deexcitation of ^{13}C are at 3.684 and 3.853 MeV (Tables 1 and 2). The cross section for proton excitation of these levels, measured by Guratzch et al. (1969) at 7 MeV, are, respectively, about 80% and 30% of that for the 4.439 MeV level in ^{12}C. Using the branching ratios of de Meijer, Plendl and Holub (1974), we estimate the 3.684 and 3.853 MeV gamma ray production cross sections from (p,p') reaction on ^{13}C to be, respectively, 90% and 20% of that for 4.438 MeV gamma rays from (p,p') reactions on ^{12}C shown in Figure 2. For the production cross sections of these lines by (α,α') reactions on ^{13}C, we assume that these ratios also hold with respect to the 4.438 MeV production cross sections from (α,α') reactions on ^{12}C.

The strongest line from the deexcitation of ^{14}N is at 2.313 MeV. The various processes leading to photons at this energy are listed in Table 1, and their cross sections are shown in Figure 4. The cross section for the reaction $^{14}N(p,p'\gamma_{2.313})^{14}N$, shown by the solid curve, includes the deexcitations of all the levels in ^{14}N which cascade to the ground state through the 2.313 MeV level. The data from 3.8 to 6.4 MeV are from Phillips et al. (1972), from 6.5 to 10 MeV from Boreli et al. (1968), at 10.2 MeV from Donovan et al. (1964), and from 9 to 26 MeV from Hansen et al.

(1973). The branching ratios are from de Meijer et al. (1974). The other two strong deexcitation lines from ^{14}N are at 1.632 MeV and 5.105 MeV (Tables 1 and 2). The cross sections for the production of these lines, derived from the above measurements and branching ratios, are approximately 60% and 70% of the cross section for the reaction $^{14}N(p,p'\gamma_{2.313})^{14}N$ shown by the solid curve in Figure 4. Other lines resulting from cascades in ^{14}N have cross sections less than 10% of the 2.313 MeV line cross section

The cross section for the reaction $^{14}N(p,x\gamma_{2.313})^{14}N$ shown by dashed curve is the sum of the cross section shown by the solid curve and of the cross section of the reaction $^{14}N(p,n)^{14}O$, since ^{14}O decays essentially 100% of the time to $^{14}N^{*}2.313$. The cross section for this (p,n) reaction from 6.5 to 12 MeV is taken from Kuan and Risser (1964). This cross section, however, is quite uncertain, since preliminary data from Dyer and Bodansky (private communication 1977) suggests that the cross section for the reaction $^{14}N(p,n)^{14}O$ may be much lower than reported by Kuan and Risser (1964). The cross section for the reaction $^{14}N(p,x\gamma_{2.313})^{14}N$ between 20 and 24 MeV is from the preliminary data of Dyer and Bodansky (1977) and the data point at 120 MeV is from Clegg et al. (1961).

The dashed-crossed curve in Figure 4 is the cross section for the reacion $^{14}N(\alpha,\alpha'\gamma_{2.313})^{14}N$. This cross section is based on the measurements of Ploughe (1961) at 4.8 MeV/nucleon, Garcia, Milio and Senent (1970) at 5.4 MeV nucleon, and Harvey et al. (1966) at 10.1 MeV/nucleon, and the branching ratios of de Meijer et al. (1974). We assume that the relative intensities of the 5.105 and the 1.632 MeV lines compared to the 2.313 MeV are the same for (α,α') excitations as for (p,p') excitations, i.e. about

70% and 60%, respectively. These values are consistent with the measurements of Garcia et al. (1970).

Gamma rays at 2.313 MeV resulting from proton interactions with ^{16}O (Tables 1 and 2) have been measured by Zobel et al. (1968) and their data is shown by the closed circles in Figure 4. These gamma rays result from the direct production of $^{14}N^*$ and from the decay of ^{14}O, with a possible contribution from excited states of ^{13}N. The dashed-dotted curve through the data points of Zobel et al. (1968) is our estimate of the cross section for 2.313 MeV photon production from ^{16}O.

Nuclear excitation of ^{16}O can produce several gamma ray lines (Table 2). The first excited state of ^{16}O at 6.05 MeV decays by $e^+ - e^-$ pair emission. The second, third and fourth excited states at 6.131, 6.919 and 7.119 MeV decay almost exclusively to the ground state producing gamma rays at 6.129, 6.917 and 7.117 MeV, respectively. The fifth excited state at 8.872 MeV decays 75% of the time to 6.131 MeV level and hence produces lines at 2.741 MeV and 6.129 MeV. Other transitions between the states of ^{16}O are also possible (de Meijer et al. 1974). In particular, excited levels at 10.94 and 11.07-MeV cascade to the ground state via the excited states at 6.131, 6.919 and 7.119 MeV with branching ratios given by Ajzenberg-Selove and Lauritsen (1968).

The cross section for producing gamma rays at 6.129 MeV from proton interaction with ^{16}O is shown in Figure 5 by the solid curve. This cross section is sum of the cross sections of the reaction $^{16}O(p,p')\ ^{16}O^*6.131$ and 76% of the cross section for the reaction $^{16}O(p,p')\ ^{16}O^*8.872$ and about 50% of the cross section of the reaction $^{16}O(p,p')\ ^{16}O^*11.07$. These cross sections were measured by Dangle et al. (1964) between 7 and 10.5 MeV, by Kobayashi (1960) between 11 and 15 MeV, by Daehnick (1964) between 15 and 19 MeV, by

Hornyak and Sherr (1955) at 19 MeV, by Crawley and Garvey (1967) at 17.5 MeV, by Austin et al. (1971) between 17 and 45 MeV, by Sundberg and Tibell (1969) at 185 MeV, and by Friedes et al. (1967) at 1 GeV.

The dashed-dotted curve in Figure 5 is the cross section for the reaction $^{16}O(\alpha,\alpha'\gamma_{6.129})^{16}O$. This cross section was measured by Mehta, Hunt and Davis (1967) from 2.5 to 4.7 MeV/nucleon, by Corelli, Bleuler and Tendam (1959) at 4.5 MeV/nucleon, by Blatchley and Bent (1965) at 5.6 MeV/nucleon, by Yavin and Farwell(1959) at 10 MeV/nucleon, and by Harvey et al. (1964) at 16.2 MeV/nucleon.

Most of the experimental measurements of the cross sections for excitation of the 6.919 and 7.119 MeV levels in ^{16}O by (p,p') reactions do not resolve these two levels. Therefore, in Figure 6 the solid curve gives a fit to the sum of the cross sections for the excitation of these levels based on measurements of Zobel et al. (1968). Measurements of (p,p') reactions to these levels by Kobayashi (1960) at 5.6 MeV and Crawley and Garvey (1967) at 17.5 MeV coincide with this curve. At higher energies the measurements of (p,p') reactions by Hornyak and Sherr (1955) and Sundberg and Tibell (1969) give lower values. The difference should be attributed to contributions of spallation lines such as the 7.299 MeV from ^{15}N, which show up at high incident proton energies. In our calculations we use the cross section of Figure 6, and we assume that half of the resultant photons are at 6.917 MeV and half are at 7.117 MeV.

The 2.741 MeV line is produced by transitions between the 8.872 level to the 6.131 MeV level in ^{16}O with a branching ratio 76%. The dashed curve in Figure 6 is based on the (p,p') measurements of Crawley and Garvey (1967) at 17.3 MeV, and of Austin et al. (1971) between 17 and 45 MeV. The data of Zobel et al. (1968) are in agreement with the (p,p') measurements. The

$^{16}O(\alpha,x\gamma_{6.9,7.1,7.3})^{16}O$ or ^{15}N cross section is shown by the dashed-dotted curve in Figure 6. This curve is based on measurements of Corelli et al. (1959) at 4.5 MeV/nucleon, of Harvey et al. (1966) at 10 MeV/nucleon and of Zobel et al. (1963) at 13 MeV/nucleon.

Gamma ray lines from ^{16}O can also be produced by spallation reactions which populate excited levels in ^{12}C, ^{15}N, ^{15}O, ^{14}O, ^{13}C and ^{10}B (Table 2). The production of 4.438 MeV gamma rays by the reaction $^{16}O(p,x\gamma_{4.438})^{12}C$ has been discussed above.

The strongest lines from ^{15}N are at 6.322, 5.270 and 5.298 MeV and from ^{15}O at 5.180, 5.241 and 6.176 MeV. Because of poor energy resolution the 6.2 MeV gamma ray production cross sections of Zobel et al. (1968) and Alard et al. (1976) shown by the data points in Figure 5 include the lines at 6.129 MeV from ^{16}O, at 6.176 from ^{15}O and 6.322 MeV from ^{15}N. Thus, the difference between the dashed and solid curves, and between the dashed-crossed and dashed-dotted curves, in Figure 5 give the sum of the cross sections for the production of the 6.176 and 6.322 MeV lines in proton and alpha particle induced reactions, respectively. There is only one direct high-resolution measurement of gamma rays from ^{16}O which can resolve the 6.129, 6.176 and 6.322-MeV lines (Goryachev et al. 1973). This measurement at ~1 GeV shows the 6.322-MeV line to be stronger than the line at 6.176 MeV by about a factor of 2. Assuming that this ratio holds also at lower energies, we take the cross sections for the production of the 6.322-MeV and the 6.176-MeV lines as 2/3 and 1/3, respectively, of the combined cross sections of these two lines.

The sum of the cross sections for the reactions $^{16}O(p,x)^{14}N^*$, $^{16}O(p,pn)^{15}O^*$, and $^{16}O(p,2p)^{15}N^*$ leading to ~5.2 MeV photons is shown by curve 2 in Figure 3 based on data by Zobel et al. (1968). In our calculations we arbitrarily assume that the cross sections for the production of the 5.105, 5.180, 5.241, 5.270 and 5.298 MeV lines are each 20% of this cross section. The cross section for the production of ~5.2 MeV photons in α particle induced spallation reactions is shown by curve 7 in Figure 3. As with the proton induced reactions, we assume that the cross sections for the individual lines are 20% of the total.

The ^{10}B lines at 0.717 and 1.023 MeV can be produced by the spallation of ^{16}O. Foley et al. (1962a) find that for 140 MeV protons the cross section of these two lines are about equal to each other, and each of them is about half of the cross section for producing the 4.438 MeV line from ^{16}O spallation. We therefore approximate each of these cross sections by curve 3 in Figure 3. Spallation of ^{16}O can also populate excited levels of ^{13}C leading to line emission at 3.684 MeV and 3.853 MeV. In Figure 3 we show the data of Zobel et al. (1968) for the combined production of both these lines and our estimate (curve 5) for the energy dependence of this cross section.

c. Lines from Ne, Mg, Al, Si, S, Ca and Fe Reactions

The strongest deexcitation line from ^{20}Ne is at 1.634 MeV resulting from the deexcitation of its first excited state. The various production modes of this line are given in Table 1. The solid curve in Figure 7 is the cross section for the reaction

$^{20}Ne(p,p')^{20}Ne^{*1.634}$. From 5 to 14.2 MeV the data are from Oda et al. (1960) and references therein, at 17 MeV from Schrank et al. (1962), and at 24.5 MeV from de Swiniarski et al. (1969). At low energy we have averaged the data over resonances.

The cross section for the reaction $^{20}Ne(p,p'\gamma_{1.634})^{20}Ne$ which includes the cascades from the 4.247 and 4.968 MeV levels is shown by the dashed curve in Figure 7. The cross sections for populating these levels were measured by Oda et al. (1960) from 7.6 to 14.2 MeV, Schrank et al. (1962) at 17 MeV, and de Swiniarski et al. (1969) at 24.5 MeV, and we have used the branching ratios of de Meijer at al. (1974). Since there is no data above 24.5 MeV, the dashed curve at these energies is an approximation based on similar excitation functions of ^{16}O and ^{24}Mg. Below 5 MeV we have used preliminary data from gamma ray measurements (P. Dyer, and D. Bodansky, private communication 1977) which at higher energies are consistent with the above measurements and calculations.

The dashed-dotted curve in Figure 7 is the cross section for the reaction $^{20}Ne(\alpha,\alpha')^{20}Ne^{*1.634}$. This cross section has been measured by Seidlitz, Bleuler and Tendam (1958) at 9.5 MeV/nucleon and by Rebel et al. (1972) at 41 MeV/nucleon. There is no data on this cross section at lower energies and we have based our estimate on the expected behavior of the cross section near the Coulomb barrier. The dashed-crossed curve is the cross section for the reaction $^{20}Ne(\alpha,\alpha'\gamma_{1.634})^{20}Ne$. At 4.5 Mev we calculate the contributions of the cascades from the measurements of Seidlitz et al. (1958), and we assume that the ratio (~2) between the cross sections for the reactions $^{20}Ne(\alpha,\alpha'\gamma_{1.634})^{20}Ne$ and $^{20}Ne(\alpha,\alpha')^{20}Ne^{*1.634}$ remains constant at higher energies.

Transitions from the 4.247 and 4.968 MeV levels provide the

next strongest deexcitation lines in ^{20}Ne, at 2.613 MeV and 3.334 MeV. At 17 MeV Schrank et al. (1962) find that the intensities of these lines are about 25% and 10% of the 1.634 MeV line. We have assumed that these ratios are the same at all energies.

There is no data on spallation gamma ray lines from ^{20}Ne. But as can be seen from the measurements of Zobel et al. (1968) and Chang et al. (1974) the most important proton-induced reactions are (p,n), (p,2p), (p,pn) and p,pα). For ^{20}Ne (p,n) reactions lead to ^{20}Na which is radioactive and decays back to ^{20}Ne producing gamma rays at 1.634 MeV about 80% of the time. Because of the short mean life (0.64 sec) of ^{20}Na, the contributions of these gamma rays are included in the measurements of Dyer and Bodansky (private cummunication 1977). From the comparison of these measurements and the (p,p') data discussed above, we estimate that the contribution of ^{20}Na to the total 1.634 MeV line is less than a few percent. For the other reactions, the strongest lines are likely to result from the deexcitation of the first two excited states of the product nuclei. Therefore, we expect lines at 0.110 MeV and 0.197 MeV from ^{19}F at 0.238 MeV and 0.275 MeV from ^{19}Ne and at 6.129 MeV from ^{16}O. We assume that the sum of the cross sections of the four lines from ^{19}F and ^{19}Ne equals the cross section for ~5.2 MeV photon production from ^{16}O spallation given by curve 2 in Figure 3, and that the cross section for the reaction $^{20}Ne(p,x\gamma_{6.129})^{16}O$ is the same as the cross section for the reaction $^{16}O(p,x\gamma_{4.438})^{12}C$ given by curve 1 in this figure.

The principal deexcitation line from ^{22}Ne is at 1.275 NeV from the first level. Measurements of the cross section for proton

excitation of this level have been made at 1.9 to 3.2 MeV by Sorokin et al. (1963), at 4.8 to 14 MeV by Hulubei et al. (1969), and at 24.5 MeV by de Swiniarski et al. (1972). These measurements suggest that this cross section is roughly 2/3 of that for proton excitation of the 1.634 MeV level in ^{20}Ne. We therefore assume that the ^{22}Ne $(p,p'\gamma_{1.275})^{22}$Ne and ^{22}Ne$(\alpha,\alpha'\gamma_{1.27})^{22}$Ne cross sections are equal to the product of this fraction and the ^{20}Ne$(p,p'\gamma_{1.634})^{20}$Ne and the ^{20}Ne$(\alpha,\alpha'\gamma_{1.634})^{20}$Ne cross sections, respectively, in Figure 7.

The nuclear interactions between energetic particles and comple nuclei ($A \geq 20$) produce many more gamma ray lines than those resulting from the deexcitation of the low-lying levels discussed above. These lines result from the cascade deexcitations of the many high-lying levels that are populated both by direct excitations and spallation reactions. Zobel et al. (1968) have measured the total production cross section, σ_γ, of gamma rays of energies greater than 0.7 MeV in interactions of protons and alpha particles with complex nuclei. They find that for C and O this total cross section is essentially the same as the sum of the cross sections for the excitation of individual lines; but for heavier targets the resolvabl lines can account for only a fraction of the total gamma ray cross section, σ_γ.

The measurements of Zobel et al. (1968) for σ_γ were done at proton energies of 16 MeV, 33 MeV, 56 MeV and 160 MeV for C, O, Mg, Al, Fe and Co targets and at an α particle energy of 15 MeV/nucleon for C, O, Al and Fe targets. We have interpolated these results for Ne, and the resultant cross sections at the above energies are shown by the diamonds in Figure 7. The crossed and

crossed-dotted curves are our estimates of the energy dependences of σ_γ for proton and α particle induced reactions, respectively. At high energies we have assumed a constant ratio between these two curves, and at low energies we have merged them with the appropriate cross sections for the excitation of the first excited level of ^{20}Ne.

In addition to the lines discussed above, gamma ray emission is also produced from the decay of long lived radioactive spallation products. Radioisotopes with mean lives longer than 1 day that we consider are are ^{7}Be, ^{22}Na, $^{26}A\ell$, ^{52}Mn, ^{54}Mn, ^{55}Co and ^{56}Co. We have already discussed the production of ^{7}Be in IIa. In order of increasing nuclear mass, we next consider ^{22}Na which produces a gamma ray line at 1.275 MeV by decaying into the first excited state of ^{22}Ne.

For Ne isotopes, an important production mode of ^{22}Na is the reaction $^{22}Ne(p,n)^{22}Na$. Although the cross section of this reaction has not been measured, we estimate from the systematics of other (p,n) reactions that this cross section should be roughly equal to that of $^{26}Mg(p,n)^{26}Al$ (shown in Figure 9) and we use these values in our calculations. The production of ^{22}Na from Mg and Si is discussed below.

The strongest deexcitation line in ^{24}Mg is at 1.369 MeV. The solid curve in Figure 8 is the cross section for the reaction $^{24}Mg(p,p')^{24}Mg^{*1.369}$. The data for this reaction from 3 to 5.5 MeV is from Duray et al. (1972), at 5.4 to 7 MeV from Seward (1959), at 12 MeV from Conzett (1957), at 17.5 MeV from Crawley and Garvey (1967), at 40 MeV from Stoval and Hintz (1964), and at 100 MeV from Horowitz et al. (1969).

The cross section for gamma ray emission at 1.369 MeV from proton bombardment of ^{24}Mg, including cascades from higher levels, has been measured at 30.3 MeV by Zobel et al. (1968) and at 143 MeV by Foley et al. (1962b). These data are shown by the open square and triangle in Figure 8. These measurements are consistent with estimates of the total 1.369 MeV emission mode from the measurements of Crawley and Garvey (1967) and Horowitz et al. (1969), using the branching ratios given by de Meijer, Drentje and Plendl (1975) and Endt and Van der Leun (1973). These estimates suggest that the contribution of the cascades from the first 10 excited states out of about 40 bound states is about equal to the contribution of the direct excitation of the first excited level. The dashed curve in Figure 8 is our estimate of the cross section for the reaction $^{24}Mg(p,p'\gamma_{1.369})^{24}Mg$. We find that this estimate is in good agreement with the preliminary gamma ray data of Dyer and Bodansky (private communication 1977).

The cross section for the reaction $^{24}Mg(\alpha,\alpha')^{24}Mg^{*1.369}$ is shown by the dashed-dotted curve in Figure 8. This cross ection has been measured by Sauter and Singh (1974) from 2.5 to 3.5 MeV/nucleon, by Eberhard and Trombik (1972) from 3.9 to 4.8 MeV/nucleon, by McNeilley et al. (1973) at 4.2 MeV/nucleon, and by Janus and McCarthy (1974) at 10 MeV/nucleon. Since there is no data below 2.5 MeV/nucleon, our estimate in this energy range is based on the expected behavior of the cross section near the Coulomb barrier. The 1.369 MeV level will also be populated by cascading from highler lying levels. From Eberhard and Trombik (1972), who have measured the excitation cross sections of the 4.122, 4.239

and 5.236 MeV levels, we estimate that the cascades in ^{26}Mg increase the effective 1.369 MeV gamma-ray production cross section by about a factor of 2.5. Similarly, from the measurements of Thompson et al. (1967) at 2.7 MeV/nucleon, we find that this factor is about 1.4. The dashed-crossed curve in Figure 8 is our estimate of the cross section for the reaction $^{24}Mg(\alpha,\alpha'\gamma_{1.369})^{24}Mg$.

Although many more deexcitation lines can result from transitions among the ~ 40 bound states of ^{24}Mg, we estimate from the cross sections of Crawley and Garvey (1967) and the branching ratios of de Meijer et al. (1975) that none of these lines is stronger than 10% of the 1.369-MeV line. These lines are included in the total unresolved nuclear radiation from ^{24}Mg. In Table 1 we include only the line at 2.754 MeV. This line results from transitions between the second and first excitated states of ^{24}Mg, and estimate that its intensity is 10% of the 1.369 MeV line intensity.

The two strongest lines resulting from the spallation of ^{24}Mg are at 1.634 and 1.636 MeV. These lines are due to the deexcitation of ^{20}Ne and ^{23}Na which result from (p,pα) and (p,2p) reactions, respectively. Zobel et al. (1968) have observed a feature at ~ 1.6 MeV from the bombardment of ^{24}Mg with 30 MeV protons, and found that its intensity is about twice that of the 4.44 MeV line from ^{16}O, whereas Foley et al. (1962b) found that this ratio at 143 MeV is about unity. In our calculations we take the sum of the cross section for producing 1.634 and 1.636 MeV photons from ^{24}Mg spallation to be, at all incident energies, 1.5 times the cross section for the reaction $^{16}O(p,x\gamma_{4.438})^{12}C$

shown in Figure 3. This assumption is consistent with the preliminary data of Dyer and Bodansky (private communication 1977) for incident proton energies from about 16 to 23 MeV. We further assume that these lines have equal cross sections. The 1.6 MeV feature observed by Zobel et al.(1968) could also include the 1.600 MeV line of ^{23}Mg, and the comparison between these measurements and those of Dyer and Bodansky (which have much better energy resolution) suggests that the cross section for producing 1.600 MeV photons from ^{24}Mg spallation is about 50% of the $^{16}O(p,x\gamma_{4.438})$ cross section.

Other spallation lines from ^{24}Mg are at 2.613 MeV and 2.640 MeV resulting from deexcitations in ^{20}Ne and ^{23}Na, respectively. From the measurements of Zobel et al. (1968), at an incident proton energy of 30 MeV, the sum of the cross sections of these two lines is about 60% of the $^{16}O(p,x\gamma_{4.438})^{12}C$, cross section, whereas from the measurements of Foley et al.(1962b), at 143 MeV the corresponding ratio is about 1.5. We assume a constant ratio of 2, and we take the cross sections for producing the 2.613 and 2.640 MeV lines equal to each other. Foley et al. (1962) observed another spallation feature at 0.92 MeV with half the strength of the 4.438 MeV line from ^{16}O at ~ 143 MeV. They identified this feature as the 0.891 MeV line from ^{22}Na, and we take its cross section, at all incident energies, equal to 0.5 times the $^{16}O(p,x\gamma_{4.438})^{12}C$ cross section.

Neither Foley et al. (1962b) nor Zobel et al. (1968) looked for gamma-rays below 0.7 MeV, but both the 1.636 and 1.600 MeV lines imply additional lines of at least equal intensities, at

0.440 and 0.451 MeV, respectively.

Because of the multitude of excited states of ^{24}Mg and its spallation products, nuclear interactions produce many weaker lines in addition to the lines that we have discussed above. The crossed and crossed-dotted curves in Figure 8 show the total gamma ray production in ^{24}Mg. The closed square is a measurement by Zobel et al. (1968), while the diamonds have been obtained from interpolations similar to those done for Ne. At low incident energies, these total cross sections approach those for the direct excitation of the 1.369 MeV level.

The cross section for ^{22}Na production from Mg is shown in Figure 9. Measurements of this cross section for proton spallation of both ^{24}Mg and ^{25}Mg are reported and reviewed by Furukawa et al. (1971) for proton energies up to 52 MeV, by Korteling and Caretto (1970a, b) at 100 to 400 MeV, and by Raisbeck and Yiou (1975) above 1 GeV.

The less abundant (11%) isotope ^{26}Mg is a significant source of gamma ray line emission at 1.809 Mev from deexcitation of the first level and by (p,n) production of long-lived ^{26}Al which decays back to ^{26}Mg through the 1.809 MeV level. ^{26}Al is also listed in Table 3 as an important long-lived gamma ray producing radioisotope. The cross section for direct excitation of the 1.809 MeV level, measured at 17.5 MeV by Crawley and Garvey (1967) is about 35% of that for excitation of the 1.369 MeV level in ^{24}Mg. In our subsequent calculations we assume that the $^{26}Mg(p,p'\gamma_{1.809})^{26}Mg$ and $^{26}Mg(\alpha,\alpha'\gamma_{1.809})^{26}Mg$ cross sections are one half of the $^{24}Mg(p,p'\gamma_{1.368})^{24}Mg$ and $^{24}Mg(\alpha,\alpha'\gamma_{1.368})^{24}Mg$

cross sections, respectively, shown in Figure 8. The cross section for the (p,n) reaction leading to long-lived ^{26}Al has been measured from 8 to 14 MeV by Wong et al.(1967) and from 6 to 52 MeV by Furukawa et al.(1971), and is shown in Figure 9. We also include for completeness in ^{26}Al production the ^{27}Al(p,pn)^{26}Al cross section measured by Furukawa et al.(1971). The production of ^{26}Al from ^{28}Si spallation is discussed below.

The stronest deexcitation line in ^{28}Si is at 1.779 MeV. The solid curve in Figure 10 is the cross section for the reaction ^{28}Si (p,p')^{20}Si*1.779. This cross section was measured by Conzett (1957) at 12 MeV, Crawley and Garvey (1967) at 17.5 MeV, deSwiniarski et al. (1973) at 25.25 MeV and Horowitz et al. (1969) at 100 MeV. Foley et al. (1962b) measured the cross-section for 1.779 MeV gamma rays at proton energies of 141 MeV. Their result is shown by the open square in Figure 10. As with ^{24}Mg, the reason for the high value of this measurement is the contribution of the cascades from the numerous (> 40) bound states of ^{28}Si which deexcited mainly through the 1.779 MeV level. The dashed curve in Figure 10 is our estimate of the cross section for the reaction ^{28}Si(p,p'$\gamma_{1.779}$)^{28}Si* based on preliminary gamma ray data of Dyer and Bodansky (private communication, 1977) up to proton energies of 25 MeV and the measurements of Foley et al. (1962b) at higher energies.

Two other strong lines from ^{28}Si are those at 6.878 and 5.099 MeV from deexcitation of ^{28}Si*6.879. The cross section for proton excitation of this level, measured from 12 to 15 MeV by Shotter, Fisher and Scott (1970), at 17.5 MeV, Crawley and Garvey (1967) and

at 100 MeV by Horowitz et al. (1969), is roughly 17% of that for excitation of $^{28}Si(p,p'\gamma_{1.779})^{28}Si$. Using the branching ratios of de Meijer et al. (1975) and assuming a 20% cascade contribution from higher levels we estimate the 6.878 and 5.099 MeV gamma-ray production cross sections to be, respectively, 13% and 6% of that for 1.779 MeV gamma-rays in Figure 10 above an effective proton threshold energy of 8 MeV.

The cross section for the reaction $^{28}Si(\alpha,\alpha')^{28}Si^{*1.779}$ is shown by the dashed-dotted curve in Figure 10. This cross section has been measured by Blatchley and Bent (1965) at 5.6 MeV/nucleon, by Kokame et al. (1965) at 7.1 MeV nucleon and by Rebel et al. (1972) at 26 MeV/nucleon. At 4.5 MeV/nucleon we use scaled data of Corelli et al. (1959) for the reaction $^{32}S(\alpha,\alpha')^{32}S^{*2.230}$. At lower energies, we again extrapolate the data according to the expected behavior near the Coulomb barrier. The dashed-crossed curve in Figure 10 is our estimate for the cross section of the reaction $^{28}Si(\alpha,\alpha'\gamma_{1.779})^{28}Si$. In analogy with the (p,p') reaction, we take a factor of 2 for the ratio of the cross sections of the reactions $^{28}Si(\alpha,\alpha'\gamma_{1.779})^{28}Si$ and $^{28}Si(\alpha,\alpha')^{28}Si^{*1.779}$ at energies well above the Coulomb barrier energy.

The cross section for α particle excitation of $^{28}Si^{*6.879}$ which leads to 6.878 and 5.099 Mev gamma-rays has been measured at an α energy of 7.1 Mev/nucleon by Kokame et al. (1966). As with (p,p') excitation, these measurements show that the $^{28}Si(\alpha,\alpha')^{28}Si^{*6.879}$ cross section is roughly half that for $^{28}Si(p,p')^{28}Si^{*1.779}$. Using the branching ratios of de Meijer et al. (1975), we estimate the 6.878 and 5.099 MeV gamma-ray production cross

section from (α,α') to be, respectively, 13% and 6% of that for 1.779 MeV gamma-ray production.

Foley et al. (1962b) observed a rich spectrum of proton induced spallation lines from ^{28}Si. The strongest such line is at 1.369 MeV from ^{24}Mg. The cross section for this reaction is larger by about a factor of 2 than the cross section for the production of the 4.438 MeV line from ^{16}O at this energy. Based on this measurement, we assume that the cross section for the reaction $^{28}Si(p,x\gamma_{1.369})^{24}Mg$ is, at all energies, 2 times the cross section for the reaction $^{16}O(p,x\gamma_{4.438})^{12}C$ shown in Figure 3. Other spallation lines of ^{28}Si are at 1.634 and 2.613 MeV from deexcitations in ^{20}Ne, at 0.780 and 0.957 from ^{27}Si, and at 0.844 and 1.014 from ^{27}Al. From the data of Foley et al. (1962b) the cross sections for producing these lines, at an incident proton energy of ~ 150 MeV, are, respectively, 65, 40, 25, 20, 30 and 40% of the 1.369 MeV line cross section. We use these ratios in our subsequent calculations, and we assume that they remain the same at all incident proton energies. Since Zobel et al. (1968) have observed the 1.014 MeV line from direct excitation of ^{27}Al, we also include in our calculations the reaction $^{27}Al(p,p'\gamma_{1.014})^{27}Al$, for which we take an average cross section of 50% of the $^{28}Si(p,p'\gamma_{1.779})^{28}Si$ cross section, based on the Zobel et al.(1968) measurements.

As with Ne and Mg, we take into account the many other weaker lines from Si and its spallation products by considering the total gamma-ray production cross section. There are no direct measurements of this cross section for Si. The diamonds in

Figure 10 are estimates obtained by interpolating the data of Zobel et al. (1968), as was done for Ne and Mg. The crossed and crossed-dotted curves in Figure 10 show the total gamma-ray production cross section in Si for proton and α particle induced reactions, respectively.

An additional contribution to ^{22}Na and ^{26}Al production is obtained from the spallation of Si. Measurements of the Si spallation production cross section for these two isotopes by protons of energy up to 52 MeV are reported and reviewed by Furukawa et al. (1971). Higher energy measurements of ^{22}Na production have been made at 50 to 150 MeV by Bimbot and Gauvin (1971), at 100 to 400 Mev by Korteling and Caretto (1970a,b), and above 1 GeV by Raisbeck and Yiou (1975). These cross sections are shown in Figure 9.

The principal gamma ray line from deexcitation of ^{32}S is at 2.230 MeV from the first level. The cross sections for excitation of this level has been measured at 5 to 5.5 MeV by Oda et al. (1959), at 5 to 14 MeV by Berinde, Neamu and Vladuca (1971) at 7.6 to 14 MeV by Oda et al. (1960), at 17.5 MeV by Crawley and Garvey (1967), and at 155 MeV by Willis et al. (1968). These cross sections are roughly 70% of that for excitation of the first level in ^{28}Si at 1.779 MeV. Assuming that cascade contributions are comparable, we use cross sections for both $^{32}S(p,p'\gamma_{2.230})^{32}S$ and $^{32}S(\alpha,\alpha'\gamma_{2.230})^{32}S$ that are 0.7 times those for $^{28}Si(p,p'\gamma_{1.779})^{28}Si$ and $^{28}Si(\alpha,\alpha'\gamma_{1.779})^{28}Si$, respectively.

Spallation of ^{32}S also leads to strong gamma ray lines at 1.779 Mev from $^{32}S(p,p\alpha)^{28}Si^*$ and at 1.249, 1.266, 2.029, 2.034,

2.232 and 2.234 MeV from $^{32}S(p,2p)^{31}P^*$ and $^{32}S(p,pn)^{31}S^*$. Foley et al. (1962b) have measured cross sections for the 1.779 Mev line and for each of the pairs at ~1.2, ~2.0 and ~2.2 MeV and find them to be 160%, 330%, 120% and 140% of that for the 4.438 MeV line from $^{16}O(p,px)^{12}C^*$, respectively. For the latter pair we have subtracted the contribution of (pp') at 2.230 MeV measured also by Foley et al.(1962b). Assuming similar excitation functions and equal yields for each of the paired lines, we take the cross sections for the 1.249, 1.266, 1.779, 2,029, 2.034, 2.232 and 2.234 MeV lines from ^{32}S spallation to be 1.7, 1.7, 1.6, 0.6, 0.6, 0.7 and 0.7 times that for the 4.44 MeV line from ^{16}O spallation (Figure 3), respectively.

For the unresolved line contribution from ^{32}S we assume that for both proton and α particle excitations the cross sections are the same as for ^{28}Si given by the crossed and crossed-dotted curves in Figure 7.

The strongest deexcitation line from ^{40}Ca is at 3.736 MeV from the first gamma decay level. The cross section for proton excitation of this level has been measured at 14.6 and 17.3 MeV by Gray, Kenefick and Kraushaar (1965), at 30 MeV by Ridley and Turner (see Satchler, 1973), at 55 MeV by Yagi et al. (1964), and at ~155 MeV by Willis et al. (1968) and Roos and Wall (1965). These cross sections lie essentially halfway between those for proton excitation of the first levels in ^{28}Si and ^{56}Fe or 150% of that for ^{28}Si. Assuming that the cascade contribution is also an average between that in ^{28}Si and ^{56}Fe, we take the cross sections for $^{40}Ca(p,p'\gamma_{3.736})^{40}Ca$ and $^{40}Ca(\alpha,\alpha'\gamma_{3.736})^{40}Ca$ to be equal to 1.5 times the $^{28}Si(p,p'\gamma_{1.779})^{28}Si$ and the $^{28}Si(\alpha,\alpha'\gamma_{1.779})^{28}Si$

cross sections, respectively. For the unresolved lines of Ca we again assume a cross section that is 1.5 times the corresponding one in ^{28}Si.

The strongest deexcitation line of ^{56}Fe is at 0.847 MeV. The cross section for direct excitation of this level by the reaction $^{56}Fe(p,p')\ ^{56}Fe\ ^{*}0.847$ is shown by the solid curve in Figure 11. From 3.5 to 6 MeV the data is from Nichols et al. (1969), at 6 MeV from Andronov et al. (1970, at 11 MeV from Perey et al. (1970) at 19.6 MeV from Hendrie et al. (1969), at 17.5 MeV from Peterson (1969), at 30.3 MeV from Karban et al. (1970, and at 49.35 MeV by Mani (1971).

The cross section for the reaction $^{56}Fe(p,p'\gamma_{0.847})^{56}Fe$ was measured by Zobel et al. (1968) at 15.7 and 31.4 MeV, and by Chang et al. (1974) and Jastrzebski et al. (1976) at 100 MeV. Their data are shown in Figure 11 by open squares and triangle and circle. As can be seen, there is an inconsistency of a factor of 3 between the data of Chang et al. (1974) and Jastrzebski et al. (1976), which hopefully will be resolved by new measurements (N. S. Wall, private communication 1977).

The cross sections for producing 0.847 MeV gamma rays shown in Figure 11 are much larger than the cross section for the reaction $^{56}Fe(p,p')^{56}Fe^{*}0.847$ due to the contribution of cascades from higher excited levels of ^{56}Fe. This nucleus has more than 100 bound states (Nuclear Data Group 1973) which are known to decay almost exclusively by cascades via the 0.847-MeV level. From Peterson (1969) at 17.5 MeV, and Mani (1971) at 49.35 MeV, we

see that the cross section for the excitation of each excited state is on the average about 10% of the cross section for the excitation of the 0.847 MeV level. Thus at these energies the cross section for 0.847 MeV gamma ray production should be larger by about an order of magnitude than the $^{56}Fe(p,p')^{56}Fe^{*}0.847$ cross section. In our calculations we use the cross sections given by the dashed curve in Figure 11. The comparison of this curve with the preliminary data up to 32 MeV based on gamma-ray measurements (P. Dyer, and D. Bodansky, private communication 1977) gives a good agreement.

The cross section for producing 0.847 MeV gamma rays from ^{56}Fe $(\alpha,\alpha'\gamma_{0.847})^{56}Fe$ has been measured by Zobel et al. (1968) who find a value of 790$\pm$ 430 mb at 14.3 MeV/nucleon. Because of the effe of the Coulomb barrier at low energies, we assume that this cross section is proportional to the dashed curve in Figure 11, with a constant of proportionality of 1.5 based on the data of Zobel et al. (1968).

Another strong line from ^{56}Fe is at 1.238 MeV produced by transitions from the 2.085 MeV to the 0.847 MeV levels; these transitions are always followed by the emission of 0.847 MeV photons. In (p,p') reactions the strength of the 1.238 MeV line relative to that of the 0.847-MeV line is 57% at 15.7 MeV (Zobel et al. 1968) and 45% at 100 MeV (Chang et al. 1974). At 31.4 MeV Zobel et al. (1968) give a cross section for the 1.238-MeV line larger by about a factor of 2 than that for the 0.847 MeV line. This is inconsistent with the fact that every 1.238 MeV photon should be followed by a 0.847 MeV photon, but because of

poor detector resolution, the measurements of Zobel et al. (1968) of ~1.3-MeV photons probably included a large contribution from spallation lines at energies other than 1.238 MeV. Since spallation reactions contribute less at lower energies, the measurements at 15.7 MeV probably give a more correct value for the 1.238-MeV line cross section. At 100 MeV, the measurements of Chang et al. (1974) have adequate energy resolution to resolve the 1.238-MeV line from spallation lines which are quite dominant at this energy. In the subsequent calculations we have taken a value of 0.5 for the ratio of 1.238 to 0.847 MeV gamma-ray production. This value is roughly consistent with the preliminary data of Dyer and Bodanksy (private communication 1977).

In addition to emission at 0.847 and 1.238 MeV, deexcitations of excited states in ^{56}Fe lead to gamma ray production also at a variety of other energies (Table 2). We have included in Tables 1 and 2 all lines whose intensities are expected to be more than 10% of the 0.847-MeV line intensity. From Rao (1970) and Chang et al. (1974) such lines are at 1.772, 1.811, 2.094 and 2.113 MeV, with intensities relative to that of the 0.847-MeV line of approximately 14, 50, 12 and 10%, respectively. As with the 1.238-MeV line, we assume that the energy dependences of the cross sections of these lines are the same as that of the line at 0.847 MeV.

Spallation of ^{56}Fe leads to several important prompt gamma ray lines (Table 2). At low energies (<20 MeV), Dyer and Bodansky (private communication 1977) find a strong line at 0.812 MeV from the reaction $^{56}Fe(p,n)^{56}Co^{*}0.812$, whose cross section at 10 MeV

is about 30% of that of the reaction $^{56}Fe(p,n)^{56}Co$ given in Figure 12. We assume this ratio at all energies in our subsequent calculations. The line at 0.812 MeV implies an additional de-excitation leading to 0.158 MeV photons, whose intensity is at least equal to that of the 0.812 MeV line.

At 100 MeV Chang et al. (1974) find the strongest spallation line is at 1.434 MeV from the reactions $^{56}Fe(p,x)^{52}Cr^*$ and $^{56}Fe(p,x)^{52}Mn^*(e^+;\varepsilon)^{52}Cr$. The latter reaction populates the isomeric state of ^{52}Mn which decays directly into the excited state of ^{52}Cr. There are no measurements of the cross section for $^{52}Cr^*$ production at other energies. However, we can estimate this cross section by comparing it with the reaction $^{16}O(p,x\gamma_{4.44})^{12}C$ in Figure 3. By using the results of Jastrzebski et al. (1976), we take the cross section for the reaction $^{56}Fe(p,x\gamma_{1.434})^{52}Cr$ equal to 3 times the values given by curve 1 in Figure 3.

The other prompt spallation lines of ^{56}Fe shown in Tables 1 and 2 are those whose cross sections at 100 MeV are at least 10% of the 1.434 MeV line cross section. From Chang et al. (1974) such lines are at 0.092, 0.412, 0.477, 0.744, 0.931, 1.312, 1.334, 1.370 and 1.408 MeV with cross sections of 15, 15, 15, 20, 65, 30, 15, 10 and 60% of the 1.434 MeV cross section. We use these ratios in our calculations at all energies.

As with Ne, Mg, and Si, the total gamma-ray production cross section from ^{56}Fe is considerably larger than the cross section for the excitation of any single line from this nucleus. In Figure 11 the closed squares represent data for this total cross

section (Zobel et al. 1968). The diamond is based on an extrapolation of the measurements of Zobel et al. (1968) for ^{16}O and ^{27}Al at 56 MeV. We have assumed isotropic gamma-ray emission in transforming the differential cross sections given by these authors into total cross sections. The crossed line in Figure 11 is our estimate of the total gamma-ray production cross section by proton-induced reactions on ^{56}Fe. For the unresolved gamma-ray emission from α-particle-induced reactions on ^{56}Fe, we take cross sections that at all incident energies are 3 times larger than the crossed line in Figure 11, based on a measurement of Zobel et al. at 14 MeV/nucleon.

Spallation reactions on ^{56}Fe also produce a rich spectrum of gamma ray lines from the decay of long-lived radioisotopes. The most important such isotopes are ^{56}Co, ^{55}Co, ^{54}Mn, and ^{52}Mn, along with ^{7}Be, ^{22}Na and ^{26}Al which have already been discussed above.

Decay of ^{56}Co leads to strong line emission at 0.847 and 1.238 MeV with weaker lines at 2.599, 1.772 and 1.038; ^{55}Co decay gives a strong line at 0.931 MeV and somewhat weaker lines at 1.408 and 0.477 MeV; ^{54}Mn decay yields just a single strong line at 0.835; and ^{52}Mn decay produces three strong lines at 1.434, 0.936 and 0.744 MeV. These lines, included in Table 1, have branching ratios of at least 10% (Bowman and MacMurdo 1974).

The cross sections for production of these isotopes from proton spallation of ^{56}Fe are shown in Figure 12. Measurements of these and other ^{56}Fe spallation cross sections have been summarized and discussed by Bradzinski et al. (1971) for proton energies greater than 10 MeV. Measurements of the cross sections for

^{56}Co production at lower energies have been summarized by Jenkins and Wain (1970).

Gamma ray line emission from decay of other relatively long-lived isotopes, such as ^{51}Cr, ^{48}V and ^{46}Sc, is not significant compared to those above, either because the peak production cross section is $\lesssim$ 10 mb or the gamma ray emission probability during decay is too small (< 10%).

III. GAMMA RAY SPECTRA AND INTENSITIES

In this section we discuss the shapes of the gamma ray lines and we carry out calculations of their intensities for various assumptions on the spectrum and composition of the energetic particles. We also treat the formation of gamma ray lines in interstellar grains.

In IIIa we discuss in detail the shape of the 4.438 MeV line from (p,p') reaction on ^{12}C. Detailed measurements of the spectrum of this line have recently been made in the laboratory and we compare our calculations with these measurements. In IIIb we treat the effects of interstellar grains on gamma ray line widths, and in IIIc we discuss the kinematics of the various other lines considered in this paper. In IIId we present numerical calculations of gamma ray spectra and intensities from energetic particle interactions for a variety of spectral parameters and compositions.

a. Profiles of the 4.438 and 6.129 MeV Lines from (p,p') Reactions

Consider the 4.438 MeV gamma rays resulting from the interaction of a proton with a ^{12}C target. We take the z axis in the direction of the incident proton. The probability of photon emission per second into solid angle $d\cos\theta_o d\phi_o$ from interactions in which a proton of energy E produces a $^{12}C^{*}4.439$ nucleus with recoil velocity in $d\cos\theta_r^* d\phi_r$ in the center-of-mass frame of the reaction is given by

$$dP_\gamma = n_c v \frac{d\sigma}{d\Omega^*}(E,\theta_r^*) d\cos\theta_r^* d\phi_r \, g(E,\theta_r^*,\theta_o,\phi_r-\phi_o) d\cos\theta_o d\phi_o. \quad (1)$$

Here n_c is the number density of the carbon target, v(E) is the velocity of the proton, $d\sigma/d\Omega^*$ is the center-of-mass differential cross section, and g is the angular distribution of the gamma rays which can depend on all the variables shown in equation (1). Both θ_r^* and θ_o are measured with respect to the z axis, while the azimuthal angles ϕ_r and ϕ_o are, as usual, given in the (x,y) plane.

The gamma ray energy, E_γ, corresponding to the variables E, θ_r^*, θ_o, $\phi_r-\phi_o$ is a single valued function of these variables through the following set of equations

$$E_\gamma = E_o/(\gamma_r-(\gamma_r^2-1)^{1/2}\cos\theta_\gamma), \quad (2)$$

$$\gamma_r = \gamma_c\gamma_r^*+(\gamma_c^2-1)^{1/2}(\gamma_r^{*2}-1)^{1/2}\cos\theta_r^*, \quad (3)$$

$$E_r = m_p c^2(\gamma_r-1), \quad (4)$$

$$\cos\theta_\gamma = \cos\theta_r\cos\theta_o+\sin\theta_r\sin\theta_o\cos(\phi_r-\phi_o), \quad (5)$$

$$\cos\theta_r = [\gamma_r^*(\gamma_c^2-1)^{1/2}+\gamma_c(\gamma_r^{*2}-1)^{1/2}\cos\theta_r^*]/(\gamma_r^2-1)^{1/2}, \quad (6)$$

$$\gamma_c = (E_{cm}^2+m_2^2-m_1^2)/(2m_2E_{cm}), \quad (7)$$

$$\gamma_r^* = (E_{cm}^2+m_3^2-m_4^2)/(2m_3E_{cm}), \quad (8)$$

$$E_{cm} = [(m_1+m_2)^2+2m_2E]^{1/2}. \quad (9)$$

Here γ_c is the Lorentz factor of the center of mass of the $p^{12}C$ system, γ_r^* and γ_r are the Lorentz factors of the recoil ^{12}C in the center-of-mass and the laboratory frames, respectively, θ_r' is the angle between the velocity vectors of the incident proton and the recoil in the laboratory frame, θ_γ is the angle between the velocity vector of the recoil ^{12}C and the direction of the gamma ray in the laboratory frame, m_1 and m_4 are equal to the proton mass m_p, m_2 is the mass of the ^{12}C, and $m_3 = m_2 + \Delta\varepsilon$ where $\Delta\varepsilon = 4.439$ MeV. Because of additional recoil of the ^{12}C during photon emission, the photon energy in the rest frame of the $^{12}C^*4.439$ is given by

$$E_o = \Delta\varepsilon[1 - \Delta\varepsilon/(2m_3c^2)].$$

The total cross section for the reaction $^{12}C(p,p')^{12}C^*4.439$ was discussed in detail in Section IIb. For the differential cross section of this reaction, $d\sigma/d\Omega^*$, we use the data of Peele (1957) at E = 14 MeV for the proton energy range $12 \leq E < 20$ MeV, that of Dickens, Haner and Waddell (1963) at 24.1 MeV for $20 \leq E < 35$ MeV, the data of Fannon et al. (1967) at 50 MeV for $35 \leq E < 70$ MeV, and that of Strauch and Titus (1956) at 96 MeV for $E \geq 70$ MeV. Below 12 MeV we assume that $d\sigma/d\Omega^*$ is isotropic.

For the Monte Carlo simulation that we use for the evaluation of gamma ray spectra we shall need numerical values for the probability that $\cos\theta_r^*$ is less than a given value. Using the above data on $d\sigma/d\Omega^*$ we show these probabilities by the solid curves in Figure 13. As can be seen with increasing proton energy the $^{12}C^*$ nuclei tend to recoil more towards the backward direction in the center-of-mass frame. For example, half the nuclei have recoil angles, θ_r^*, greater than 90° if $E < 12$ MeV, whereas if E = 96 MeV half have $\theta_r^* > 155°$.

We proceed now to discuss our assumptions for the gamma-ray angular

distributions g. In previous treatments (Ramaty and Crannell 1976, Ramaty, Kozlovsky and Suri 1977) it was assumed that the photon angular distribution is isotropic in the rest frame of the $^{12}C^{*}4.439$ nucleus. This assumption, however, cannot explain the profiles of the 4.438 MeV line obtained in accelerator experiments in which a high resolution gamma ray detector was placed at a fixed angle to the direction of the beam. For example when this angle is 90°, the line profile has a deep minimum at 4.438 MeV, and two symmetrically located maxima whose separation, ΔE_γ, depends on the energy of the protons: $\Delta E_\gamma \simeq 90$ keV for E = 50 MeV (N. S. Wall, private communication 1977) and $\Delta E_\gamma \simeq 60$ keV for both E = 23 MeV (Kolata, Auble and Galonsky 1967) and E = 16 MeV (P. Dyer and D. Bodansky, private communication 1977). Below 10 MeV the two peaks can no longer be separated (P. Dyer and D. Bodansky, private communication 1977). The ratio between the maximum and minimum intensities is about a factor of 2 for all proton energies greater than 16 MeV.

Following Kolata et al. (1967), we can account for this splitting effect by assuming that the magnetic sublevels of the 2^+ state of the ^{12}C nucleus (at 4.439 MeV) are unequally populated in the $^{12}C(p,p')^{12}C^{*}4.439$ reaction. In this case the angular distribution of the gamma-ray emission can be written as

$$g = \sum_{m=-2}^{2} S_m |X_{2m}(\cos\theta_w)|^2. \qquad (10)$$

Here, $\cos\theta_w = \sin\theta_o \sin(\phi_r - \phi_o)$, where θ_w is the angle between the gamma ray and the normal to the reaction plane defined by the velocity of the proton and the recoil $^{12}C^{*}$ nucleus, and the $X_{\ell m}$ are proportional to vector spherical harmonics (e.g. Jackson 1962, page 551). The S_m's are the probabilities for populating the sublevels, and they can depend

on the proton energy E and the scattering angle θ_r^*. Schmidt et al. (1964) have measured these probabilities at 10.3 MeV. We have approximated their results by the expressions

$$S_o = 1 - (S_1+S_{-1}) - (S_2+S_{-2}) \tag{11}$$

$$S_1+S_{-1} = S_2+S_{-2} = 0.5\exp[(\cos\theta_r^*-1)/1.4], \tag{12}$$

and we have assumed that these coefficients are independent of energy.

Equations (11) and (12) coupled with the angular dependence of $d\sigma/d\Omega^*$ (Figure 13) lead to the reduced population of the $m = \pm 1$ and ± 2 sublevels, since $S_{\pm 1}$ and $S_{\pm 2}$ are largest at $\cos\theta_r^* = 1$ where $d\sigma/d\Omega^*$ is the smallest. This effect can explain the dip at the center of the 4.438 MeV line, since photons at this energy result from reactions whose reaction plane is perpendicular to the direction of observations, and because only the $m = \pm 1$ terms in equation (10) produce radiation in the $\theta_w = 0°$ direction.

We use a Monte-Carlo simulation to integrate equation (1) over $\cos_r^*$ and ϕ_r for constant E, θ_o and ϕ_o. We choose a large number of pairs of independent random numbers R_1 and R_2, each of which are uniformly distributed from 0 to 1. For every such pair we solve for $\cos\theta_r^*$ and ϕ_r from the equations

$$R_1 = [1/\sigma(E)] \int_{-1}^{\cos\theta_r^*} (d\sigma/d\Omega^*)d\Omega^* \tag{13}$$

$$R_2 = \phi_r/2\pi, \tag{14}$$

where the right hand side of equation (13) is plotted in Figure 13. We then evaluate E_γ from equations (2) through (9) and g from equations (10) through (12). The probability of observing gamma rays of energies between E_γ to $E_\gamma + \Delta E_\gamma$ is then proportional to the sum of all the g's

for which E_γ is in the range.

The results are shown by the solid curves in Figure 14 for $\theta_o = 90°$ and three values of E. As can be seen, line splitting with strong dips does indeed follow from the numerical calculation; both the depths of the dips and the separation between the peaks are essentially consistent with the accelerator data of N. S. Wall (private communication 1977) P. Dyer and D. Bodansky (private communication 1977) and Kolata et al. (1967).

Also shown in Figure 14 (dashed curves) is the line profile resulting from isotropic gamma-ray emission ($S_o = S_1+S_{-1} = S_2+S_{-2}$) at E = 50 MeV and $\theta_o = 90°$. As can be seen, this profile also shows a small amount of line splitting caused by the preferential emission of $^{12}C^*$ nuclei into the backward direction in the center-of-mass frame. This splitting, however, is insufficient to account for the large splitting and deep dips observed in the accelerator data.

If we now consider gamma ray emission from nuclear interactions of an isotropic distribution of energetic particles, then in addition to the integrations over θ_r^* and ϕ_r, equation (1) should be integrated over θ_o and ϕ_o. Furthermore, for a distribution of particle energies, an integration over E is also required. We carry out these integrations by choosing two additional random numbers, R_3 and R_4, and by solving for E and $\cos\theta_o$ from the equations

$$R_3 = C\int_o^E vN_p(E')\sigma(E')dE' \qquad (15)$$

$$R_4 = (1+\cos\theta_o)/2, \qquad (16)$$

where $N_p(E)$ is the number of energetic protons per unit energy, and C is a normalization constant; there is no need to evaluate ϕ_o explicitly

because equation (1) depends only on $\phi_r - \phi_o$. We then determine the gamma-ray spectrum as before when E and θ_o were kept constant.

The results are shown in Figure 15 for an energy spectrum $N_p(E) \propto E^{-2}$ and two choices of the angular distribution of the gamma rays. The solid line is for isotropic gamma ray emission, and the dashed line is for the S_m's as given in equation (11) and (12). As can be seen, there is no substantial difference between these two spectra. In particular the full widths at half maximum (FWHM) of these spectra are essentially identical. This result implies that the effects of the anisotropic gamma-ray emission which are very noticeable in the case of a proton beam, are essentially smeared out when the distribution of the energetic particles is isotropic. Therefore, in the subsequent discussion and calculations we consider only isotropic incident particle distributions and assume isotropic gamma-ray emission for the 4.438 MeV line as well as for all the other lines discussed in Section II. Some other observable features in gamma-ray line shapes resulting from anisotropic particle distribution in solar flares have been discussed previously (Ramaty and Crannell 1976, Kozlovsky and Ramaty 1977).

For the calculation of the 6.129 MeV line profile in (p,p′) reactions we use data for $d\sigma/d\Omega^*$ measured by Crawley and Garvey (1967) at 17.5 MeV, and by Austin et al. (1971) at 17, 29.5 and 46.1 MeV. The integrals required in equation (13), based on these data, are shown by the dashed curves in Figure 13. As for the 4.438 MeV line, we assume that $d\sigma/d\Omega^*$ is isotropic for $E<12$ MeV, and we use the 17 MeV data for the range $12 \leq E < 20$ MeV, the 24.5 MeV data for $20 \leq E < 35$ MeV, and the 46.1 data for $35 \leq E < 70$ MeV. Because of the lack of data at higher energies, we have used the ^{12}C data at 96 MeV (Stranch and Titus (1956) also for ^{16}O in the range $E \geq 70$ MeV.

b. Lines from Interstellar Grains

In calculating the profiles of the various gamma ray lines discussed in II, we have to consider the effects of interstellar grains which can lead to very narrow line emission (Lingenfelter and Ramaty 1977). This line component is produced by deexcitation of interstellar grain nuclei.

As we have seen in IIa, the energy, E_γ, of a gamma ray emitted from a given nuclear level is Doppler shifted from the rest energy E_o due to the recoil energy, E_r, acquired by the excited nucleus in the nuclear interaction. However, if this interaction takes place in a grain, at the time of photon emission the recoil energy, E_r', could be smaller than its initial value, E_r, because of the energy lost by the excited nucleus in the solid prior to deexcitation. The width of the gamma ray line could, therefore, be substantially decreased provided that the mean life of the level or of its radioactive parent (Table 1), and the distance from the site of the interaction to the grain edge along the direction of the recoil, are longer, respectively, than the slowing down time and the stopping range of the excited nucleus in the grain material.

The rate of energy loss, dE_r/dx, the mean rectilinear stopping range, $\langle X(E_r)\rangle$, and the fluctuation in X due to straggling, $(\Delta X/X)^2$ are shown in Figure 16 for ^{16}O, ^{24}Mg and ^{56}Fe nuclei slowing down in water assuming that the grains are predominantly ice. These quantities, however, are not strongly dependent on the assumed grain composition. These curves were derived by Bussard (1978) from the compilations of Northcliffe and Schilling (1970) and Winterbon (1975). Typical recoil energies from (p,p') range from about a keV for ^{56}Fe to several tens of keV for ^{16}O. For a density of 1.5g cm^{-3} such nuclei slow down in less than about 7×10^{-13}sec over distances less than $\sim10^{-4}$cm. By comparing with the mean

lives listed in Table 1 and the expected sizes of interstellar grains, it is evident (Lingenfelter and Ramaty 1977) that many lines could have significant very narrow components.

In our calculations we consider spherical grains having an exponential size distribution and containing half of the interstellar C, N, O, Ne and S and all of the Al, Mg, Si, Ca, and Fe. For such grains, the probability that a nuclear interaction takes place in a grain of radius between a and a+da is

$$P(a)da = (6a_o^4)^{-1} a^3 \exp(-a/a_o)da. \quad (17)$$

In our calculations we take $a_o = 5\times10^{-5}$cm. We also assume that the energetic particle flux is isotropic, and that the matter density and composition are constant throughout the grain. Then the probability that the recoil nucleus traverses a distance to the edge of the grain between r and r+dr is

$$P(r)dr = (12a^2-3r^2)/(16a^3)dr. \quad (18)$$

In the Monte Carlo simulation for the calculation of the total gamma-ray spectrum we take into account the effects of interstellar grains for all lines whose nuclear levels or radioactive parents have mean lives longer than 10^{-13}sec (Table 1). Each event in the simulation corresponds to a nuclear interaction in some target nucleus which has a recoil energy E_r, calculated from Equation (4). If this interaction takes place in the grain, we evaluate a grain radius from Equation (17), a distance to the grain edge from Equation (18), a stopping range $X = \langle X \rangle + \Delta x$ from Figure 16, a ΔX from a gaussian distribution, and a lifetime, t_ℓ, from an exponential distribution with mean life given in Table 1. If the nucleus stops in the grain (r>x), E_r' is evaluated from

$$\int_{E_r'}^{E_r} (\rho v)^{-1} dE/(dE_r/dx) = t_\ell, \tag{19}$$

where ρ is the density and v the recoil velocity; this case includes the possibility that $E_r' = 0$, i.e. the nucleus stops before it deexcites. Equation (19) is also used when $r < X$, provided that the nucleus deexcites before it reaches the the grain edge, i.e. when

$$\int_{E_r^{edge}}^{E_r} (\rho v)^{-1} dE/(dE_r/dx) > t_\ell. \tag{20}$$

Here E_r^{edge}, the energy of the nucleus at the edge, is obtained by solving

$$\langle X(E_r^{edge})\rangle = \langle X(E_r)\rangle - r. \tag{21}$$

If condition (20) is not satisfied, then $E_r' = E_r^{edge}$, i.e. the nucleus leaves the grain in an excited state and deexcites later in the interstellar medium where its energy remains essentially E_r^{edge}. An exception is $^{26}A\ell$, whose mean life, 3.4×10^{13} sec, is longer than the stopping time of this nucleus in the interstellar medium. Thus, for the 1.809 MeV line from $^{26}A\ell$ decay we take $E_r' = 0$, independent of the grain size.

Having evaluated the effect of the grains on the recoil energy of the excited nucleus, we evaluate the gamma ray energy, E_γ, from Equations (2) through (9), with the transformation $E_r \rightarrow E_r'$ as described above.

c. Kinematics of Other Nuclear Lines

We proceed now to evaluate the spectrum that results from the superposition of all the gamma ray emission produced by the reactions discussed in Section II.

We first discuss reactions induced by energetic protons and alpha particles. The data and assumptions used to calculate the profiles of the

4.438 and 6.129 MeV line from (p,p') reactions were given in (IIIa). For all other (p,p') and (p,n) reactions we assume that the angular dependence of $d\sigma/d\Omega^*$ is the same as that for the $^{12}C(p,p')^{12}C^*$ reaction shown in Figure 13. For (α,α') reactions, we assume that $d\sigma/d\Omega^*$ is isotropic. An can be seen from the cross sections of II, (e.g. Figure 2 for the reaction $^{12}C(\alpha,\alpha')^{12}C^*$), (α,α') reactions are important only at projectiles energies below about 10 MeV/nucleon. In this energy range, the data of Mitchel, Carter and Davies (1970), Morgan and Hobie (1970), Blatchley and Bent (1965) and Correlli, Bleuler and Tendam (1959) indicate that the (α,α') differential cross sections have considerable structure with several maxima and minima, but on the average they can be approximated by an isotropic distribution. As discussed by Kozlovsky and Ramaty (1977), it can be assumed that $d\alpha/d\Omega^*$ is isotropic for the reactions $^4He(\alpha,n)^7Be^*$ and $^4He(\alpha,p)^7Li^*$.

To calculate line profiles from spallation reactions, we in principle need data both on $d\alpha/d\Omega^*$ and on the distribution of γ_s^*, because in reactions with more than two bodies in the final state, this quantity is not a unique function of the incident energy, E. But in the absence of data on this distribution, we have assumed for multibody processes that $\gamma = \gamma_c$, i.e. that the velocity of the recoil nucleus is the same as that of the center of mass. This assumption is different from that made by Ramaty et al. (1977), and it leads to a larger width than found by these authors. From gamma-ray measurements, P. Dyer and D. Bodansky (private communication 1977) have found that the FWHM of the 4.438 MeV line from ^{16}O spallation is somewhat larger than 100 keV, a result which is more consistent with the present assumption.

For all lines from levels with mean lives longer than 10^{-13}sec we

carry out the transformation $E_r \rightarrow E_r'$ to take into account the effects of interstellar grains as discussed in IIIb.

We estimate the energy distribution of the unresolved gamma-ray lines of Ne, Mg, Si and Fe from the measurements of Zobel et al. (1968). These authors have measured the energy distribution of gamma rays from the bombardment of $^{27}A\ell$ and ^{56}Fe by protons of various energies. Their results are quoted by Shima and Alsmiller (1970). These distributions peak between about 1 to 2 MeV, with the magnitude of maximum becoming more pronounced with increasing target atomic number and proton energy. As we have discussed in IIc, the gamma rays at these energies arise mainly from transitions in high-lying levels of the nuclei and their spallation products. Indeed, from the measurements of Degnan et al. (1973) we see that for a variety of target nuclei the photon multiplicity increases with increasing excitation energy of the residual nuclei. From these multiplicities it follows that, on the average, the photon energies are in the 1 to 2 MeV range.

The energy distribution of the unresolved gamma-ray lines are shown in Figure 17 normalized to unit integral. The closed circles are data for ^{56}Fe based on the measurements of Zobel et al. (1968) at proton energies of 31.4 MeV, and the open squares show the assumed gamma-ray distribution for ^{28}Si based on measurements of $^{27}A\ell$ at 30 MeV. We expect the spectrum of unresolved gamma-ray lines to have a smooth dependence on A, as is the case for the total cross section, σ_γ, discussed in IIc. Therefore, the measured spectrum of $^{27}A\ell$ should be a good approximation for ^{28}Si. The open circles show our approximation for Ne and Mg based on measurements from $^{27}A\ell$ at 14 MeV. The choice of the

Aℓ data at lower energies for Ne and Mg is based on the trend in the data of Zobel et al. (1968) according to which the peak in the 1 to 2 MeV region becomes less pronounced for lighter targets and lower incident energies.

For the reactions induced by energetic heavy nuclei we proceed as follows. For the two-body reactions we use, with the appropriate transformations, the same kinematics and data as for the corresponding reactions induced by protons or alpha particles. For spallation reactions, we assume that the excited nucleus moves in the same direction and with the same velocity as the incident heavy nucleus. For the unresolved lines we use the same data as for the corresponding reactions induced by protons and alpha particles, but broaden the spectra shown in Figure 17 by assuming, as we just did for the spallation reactions, that the excited nuclei move in the same direction and with the same velocity as the incident nuclei.

Interstellar grains have no effect on gamma ray lines from excited energetic heavy nuclei since the stopping ranges of these particles are much longer than the dimensions of the grains. The 1.809 MeV line from ^{26}Aℓ decay produced by energetic ^{26}Mg, ^{27}Aℓ and ^{28}Si nuclei, however, will be very narrow, because the energetic (<100 MeV/nucleon) ^{26}Aℓ stops in the interstellar medium of density ~ 1 Hcm^{-3} in a time shorter than its mean lifetime.

d. Nuclear Gamma Ray Spectra and Intensities

Using the above data and assumptions, we have evaluated the total gamma-ray spectrum by employing for each of the reactions given in Section II a Monte Carlo simulation similar to the one described in IIIa for the 4.438 MeV line.

For the ambient medium we use the abundances of Ross and Aller (1976) shown in Table 2. For the energetic particles, we assume that all particle species have the same energy spectrum,

$$N_i(E) \propto \begin{cases} E^{-s} & ; E>E_c \\ \text{Const} & ; E\leq E_c \end{cases} , \qquad (22)$$

where $N_i(E)$ is the number density of species i per unit energy per nucleon interval around E, and s and E_c are spectral parameters; steep spectra correspond to large s and low E_c, and flat spectra to low s or large E_c. We use two sets of abundance ratios for the energetic particles at the same E: solar abundances from Ross and Aller (1976) (Table 3, column 1) and cosmic ray source abundances from Shapiro, Silberberg and Tsao (1975) (Table 3, column 2).

The results are shown in Figures 18, 19 and 20 for $E_c = 0$ and s = 2, 3 and 4 and solar abundances, and in Figures 21 and 22 for s = 3 and E_c = 0 and 20 MeV/nucleon and cosmic ray abundances. There are 10^5 photons in each of these spectra, and they are binned into energy intervals of widths ranging from 2 to 5 keV, as indicated in the figures. Such widths are consistent with the energy resolution of Ge detectors used in current and planned gamma ray astrophysical spectroscopy missions (Lingenfelter and Ramaty 1978).

For comparison, in Figures 23 and 24 we show gamma ray spectra obtained by binning the photons into 100 keV intervals. In these figures, we also use cosmic ray abundances for the energetic particles, and s = 3 and E_c = 0 or 20 MeV/nucleon. The solid lines show total spectra, while the dashed lines are spectra produced by only the energetic heavy nuclei ($A\geq 12$).

Three line components contribute to the spectra of Figures 18 through

24. There is a broad component from the deexcitation of energetic heavy nuclei which interact with ambient H and He, a narrow component from ambient nuclei excited by energetic protons and alpha particles, and a very narrow component from deexcitation of those excited nuclei that can come essentially to rest before deexcitation because the lifetime of the level, or its radioactive parent, is long enough and the ambient density high enough. The very narrow component is mostly due to the interactions of protons and alpha particles with heavy nuclei is interstellar grains (Lingenfelter and Ramaty 1977).

The broad lines tend to overlap, and therefore only a few well defined features can be distinguished in this component. Such features are most noticeable for steep particle spectra and cosmic ray abundances, and can be seen, for example, in Figures 21 and 23 at about 0.85, 1.3, 1.7, 4.4 and 6.2 MeV.

Many narrow and very narrow lines are superimposed on the continuum defined by the broad component. These are particularly numerous if the energetic particles have the same composition as the ambient medium (Figures 18, 19 and 20); if the relative abundances of heavy nuclei are enhanced as in cosmic ray sources, then the underlying continuum becomes higher, and therefore fewer narrow and very narrow lines can be seen (Figures 21 and 22).

The strongest narrow line is at 4.44 MeV resulting from deexcitations of excited states in ^{12}C and ^{11}B (Table 1). Because of the short mean lives of these levels, the 4.44 MeV line has no very narrow component. However, the second strongest line, at 6.129 MeV, has a prominent very narrow component which can be clearly seen in Figures 18 through 22. In addition, there are many other lines which exhibit very narrow components.

The strongest among these, at 0.847 and 1.238 MeV from ^{56}Fe, at 1.369 MeV from ^{24}Mg, at 1.634 MeV from ^{20}Ne, and at 1.779 MeV from ^{28}Si, are visible even for a cosmic ray composition, as can be seen in Figures 21 and 22. The 1.809 MeV line from ^{26}Aℓ decay is very prominent in Figure 22. This line is produced in the interstellar medium which slows down the excited ^{26}Aℓ nuclei resulting from energetic ^{28}Si, ^{27}Aℓ and ^{26}Mg before they decay into the 1.809 MeV level of ^{26}Mg.

The production rates, q, of the 4.44, 6.129 and 0.847 MeV lines and of the total nuclear radiation, normalized to the energy density, W, in energetic particles and 1H atom in the ambient medium are shown in Figure 25. These results are based on solar abundances for both the ambient medium and the energetic particles. For the 4.44, 6.129 and 0.847 MeV lines, the q's of Figure 25 are those resulting from proton and alpha interactions, i.e. the narrow component of the 4.44 MeV line and the sums of the narrow and very narrow components of the other two lines. For the total, q is the sum of the production rates of photons of all energies in all three line components.

As can be seen from Figure 25, the q/W's are maximal for a given s when E_c is between about 10 to 30 MeV/nucleon. This is due to the fact that the nuclear cross sections peak in this energy region.

The production rates, q, can also be normalized to the energy deposition rate, $\dot{W}$, of the energetic particles in the ambient medium. The ratios $q/\dot{W}$ are shown in Figures 26 and 27 for a neutral and ionized ambient medium, respectively. As in Figure 25, the q's are the production rates of the narrow 4.44 MeV and narrow plus very narrow 6.129 MeV line, and both the ambient medium and energetic particles have solar abundances. The energy loss rates in a neutral medium of 90% H and 10% He are from Northcliffe and Shilling (1970) and Barkas and Berger (1964). The energy loss rates in an ionized medium are from Ginsburg and Syrovatskii (1964)

calculated for a temperature of 10^4K and electron density $1cm^{-3}$. As can be seen, in a neutral medium $q/\dot{W}$ is larger by about a factor of 4 than in an ionized one, because for a neutral gas $\dot{W}$ is smaller by this factor. By comparing Figures 26 and 27 with Figure 25, we see that the $q/\dot{W}$'s tend to peak at higher E_c than q/W. This is due to the fact that the energy loss rates of fast particles increase very rapidly as their energies decrease.

The ratio of the production rates of the narrow plus very narrow 6.129 MeV line to the narrow 4.44 MeV line is shown in the upper panel of Figure 28 as a function of s and E_c for solar abundances. As can be seen, this ratio is quite insensitive to the spectral parameters, its value ranging from about 0.3 to 1.

The production of nuclear gamma ray lines by energetic particle interactions is accompanied by positron production from the decay of radioactive positron emitters. Such positron production has been treated in considerable detail by Ramaty et al. (1975). We have updated the cross sections used by these authors, and we have added several new positron emitters such as $^{16}O^*6.052$ and ^{56}Co. We shall present a detailed discussion of positron production elsewhere. In the lower panel of Figure 28 we show the ratio of positron production to the narrow 4.44 MeV line production as a function of s and E_c for solar abundances. We note that $q_+/q_{4.44}$ is not a strong function of the spectral parameters. Nonetheless, for extreme flat spectra, this ratio is larger by about a factor of 6 than for very steep spectra, reflecting the fact that positron production does not drop off at high energies as does the cross section for 4.44 MeV line production (Figure 2). We note that q_+ in Figure 28 does not include positron production from $\pi+$ decay.

IV. AN ASTROPHYSICAL SOURCE: NUCLEAR GAMMA RAYS FROM THE INTERSTELLAR MEDIUM

Detectable nuclear gamma ray line emission may be produced by energetic particle interactions in various sources. Nuclear gamma ray production in solar flares has been treated in detail by Ramaty et al. (1975, 1977) and other sources which could be observed in gamma-ray lines have been reviewed recently by Lingenfelter and Ramaty (1978). In this section we shall apply the theory developed in the previous two sections to the nuclear gamma ray line emission resulting from low energy ($<$100 MeV/nucleon) cosmic ray interactions with the interstellar gas and dust. We calculate the expected line intensities and we compare our results with previous estimates, as well as with reported observations of nuclear lines from the galaxy. We shall also compare the calculated nuclear line intensities with other diffuse lines expected from annihilation of positrons from various sources and from the decay of long-lived ($>10^5$yrs) radioisotopes synthesized in novae and supernovae.

Gamma ray line emission from cosmic ray interactions in the interstellar medium should constitute a spatially diffuse galactic source with maximum intensities in the galactic plane in the general direction of the galactic center, reflecting the distributions of matter and energetic particles along the line of sight. The intensity in any particular direction depends primarily on the distributions of the density and composition of interstellar matter, and the energy density, spectrum and composition of low energy cosmic rays. The intensity of the very narrow line component also depends on the size, composition and distribution of the dust grains.

Although these distributions are at best only poorly known, the line intensities can be calculated from the measured (Fichtel et al. 1975; Paul et al. 1978) intensity of high energy galactic gamma rays and the comparison

of the relative emissivities of nuclear lines and these gamma rays. A large fraction of the high energy gamma rays are believed to be due to the decay of π° mesons produced by the interaction of high energy (>100 MeV/nucleon) cosmic rays with interstellar matter. The nuclear line intensities are further constrained by x-ray and low energy gamma ray observations. The x-ray observations can set limits on the column depth in the galactic plane of O and heavier elements through studies of the absorption of radiation from x-ray sources (Ryter, Cesarsky and Audouze 1975); x-ray observations can also limit low energy cosmic ray fluxes through investigations of the nonthermal 6.8 keV iron line produced by charge exchange of energetic iron ions with interstellar gas (Bussard, Ramaty and Omidvar 1978). A further limit on the individual nuclear line intensities is given by upper limits on the total gamma ray emission from the galactic disc in the MeV region (Gilman et al. 1978). We shall discuss these constraints below together with much more model dependent constraints related to the ionization of the interstellar medium and Li production. But first we set up the formalism for calculating the intensities of the nuclear lines.

Let q_i and q_{π° be the emissivities per H atom of gamma rays in a nuclear line i and from π° decay, respectively, as functions of galactocentric radius, ω. The fluxes that result from these emissivities, integrated over galactic latitude, b, at a given longitude, ℓ, can be written as

$$I_i(\ell) = 1/4\pi \int_{-10^\circ}^{10^\circ} db \int_0^h \cot b \, dr \; n_p(\omega) q_i(\omega) \tag{23}$$

and

$$I_{\pi^\circ}(\ell) = q_{\pi^\circ}(0)/4\pi \int_{-10^\circ}^{10^\circ} db \int_0^h \cot b \, dr \; n_p(\omega) q_{\pi^\circ}(\omega)/q_{\pi^\circ}(0), \tag{24}$$

where r is the distance from the observing point along the line of sight, n_p is the number density of protons (in both atomic and molecular form)

at ω, and $q_{\pi^\circ}(\theta)$ is the local π° decay emissivity (i.e. at $\omega=\omega_\theta$ = 10 kpc). The relationship between r, ℓ, and ω is $\omega = (\omega_\theta^2 + r^2 - 2\omega_\theta r \cos\ell)^{\frac{1}{2}}$; the limits of integration on b are consistent with presently used gamma ray line detectors.

Let $W(\omega)$ be the energy density in low energy cosmic rays as a function of galactocentric radius, and $W(\theta)$ the local energy density in these cosmic rays. If we assume that the low and high energy cosmic rays have the same spatial distribution in the galaxy, and if their energy spectra are spatially independent, then

$$W(\omega)/W(\theta) = q_{\pi^\circ}(\omega)/q_{\pi^\circ}(\theta). \tag{25}$$

From equations (23), (24) and (25) we obtain that

$$I_i(\ell) = W(\theta)\ I_{\pi^\circ}(\ell)/q_{\pi^\circ}(\theta)\langle q_i/W\rangle, \tag{26}$$

where $\langle q_i/W\rangle$ is the emissivity in line i per H atom per unit energy density averaged along the line of sight.

We shall use equation (26) to calculate the fluxes of the various gamma ray lines. For $W(\theta)$ we take the nominal value of $1 eV/cm^3$, roughly equal to the measured energy density of the high energy cosmic rays. The energy density in low energy cosmic rays outside the solar system is not known because solar modulation excludes these particles from the inner solar system (e.g. Goldstein, Fisk and Ramaty 1970).

The second term in equation (26), $I_{\pi^\circ}/q_{\pi^\circ}$ follows from high energy gamma ray observations and theory. The high energy gamma ray spectrum has been measured by Paul et al. (1978) from several directions in the galaxy. We shall use their data from the general direction of the galactic center, integrated over about $\pm 10°$ of galactic latitude from 355° to 15° of galactic longitude. This data is shown in Figure 29. The general longitude dependence of the galactic high energy gamma rays was determined by Fichtel et al. (1975). For galactic longitudes between about 330° to 30°,

the high energy gamma ray intensity is constant to within a factor of 2. At gamma ray energies less than about 200 MeV the spectrum can be fitted by a π°-decay gamma ray spectrum plus an apparent electron bremsstrahlung component which we shall discuss below. But above 300 MeV the measured spectrum is consistent with that expected (e.g. Stecker 1976) purely from π°-decay gamma rays (see Figure 29). Normalization of the measured flux at these energies to the calculated π°-decay spectrum gives $I_{\pi^\circ}(\ell)/q_{\pi^\circ}(0) = 5\times10^{20}$ H atom/(cm^{2}rad) for longitudes ℓ near the galactic center.

The emissivities per unit energy density, $\langle q_i/W\rangle$, depend on the compositions of interstellar matter and low energy cosmic rays, and the energy spectrum of these cosmic rays. We first consider the composition of interstellar matter.

There may be evidence for large radial gradients in the relative abundance of elements in our galaxy, based on observations of HII emission nebulae in both our own and other spiral galaxies (e.g. Searle 1971, Shields 1974, Smith 1975, Peimbert 1975, and Peimbert, Torres-Peimbert and Rayo 1978). Such composition gradients are expected from galactic evolutionary models (Tinsley and Larson 1978). Within a few kiloparsecs of the Sun, Peimbert et al. (1978) find radial gradients for O and N of $d \log (O/H)/d\omega = 0.13 \pm 0.04$ kpc^{-1} and $d \log (N/H)/d\omega = 0.23 \pm 0.06$ kpc^{-1}. Measurements (Burton 1976) of the longitude-velocity distribution of CO emission suggest a maximum in the molecular density in a region at galactocentric radius of 4 to 6 kpc. Since it is believed (Stecker 1976) that a major fraction of gamma rays from π° decay are produced in this region, we calculate $\langle q_i/W\rangle$ for O/H and N/H at $\omega \simeq 5$kpc. From the local abundance gradients, these ratios should be larger than solar system abundances by factors of $\sim$5 and $\sim$15, respectively. The solar system abundances and the

assumed ambient medium abundances at 5kpc are shown in the first and third columns of Table 3. In the latter, the abundances of all elements heavier than He, except N, are larger by a factor of 5 than solar system abundances; the N abundance is larger by a factor of 15.

The assumptions regarding the enrichment of heavy elements in the interstellar medium are limited by the column density of these elements as determined by interstellar absorption of x rays, and by the lower limit on the hydrogen column density obtained from 21cm observations. The column density of O is about $7 \times 10^{19} cm^2$ (Tucker et al. 1973, Ryter, Cesarsky and Audouze 1975), while that of H should be greater than $\sim 10^{22} cm^2$, the value obtained from 21cm emission. These two column densities would allow a maximal O/H ratio larger by about a factor of 10 than the solar O/H. The enrichment factor of 5 used in Table 3, however, is more consistent with the presence of comparable amounts of atomic and molecular hydrogen along the line of sight.

We next consider the composition of the low energy cosmic rays. Since this cosmic ray component has not been directly observed, we base our assumptions about its composition on information obtained from the high energy component. The composition of high energy cosmic rays at their sources has been calculated by several authors (e.g. Shapiro et al. 1975). From these calculations we assume a low energy cosmic ray composition as shown in the second column of Table 3. It is believed that the cosmic rays observed near Earth reflect galactic conditions in a region extending to a distance of not more than ~ 1 kpc from the solar system (e.g. Ramaty, Reames and Lingenfelter 1970). In the fourth column of Table 3 we present a possible cosmic ray source composition at 5kpc, where we assume that the abundances of nuclei heavier than He are enhanced relative to local cosmic ray source

abundances by the same factors as the ambient medium, i.e., by a factor of 5, except for N whose abundance is enhanced by a factor of 15.

In our subsequent calculations we shall consider four combinations of abundance ratios, which we shall refer to as cases (1) through (4). For case (1) both the ambient medium and low energy cosmic rays have solar abundances; for case (2) the ambient medium has solar abundances and the cosmic rays have local cosmic ray source abundances; for case (3) both the ambient medium and the low energy cosmic rays have the same composition as the enhanced ambient medium composition at 5kpc; and for case (4) the ambient medium has the same composition as for (3), but the cosmic rays have an enhanced cosmic ray source composition.

The dependence of q_i/W and $q_i/\dot{W}$ on the spectral parameters of the energetic particles, s and E_c, was treated in IIId for solar abundances, and the results are shown in Figures 25, 26 and 27. In Table 4 we present $\langle q/W \rangle$ and $\langle q/\dot{W} \rangle$ for the narrow and broad 4.44 MeV lines for cases (1) through (4), and s = 4 and E_c = 20 MeV/nucleon which essentially maximize these emissivities; $\dot{W}$ in this table is calculated for a neutral ambient medium. As can be seen, q/W and $q/\dot{W}$ increase, in general, with increasing relative abundance of the heavier nuclei. But this increase is not linear, because for large heavy element abundances in the energetic particles, a large fraction of W and $\dot{W}$ are due to the heavy nuclei themselves. The contribution of nuclei heavier than He to the total W is about 1.5%, 14%, 8% and 47% for cases (1), (2), (3) and (4), respectively, and their contribution to $\dot{W}$ is 7%, 51%, 29% and 84%, again for cases (1) through (4), respectively. Thus, for case (4), for example, half the energy density and almost all the energy loss of the energetic particles is due to nuclei heavier than He.

Also shown in Table 4 is the ratio of positron production to the total (narrow + broad) 4.44 MeV line production. As can be seen, this ratio is essentially independent of the assumed abundance combination, since both the positron emitters and the 4.44 MeV photons are produced predominantly from C, N and O.

For the comparison of the calculations with the data of Haymes et al. (1975) and Gilman et al. (1978), we also need the production rates of the total nuclear radiation, q(tot), and the production rates of gamma rays in the energy bands from 0.6 to 5.2 MeV, q(0.6-5.2), and 4.09 to 4.79 MeV q(4.09-4.79). For s=4 and E_c = 20/MeV nucleon and cases (3) and (4), respectively, $\langle q(tot)/W \rangle = 1.4 \times 10^{-24}$ and 6.0×10^{-24} photons/(sec Hatom eV cm^{-3}); q(0.6-5.2)/q(tot) = 0.72 and 0.80; and q(4.09-4.79)/q(tot) = 0.17 and 0.085.

Having discussed the three terms that are required to evaluate equation (26), we now proceed to calculate the fluxes of gamma ray lines from the general direction of the galactic center. By substituting $W(\theta) = 1$ eV/cm^3 and $I_{\pi^o}(\ell)/q_{\pi^o}(\ell) = 5 \times 10^{20}$ Hatom/cm^2rad into this equation, we evaluate the fluxes of the narrow 4.44 MeV line, the narrow plus very narrow 6.129 MeV and 0.847 MeV lines, and the 0.511 MeV line for cases (1) through (4). The results are given in Table 5 for s=4 and E_c = 20 MeV/nucleon. For the 0.511 MeV line, we take a photon-to-positron ratio of 0.6. This ratio is based on the calculations of Bussard, Ramaty and Drachman (1979) who find that in the interstellar medium about 93% of the positrons should annihilate from bound states of positronium with a 0.511 MeV photon-to-positron ratio of 0.5, and the remainder by direct annihilation with a ratio of 2.

The calculated line intensities given in Table 5 can be compared with earlier calculations. For the narrow 4.44 MeV line, for example, Meneguzzi and Reeves (1975) find an intensity of 5×10^{-4} photons/cm^2sec sr MeV if the local local low energy cosmic rays have an energy density of $\sim$ 0.4 eV/cm^3.

Since the width of the 4.44 MeV line is 110 keV and the thickness in latitude of the galactic ridge is about 4°, this intensity yields a flux of $\sim 4 \times 10^{-6}$ photons/(cm^2 sec rad) which is smaller by about a factor of 3 than our predictions of (1.2 to 1.3)$\times 10^{-5}$ photons/cm^2 sec rad for local conditions (cases 1 and 2). This difference is due to the lower energy density used by these authors, and the lower q/W resulting from their choice of spectral parameters (E_c = 5 MeV/nucleon and s = 3.5 and 5.5). Meneguzzi and Reeves (1975) chose these values to limit the rates of ionization of interstellar H and ^{7}Li production (by the reactions ^{4}He(α,p)^{7}Li and ^{4}He(α,p)^{7}Be) to 2×10^{-15} (H atom sec)$^{-1}$ and 3×10^{-27} (H atom sec)$^{-1}$, respectively. For the choice of parameters of Table 4 (s=4, E_c = 20 MeV/nucleon) and W(Θ) = 1 eV/cm^3, the rate of ionization is 1.6×10^{-15} and 2.6×10^{-15} (H atom sec)$^{-1}$ for cases (1) and (2), and the rate of ^{7}Li production (using the cross sections of Figure 1) is 6×10^{-26} (H atom sec)$^{-1}$ for both these cases. Thus, our local conditions do not conflict with an ionization rate of $\sim 10^{-15}$; the ^{7}Li production could be reduced by a lower alpha particle abundance in the low energy cosmic rays and a steeper energetic particle spectrum. Furthermore, processing of interstellar matter through stars could destroy some of the ^{7}Li, and the infall of extragalactic gas could introduce further uncertainties in the problem of the origin of this isotope (see Reeves 1978).

The calculated 4.44 MeV narrow line intensity for cases (3) and (4) in Table 5 are larger by about an order of magnitude than that calculated by Meneguzzi and Reeves (1975), mainly due to the enhanced abundance of elements heavier than He along the line of sight.

Bussard et al. (1978) have related the production of nuclear gamma rays to x-ray iron line production, $q_{6.8}$, resulting from charge exchange of low energy cosmic rays with interstellar matter. For the abundances of case

(2), and s=4 and E_c = 20 MeV/nucleon, they find that $q_{4.44}(\text{narrow})/q_{6.8}$ is about 4.5×10^{-4}. This ratio also applies to case (4), since $q_{6.8}$ depends only weakly on the ambient medium abundances (Bussard et al. 1978 and R. W. Bussard private communication 1978) and both $q_{6.8}$ and $q_{4.44}$ scale linearly with the cosmic ray abundances. Thus from Table 5, the 6.8 keV flux for case (4) should be $\sim$ 0.1 photons/cm^{2}sec rad, or $\sim$0.02 photons/cm^{2}sec from a longitude interval of 13° around the galactic center. This is consistent with the upper limit of 0.024 given by Bussard et al. (1978) for that region.

The nuclear line emission discussed above is superimposed on the possible bremsstrahlung continuum that is apparently required to account for the difference between the observed high energy gamma rays and the π° decay spectrum at energies between about 50 and 300 MeV (see Figure 29). It should be noted, however, that unresolved discrete sources (Higdon and Lingenfelter 1976, Bignami, Caraveo and Maraschi 1978) may also account for some of the observed high energy gamma ray emission.

The bremsstrahlung flux shown by the dashed line in Figure 29 has a numerical value given by $5\times10^{-4}E_\gamma^{-1.6}$ photons/(cm^{2}sec rad MeV). If the electrons that produce this flux have the same spatial distribution as $q_{\pi^\circ}(\omega)/q_{\pi^\circ}(0)$, then the local bremsstrahlung emissivity, q_B, and the corresponding local electron intensity, j_e, are

$$q_B(E_\gamma) \simeq 10^{-24}E_\gamma^{-1.6} \text{ photons/(H atom sec MeV)}, \tag{27}$$

and

$$j_e(E) \simeq 1.4\ E^{-1.6} \text{ electrons/(cm}^2\text{ sec sr MeV)}; \tag{28}$$

equation (28) is obtained from (27) by using the bremsstrahlung formula given by Ramaty and Westergaard (1976). This local electron intensity, j_e, joins smoothly at about 200 MeV with the electron intensity deduced by

Goldstein, Ramaty and Fisk (1970) from the galactic nonthermal radio emission. However, a power law extrapolation of j_e to energies below about 50 MeV is not required by the gamma ray data; nor is it required by the galactic nonthermal radio emission.

The resulting sums of the nuclear and bremsstrahlung fluxes are shown in Figures 30 and 31 for the abundance combinations of cases (3) and (4), respectively. Many narrow and very narrow lines are visible, especially in Figure 30 where the ambient medium and low energy cosmic rays have the same composition. The intensities of the strongest lines are given in Table 5; case (3) corresponds to Figure (30) and case (4) to Figure 31. The width of the 4.44 MeV line is about 110 keV and this line has no very narrow component. The very narrow component of the 6.129 MeV line contains about 20% of the line photons for our assumed conditions (grains with mean radius $a_o = 5 \times 10^{-5}$ cm containing half the interstellar O). But the relative importance of the very narrow component depends strongly on the fraction of O locked in grains, on the grain sizes, and on the spectrum of the energetic particles, as discussed in IIIb. The width of very narrow grain lines is determined principally by differential galactic rotation. In Figures 30 and 31 all of the photons of the very narrow 6.129 MeV line are in a 5 keV bin, and about 80% of the narrow plus very narrow 0.847 MeV line photons are in a 2 keV bin. Other potentially detectable lines seen in these figures are at 1.238 MeV from ^{56}Fe, at 1.369 MeV from ^{24}Mg, at 1.634 MeV from ^{20}Ne, at 1.779 MeV from ^{28}Si, at 1.809 MeV from ^{26}Mg and at 2.313 MeV and 5.105 MeV from ^{14}N.

The 0.511 MeV line fluxes in Figure 30 and 31 are 6×10^{-5} and 1.7×10^{-4} photons/cm^{2}sec rad, as given also in Table 5. In these figures, all the 0.511 MeV photons were placed in a 2 keV energy bin, as indicated. Such a

narrow line width would result from positron annihilation in a partially ionized gas (Bussard et al. (1979). For annihilation in cold clouds, however, these authors find that the FWHM of the 0.511 MeV line is about 5 keV.

Although many of the very narrow gamma ray lines shown in Figures 30 and 31 may be observable only with high resolution detectors, the strongest lines and line complexes should be observable with detectors of much lower energy resolution. This can be seen from the nuclear spectra shown in Figure 29, which are the same as those shown in Figures 30 and 31 except that they are averaged over broader energy bins as indicated in the figure. Even with such low energy resolution considerable structure is still quite evident. Prominent lines at 0.5 and 4.4 MeV and a broad feature between about 1 and 2 MeV can be seen for case (4). For case (3), line features at approximately 0.85, 1.3, 1.7, 2.3 and 6.1 MeV can also be seen.

The nuclear lines resulting from low energy cosmic ray interactions can be compared with other diffuse interstellar gamma ray lines which are expected from decay of radioisotopes synthesized in supernova and nova explosions and from annihilation of positrons produced both by decay of such radioisotopes and by other processes.

The most important of such radioisotopes thought to be synthesized in supernovae (Clayton, Colgate and Fishman 1969; Clayton 1973; Ramaty and Lingenfelter 1977; Arnett 1977) are ^{26}Al, which produces a line at 1.809 MeV, and ^{60}Fe with lines at 0.059, 1.173 and 1.332 MeV. Following Lingenfelter and Ramaty (1978), we take the production rate of these isotopes at the present epoch to be about 10% of the average rates required to produce over the age of the galaxy 0.1% and 1% of the galactic ^{26}Mg and ^{60}Ni abundances, respectively. The flux in each of the above four lines is then about 7×10^{-5} photons/(cm^2 sec rad), comparable to our highest predicted 4.44 MeV flux

from low energy cosmic ray interactions. The widths of the ^{26}Al and ^{60}Fe decay lines are about 0.3% of the line energy, resulting primarily from differential galactic rotation. The estimated fluxes per unit energy interval in these lines are therefore quite strong; the 1.809 MeV line from radioactivity produced in supernovae could be stronger by about an order of magnitude than the line at this energy resulting from cosmic ray interactions (Figure 31).

Accretion from a large, cool companion onto a white dwarf leading to thermonuclear runaway in the CNO cycle has been suggested as the cause of novae (e.g. Starrfield et al. 1972). If so, novae could also be sources of gamma-ray line emission from the decay of synthesized radionuclei (Clayton and Hoyle 1974). The easiest line to detect should be at 1.275 MeV from ^{22}Na decay with a mean life 3.8 years. Since the estimated nova rate is $\sim$20/year, the time between nova explosions in the galaxy is much shorter than the ^{22}Na mean life. Thus, a detector with a broad field of view observing the galactic plane in the direction of the galactic center should observe diffuse emission at 1.275 MeV. For a ^{22}Na yield per nova of 10^{48} nuclei (Truran, Starrfield and Sparks 1978) and the above nova rate, the intensity of the 1.275 MeV line should be comparable to the intensities of the ^{26}Al and ^{60}Fe lines given below.

The decays of ^{26}Al and ^{22}Na are accompanied by positron emission with 0.85 and 0.9 positrons per 1.809 and 1.275 MeV photons, respectively. Taking, as above, 0.6 photons per positron in the 0.511 MeV gamma ray line (because of positronium formation), we find that these decays should produce a 0.511 MeV line with intensity of about 7×10^{-5} photons/cm^{2}sec rad. This is comparable to the 0.511 MeV line intensity resulting from low energy cosmic rays for cases (2) and (3), and is about half the value produced by cosmic

rays in case (4) (see Table 5). Positrons in interstellar space could also originate from pulsars (Sturrock 1971), and from shorter lived radioisotopes such as ^{44}Ti (Clayton 1973).

We now compare these calculations with the available observations. Haymes et al. (1975) have observed gamma ray lines from the galactic center at 0.53 $\pm$0.01 MeV and 4.6 $\pm$0.1 MeV with fluxes (8.0 $\pm$2.3)x10^{-4} and (9.5 $\pm$2.7)x10^{-4} photons/cm^{2}sec, respectively, and a feature between 1.2 to 2 MeV with flux (2.6 $\pm$0.6)x10^{-3} photons/cm^{2}sec. The detector had an opening angle of 13° and was centered on the galactic center. The measured width of the $\sim$4.6 MeV line was about 0.7 MeV, larger than the detector resolution.

Line emission above about 4 MeV should be due to energetic particle reactions; other mechanisms, such as decays of long lived radioactive nuclei from processes of nucleosynthesis are not expected to produce lines at these high energies . For low energy cosmic ray interactions in the interstellar medium, the calculated diffuse fluxes (Figure 29) in a 0.7 MeV energy bin around 4.44 MeV and in a longitude interval of 13° are 2.6x10^{-5} and 5.8x10^{-5} photons/cm^{2}sec, for cases (3) and (4), respectively. This assumes that the gamma ray intensity is essentially independent of longitude within 1 radian of the galactic center, based on the rough constancy of the high energy gamma ray intensity in this longitude interval.

These calculated fluxes are smaller than the observed flux at 4.6 $\pm$0.1 MeV by more than an order of magnitude. Similarly, the calculated fluxes in the broad feature between 1.2 to 2 MeV and in the 0.51 MeV line are also much lower than those observed. But the line ratios, nonetheless, are consistent, within errors, with the ratios expected from energetic particle reactions.

To increase the fluxes calculated for low energy cosmic ray interactions to values that would match the observations would violate the constraints discussed earlier. Thus, it is unlikely that the lines observed by Haymes

et al. (1975) are produced by such cosmic rays in the interstellar medium.

Additional information on the nature of the source of the lines observed by Haymes et al. (1975) can be obtained by comparing these observations with the data of Gilman et al. (1978) shown in Figure 29. From measurements on board Apollo 16, they have set an upper limit of 1.2×10^{-2} photons/cm^{2}sec on the gamma ray emission from the galactic disk in the longitude interval -50° to 22°. This upper limit can be compared with the data of Haymes et al. (1975) as follows.

The measured flux of 9.5×10^{-4} photons/cm^{2}sec at ~4.6 MeV in the energy interval ~0.7 MeV and longitude interval of 13° (Haymes et al. 1975) implies a total nuclear gamma ray flux from 0.6 to 5.2 MeV of 4.0×10^{-3} and 9.0×10^{-3} photons/cm^{2}sec in the same longitude interval, for cases (3) and (4) respectively. These values are lower than the upper limit of Gilman et al. (1978) and hence consistent with it as long as the longitude distribution of the nuclear gamma rays is sufficiently strongly peaked toward the galactic center. However, if the nuclear gamma rays have the same longitude distribution as the high energy gamma rays (Fichtel et al. 1975), the fluxes of nuclear radiation from 0.6 to 5.2 MeV in the longitude interval -50° to 22° should be about 2×10^{-2} and 4.5×10^{-2} photons/cm^{2}sec for cases (3) and (4), and these are larger than the upper limit of 1.2×10^{-2} photons/cm^{2}sec (Gilman et al. 1978). We conclude that the nuclear radiation reported by Haymes et al. (1975) is mostly confined to longitudes not exceeding the interval of about 13° around the galactic center. The possibility of producing nuclear gamma rays by a massive black hole at the galactic nucleus was suggested by Lingenfelter, Higdon and Ramaty (1978).

Leventhal et al. (1978a,b) have recently made high resolution spectral measurements of positron annihilation radiation from the galactic center. The observed line at 0.511 MeV line has an intensity of $(1.21 \pm 0.22) \times 10^{-3}$

photons/cm^{2}sec), and a FWHM of less than 3.2 keV. There is also evidence for the 3-photon continuum from triplet positronium annihilation. The detector used had an opening angle of 15° centered on the galactic center. The observed line intensity is consistent with the lower resolution measurements of Haymes et al. (1978) of the line at ~0.53 MeV.

By the same argument as presented above for the 4.4 MeV line, the 0.511 MeV line intensity measured by Leventhal et al. (1978a, b) is also much greater than that expected for diffuse emission from the interstellar medium. The intensity of the 0.511 MeV line from low energy cosmic ray interactions is, from Table 5, 6×10^{-5} and 1.7×10^{-4} photons/cm^{2}sec rad, for cases (3) and (4), respectively. Since the intensity of this line from ^{26}Al and ^{22}Na decays is $\sim7\times10^{-5}$ photons/cm^{2}sec rad, as discussed above, the total 0.511 MeV line intensity from diffuse emission is about 1.3×10^{-4} and 2.4×10^{-4} photons/cm^{2}sec rad for these two cases. If we assume that the longitude dependence of this emission is the same as that of the high energy gamma rays, as we did for the 4.4 MeV line, then we obtain 0.511 MeV line fluxes of 3.4×10^{-5} and 6.3×10^{-5} photons/cm^{2}sec in the longitude interval of 15° around the galactic center, for the above two cases, respectively; these values are much smaller than the observed flux.

The origin of the positrons responsible for the observed 0.511 MeV line is not known, and all the mechanisms discussed above (see also discussion by Ramaty 1978) could be possible candidates.
If, however, the positrons are produced predominantly in energetic particle reactions, then the 0.511 MeV line should be accompanied by strong nuclear lines such as the 4.44 MeV line from ^{12}C deexcitation. The observations of Haymes et al. (1975), discussed above, would support this possibility as we shall show, but these measurements need to be confirmed by independent observations.

The relative intensities of the measured positron annihilation and ^{12}C deexcitation lines are consistent with energetic particle reactions. For s=4 and E_c = 20 MeV/nucleon, the ratio of positron production to gamma ray production in the 0.7 MeV interval around 4.4 MeV is 0.82 and 1.1, for cases (3) and (4), respectively; for 0.6 gamma rays in the 0.511 MeV line per positron, the ratio of the 0.511 MeV line to these gamma rays is 0.5 and 0.65 for these two cases. The observed ratio is 1.27 $\pm$0.42, if we use the Leventhal et al. (1978a,b) flux for the 0.511 MeV line, and 0.84 $\pm$0.34, if we use the flux given by Haymes et al. (1975) for the line at $\sim$0.53 MeV. (The line at $\sim$4.6 MeV was measured only by Haymes et al. 1975). The latter ratio is consistent, within errors, with the calculations, while the former would allow some additional positrons from sources other than energetic particle reactions. But in any event, the positive detection of a 4.4 MeV line with intensity comparable to that observed by Haymes et al. (1975) would imply that a major fraction of the positrons are produced in energetic particle reactions.

As discussed above, the source of the nuclear radiation responsible for the lines observed by Haymes et al. (1975) should have a small angular size ($\leq$13°) since otherwise there is a conflict between the observed line intensities and the upper limits of Gilman et al. (1978). A similar argument can be made for the source of the 0.511 MeV line if the positrons are produced by energetic particle reactions. Moreover on the basis of the very narrow observed width of the 0.511 MeV line, Bussard et al. (1979) find that a large fraction of the positrons should annihilate in an ionized medium, and a possible implication of this result is that the positrons originate in a point-like source at the galactic center and annihilate in the HII regions close to the galactic nucleus. The size of the 0.511 MeV line source would in this case be less than about 2°. Johnson and Haymes (1973)

have observed the galactic center during a lunar occultation and found a 2.3 standard deviation decrease of the 0.44 to 0.54 MeV flux during the occultation. This result also suggests a small ($\leq 0.5°$) angular size for the source of the 0.511 MeV line.

If the bulk of 0.511 MeV line is from nuclear reactions of energetic particles, we can calculate from Table 4 the rate of energy depositions associated with the production of the positrons. This amounts to approximately 1 erg per 0.511 MeV photon for cases (3) and (4), so that the observed flux requires the deposition of $\sim 10^{43}$ erg/sec. For a source size less than about 2° this energy deposition rate is larger than the infrared luminosity of the galactic center (Hofmann, Frederick, and Emery 1971) by about an order of magnitude. Some of the excess energy could be in the form of mass motions (Oort 1977) or lost beyond the event horizon of a massive black hole (Lingenfelter et al. 1978). Less energy deposition, however, is required if the positrons are produced from radioisotopes synthesized in supernovae (e.g. ^{44}Ti) or by pulsars. The key to the question of the origin of the positrons is the detection of other gamma ray lines that are characteristic of the prevailing positron production mechanism.

V. SUMMARY.

We have studied the production of gamma ray lines from the interaction of energetic particles with the abundant constituents of cosmic matter. We consider the reactions induced by energetic protons and alpha particles in ambient nuclei (He, C, N, O, Ne, Mg, Al, Si, S, Ca and Fe), and the inverse reactions in which energetic nuclei interact with ambient H and He. We have evaluated the line production cross sections by analyzing a large body of laboratory nuclear data which we discuss in detail. We consider prompt gamma rays produced by direct excitation of nuclear levels and by spallation reactions which leave the secondary nucleus in an excited state, as well as delayed emission resulting from long-lived radioactive nuclei that are also produced in the energetic particle reactions. A list of all the lines that we consider is given in Table 1; in addition, our calculations also take into account unresolved nuclear radiation from targets heavier than O. The nuclear data is discussed systematically in Section III. The lines of He are treated in IIIa, those of C, N and O in IIIb, while those of Ne, Mg, Al, Si, S, Ca and Fe are presented in IIIc.

We determine the shapes of the gamma ray lines by taking into account the kinematics of the reactions, data on the angular distribution of both the secondary particles and the gamma rays, and the lifetimes of the excited levels or their radioactive progenitors. If these lifetimes are sufficiently long, very narrow lines can be produced in solid targets such as interstellar grains. The evaluation of line shapes is treated in IIIa, IIIb and IIIc.

We have constructed a computer program that evaluates, both digitally and graphically, nuclear gamma ray spectra from about 0.1 to 8 MeV. The bulk of the nuclear radiation from energetic particle reactions is in this energy range, although some nuclear lines of astrophysical interest can also be found at higher energies (Crannell, Crannell and Ramaty 1979).

In this computer program it is possible to vary the abundances of both the ambient medium and the energetic particles, the energy spectrum and angular distribution of these particles, and the amount of matter in grains, as well as the characteristic grain radii. Various numerical results based on this program are presented in IIId. For comparison purposes, in this subsection we also present results on positron production in energetic particle reactions based on updated values of our earlier cross section compilations (Ramaty et al., 1975).

As an application of the theory developed in this paper, we have considered gamma ray line production in the interstellar medium. The theory, however, can also be applied to other astrophysical sites such as solar flares, compact objects and nuclei of galaxies. We have evaluated the nuclear gamma ray emission from the galactic disk by normalizing the emissivity of the nuclear lines to that of high energy gamma rays, by using the observed intensities of these gamma rays from the galaxy, by assuming that the high and low energy cosmic rays have the same galactic distribution, and by taking into account the possible enhancement of heavy elements toward the galactic center. For a local low energy cosmic ray density of 1 eV/cm^3 and heavy element abundance gradients consistent with x-ray absorption observations, we find intensities of about 7×10^{-5}, 3×10^{-5} and 10^{-5} photons/cm^2 sec rad for the strongest nuclear lines at 4.44, 6.129 and 0.847 MeV. The intensity of the 0.511 MeV line from positron annihilation for the same assumptions is $\sim 10^{-4}$ photons/cm^2 sec rad. These lines should be detectable by planned high sensitivity observations. Such detection could give a wealth of information on the properties of the low energy cosmic rays and the composition and spatial distribution of interstellar gas and dust.

We have compared the results of our calculations with line observations from the direction of the galactic center. The reported fluxes at 0.511 MeV (Leventhal, MacCallum and Stang 1978 a,b) and at $\sim$ 4.4 MeV (Haymes et al. 1975) from a region of angular size $\lesssim 15^{\circ}$ around the galactic center are larger by more than an order of magnitude than those expected from diffuse low energy cosmic ray interactions. By using the theory developed in this paper, we find that the sources of these lines should be much more sharply peaked around galactic longitude $\ell \simeq 0^{\circ}$ than those of the high energy gamma rays; otherwise, the broad band nuclear radiation that accompanies the spectral lines would exceed the upper limits (Gilman et al. 1978) on the total 0.6 to 5.2 MeV radiation from the galactic disk in the longitude interval -50° to 22°. It is conceivable that the positrons and nuclear lines could be produced by one or more point sources close to the galactic center.

Note added in proof: After the completion of this manuscript, preliminary results from the A-4 experiment on HEAO-1 became available (J. L. Matteson, private communication 1978). These results do not confirm the Haymes et al. (1975) observations of the 4.44 MeV line from the galactic center. The upper limit set by the HEAO observations on the total 4 to 7 MeV radiation implies that not more than about 30% of the positrons required to account for the observed 0.511 MeV line (Leventhal et al. 1978a, b) could result from energetic particle reactions if the nuclear reaction rate does not vary on a time scale shorter than the positron annihilation time.

Figure Captions

1. Cross sections for alpha particle reactions with He. Solid curve - ^{7}Be production in its ground state plus excited state. Dashed curve - ^{7}Li production in its excited state.
2. Cross sections for 4.44 MeV photon production from ^{12}C. Solid and dashed-dotted curves - direct excitation of the 4.439 MeV level in (p,p′) and (α,α′) reactions. Dashed and dashed-crossed curves - total production of 4.44 MeV photons by protons and alpha particles, respectively.
3. Gamma ray production cross sections in spallation reactions of protons and alpha particles on ^{12}C and ^{16}O.
4. Cross sections for 2.313 MeV photon production from ^{14}N and ^{16}O. Solid curve - 2.313 MeV photon production cross sections by direct proton excitation of levels in ^{14}N; dashed curve total 2.313 MeV photon production by protons on ^{14}N including ^{14}O decay; dashed-crossed curve - 2.313 MeV photon production by direct alpha particle excitation of levels in ^{14}N; dashed-dotted curve - total 2.313 MeV production from proton bombardment of ^{16}O.
5. Cross sections of $\sim$ 6.2 MeV photon production from ^{16}O. Solid and dashed-dotted curves - 6.129 MeV photon production by direct proton and alpha particle excitation of levels in ^{16}O. Dashed and dashed crossed curves - 6.1 to 6.3 MeV photon production from proton and alpha particle bombardment of ^{16}O.

6. Cross sections for 6.917, 7.117, 7.299 and 2.741 MeV photon production by protons and alpha particles on ^{16}O. The 6.917, 7.117 and 2.741 MeV lines are from deexcitation of levels in ^{16}O, and the 7.299 MeV line is from a level in the spallation product ^{15}N.
7. Gamma ray production from ^{20}Ne. Solid and dashed-dotted curves - cross section for the direct excitation of the 1.634 MeV level in ^{20}Ne by (p,p') and (α,α') reactions. Dashed and dashed-crossed curves - total 1.634 MeV photon production from proton and alpha particles on ^{20}Ne; these cross sections include the contributions of cascades from higher lying levels in ^{20}Ne. Crossed and crossed-dotted curves - total photon production from proton and alpha particle bombardment of ^{20}Ne ($E_\gamma > 0.7$ MeV).
8. Gamma ray production from ^{24}Mg. The various curves represent quantities similar to those given by the cruves of Figure 7.
9. Cross sections for the production of ^{26}Al and ^{22}Na by protons on isotopes of Mg and Si. The dashed curve for proton bombardment of Mg includes the contributions of ^{24}Mg, ^{25}Mg and ^{26}Mg, using the isotopic ratios of Cameron (1973).
10. Gamma ray production from ^{28}Si. The various curves represent quantities similar to those given by the curves of Figure 7.
11. Gamma ray production from ^{56}Fe. The three curves represent quantities similar to those given by the curves of Figure 7. Gamma ray production by alpha particle bombardment of Fe appears to be small at low energies because of the high Coulomb threshold.

12. Cross sections for ^{56}Co, ^{55}Co, ^{54}Mn and ^{52}Mn production by protons on ^{56}Fe.

13. The angular distribution of recoil ^{12}C and ^{16}O in the center of mass frame for the reactions $^{12}C(p,p')^{12}C^*$ and $^{16}O(p,p')^{16}O^*$.

14. The profile of the 4.44 MeV gamma ray line from the reaction $^{12}C(p,p')^{12}C^*$. The bombarding protons are monoenergetic and confined to a beam, and the gamma rays are observed at 90° to the beam. The top curves are calculated for an uneven population of the spin states of the $^{12}C^*4.439$ MeV level. The lower curve is calculated for isotropic gamma ray emission.

15. The profile of the 4.44 MeV line gamma ray line from the reaction $^{12}C(p,p')^{12}C^*$ for an isotropic distribution of bombarding protons with an energy spectrum proportional to E^{-2}. The top curve is for the case of uneven spin state populations, and the lower curve is for isotropic gamma ray emission.

16. The mean stopping ranges, $\langle x \rangle$, the energy loss rates, dE_r/dx, and the range fluctuations, $\Delta x/x$, for low energy ^{16}O, ^{24}Mg and ^{56}Fe stopping in water.

17. The energy distribution in the laboratory frame of unresolved gamma rays from proton bombardment of heavy nuclei.

18. Monte Carlo simulated gamma ray spectrum for energetic particles and ambient medium having solar compositions; s and E_c are the spectral parameters of the energetic particles, and a_o is the characteristic radius of the interstellar grain distribution.

19. Monte Carlo simulated gamma ray spectrum for energetic particles and ambient medium having solar compositions.

20. Monte Carlo simulated gamma ray spectrum for energetic particles and ambient medium having solar compositions.

21. Monte Carlo simulated gamma ray spectrum for energetic particles having cosmic ray source composition and ambient medium with solar composition.

22. Monte Carlo simulated gamma ray spectrum for energetic particles having cosmic ray source composition and ambient medium with solar composition.

23. The gamma ray spectrum of Figure 21 averaged over energy intervals of 100 keV. Dashed curve - photons produced by only nuclei heavier than He; solid curve - photons produced by all the cosmic rays.

24. The gamma ray spectrum of Figure 22 averaged over energy intervals of 100 keV. Dashed curve - photons produced by only nuclei heavier

than He; solid curve - photons produced by all the cosmic rays.

25. Gamma ray emissivity per unit energy density in the energetic particles. The emissivities are for the narrow 4.44 MeV line, the narrow plus very narrow 6.129 and 0.847 MeV lines, and the total broad, narrow and very narrow emissions. Both the energetic particles and ambient medium have solar compositions. The parameters s and E_c are defined in equation (22).

26. Emissivities of the narrow 4.44 MeV and narrow plus very narrow 6.129 MeV lines per unit energy deposition rate of the energetic particles in a neutral medium. Both the energetic particles and ambient medium have solar compositions.

27. Emissivities of the narrow 4.44 MeV and narrow plus very narrow 6.129 MeV lines per unit energy deposition rate of the energetic particles in a ionized medium. Both the energetic particles and ambient medium have solar compositions.

28. Ratios of narrow plus very narrow 6.129 MeV photon production, and positron production, to the narrow 4.44 MeV production. The ambient medium has solar abundance, and $\alpha/p = 0.1$ in the energetic particles.

29. Gamma ray emission from the interstellar medium from the direction of the galactic center. The π° decay spectrum has been calculated by Stecker (1976) and is normalized here to the data of Paul et al. (1978). The nuclear gamma ray spectra are calculated for a low energy cosmic ray component with $s = 4$, $E_c = 20$ MeV/nucleon, local energy density 1 eV/cm^3, and the same spatial gradient as that implied for the high energy cosmic rays from the high energy gamma

ray data. The compositions of the ambient medium and low energy cosmic rays are for cases (3) and (4) (See text). The dashed line is a simple power law that could arise from electron bremsstrahlung.

30. High resolution plot of the sum of the nuclear gamma ray and bremsstrahlung fluxes from the direction of the galactic center. The parameters are the same as for Figure 29 case (3).

31. High resolution plot of the sum of the nuclear gamma ray and bremsstrahlung fluxes from the direction of the galactic center. The parameters are the same as for Figure 29 case (4).

Acknowledgements

We wish to acknowledge S. Austin, D. Bodansky, P. Dyer and N. S. Wall for providing nuclear data prior their publication, and R. Bussard, R. King and A. N. Suri for assisting with the numerical calculations. The research for R. E. Lingenfelter is supported by the NSF under Grant AST-76-98178 and AST-78-10289. Part of the research of Benzion Kozlovsky was done while holding a NAS/NRC Senior Resident Research Associateship at the Goddard Space Flight Center; he was also supported by NASA under Grant NGR 21-002-316 and NSG 5298 at the University of Maryland. Reuven Ramaty wishes to acknolwedge the Alexander von Humboldt Foundation of the Federal Republic of Germany for a Senior U. S. Scientist Award under which the initial phases of this research were carried out. Part of this research was also supported by the U.S.-Israel Binational Science Foundation.

Ajzenberg-Selove, F., Lauritsen, T., 1968, Nucl. Phys. A114, 1.

Alard, J. P., Baldit, A., Costilhes, J. P., Fargeix, J., Roche, R., and Tamain, J. C. , 1975, Nuovo Cimento (Letters) 10, 841.

Andronov, Y. F., Antropov, A. E., Zarubin, P. P., Ioannu, P. D., Nikitaeva, V. I., Orlov, B. N., and Romanov, V. S., 1970, Bull. Acad. Sciences USSR Phys. Ser., 34, 1934.

Arnett, W. D. 1977, Ann. N.Y. Acad. Sci. 302, 90.

Austin, S. M., Locard, P. J., Bunder, S. N., Cameron, J. M., Richardson, J. R., Verbal, J. W., Van Oers, W. T. H., 1971, Phys. Rev. C3, 1514.

Barkas, W. H. and Berger, M. J., 1964, Tables of Energy Losses and Ranges of Heavy Charged Particles, NASA SP-3013 (Washington, D. C.).

Barnard, A. C. L., Swint, J. B. and Clegg, T. B., 1966, Nucl. Phys. 86, 130.

Berinde, A., Neamu, I., and Vladuca, G., 1971, Rev. Roum. Phys. 16, 341.

Bignami, G.F., Caraveo, P. and Maraschi, L. 1978, Astron. and Astrophys. 67, 149.

Bimbot, R. and Gauvin, H., 1971, Comp. Rend. ser B, 273, 1054.

Blatchley, D. E. and Bent, R. D., 1965, Nucl. Phys. 61, 641.

Boreli, F., Shrivastava, P. J., Kinsey, B. B. and Mistry, V. D., 1968, Phys. Rev. 174, 1221.

Bowman, W. W. and Macmurdo, K. W. 1974, Atomic Data and Nucl. Data Tables, 13, 90.

Brodzinski, R. L., Rancitelli, L. A., Cooper, J. A., Wogman, N. A. 1971, Phys. Rev. C4, 1257.

Burcham, W.E., McCauley, G.P., Bredin, D., Gibson, W.M., Prowse, D.J. 1958, Nucl. Phys. 5, 141.

Burger, J.J. 1971, Ap. J. 166, 651.

Burton, W.B. 1976, The Structure and Content of the Galaxy and Galactic Gamma Rays (NASA-CP-002), 163.

Bussard, R.W. 1978, Doctoral Dissertation, University of Maryland.

Bussard, R.W., Ramaty, R., and Drachman, R.D. 1979, Ap. J. (in press).

Bussard, R.W., Ramaty, R., Omidvar, K. 1978, Ap. J. 220, 383.

Cameron, A.G.W. 1973, Space Science Rev. 15, 121.

Cavallo, G. and Gould, R.J., 1971, Nuovo Cimento 2B, 77.

Chambon, G., Hurley, K., Niel, M., Talon, R., Vedrenne, G., Likine, O.B., Kouznetsov, A.V., and Estouline, J.V. 1978, Gamma Ray Spectroscopy in Astrophysics, ed. T.L. Cline and R. Ramaty, NASA TM79619, p. 70.

Chang, C.C., Wall, N.S. and Fraenkel, Z. 1974, Phys. Rev. Letters 33, 1493.

Chupp, E.L., Forrest, D.J., Higbie, P.R., Suri, A.N., Tsai, C., Dunphy, P.P. 1973, Nature 241, 333.

Chupp, E.L., Forrest, D.J. and Suri, A.N. 1968, in Solar Gamma, X and EUV Radiations, ed. S. Kane, IAU Symp. 1968, p. 341.

Clayton, D.D., Colgate, S.A. and Fishman, D.J. 1969, Ap. J. 155, 75.

Clayton, D.D. and Hoyle, F. 1974, Ap. J. (Letters) 187, L101.

Clayton, D.D. 1973, Gamma Ray Astrophysics (NASA SP 339), p. 263.

Clegg, A.B., Foley, K.J., Salmon, G.L. and Segal, R.E. 1961, Proc. Phys. Soc. 78, 681.

Cline, T.L. and Ramaty, R. 1978, Gamma Ray Spectroscopy in Astrophysics, NASA TM79619.

Conzett, H.E. 1957, Phys. Rev. 105, 1324.

Corelli, J.C., Bleuler, E. and Tendam, D.J. 1959, Phys. Rev. 116, 1184.

Crannell, C.J., Crannell, H. and Ramaty, R. 1979, Ap. J. (to be published).

Crannell, C.J., Ramaty, R. and Crannell, H. 1977, Recent Advances in Gamma-ray Astronomy, Proceedings of the 12th ESLAB Symposium, Frascati, Italy, ESA SP 124, ed. R.D. Wills and B. Battrick, p. 213.

Crawley, G. M. and Garvey, G. T., 1967, Phys. Rev., 160, 981.

Daehnick, W. W. and Sherr, R., 1964, Phys. Rev., 133, B934.

Daehnick, W. W., 1964, Phys. Rev., 135, B1168.

Dangle, R. L., Oppliger, L. D. and Hardie, G., 1964, Phys. Rev., 133, B647.

Degnan, J. H., Cohen, B. L., Rao, G. R., Chan, K. C., and Shabason, L., 1973, Phys. Rev., C8, 2255.

de Meijer, R. S., Plendl, H. S., and Holub, R., 1974, Atomic Data and Nucl. Data Tables, 13, 7.

de Meijer, R. J., Drentje, A. G. and Plendl, H. S., 1975, Atomic Data and Nuclear Data Tables, 15, 391.

Duray, J. R., Hausman, H. J., Gearhart, N. L., Sinclair, J. W. D. and Steiner, W. S., 1972, Phys. Rev. C6, 792.

de Swiniarski, R., Bacher, A. D., Resmini, F. G., Plattner, G. R. and Hendrie, D. L., 1972, Phys. Rev. Letters, 28, 1139.

de Swiniarski, R., Glashausser, C., Hendrie, D. L., Sherman, J., Bacher, A. D. and McClatchie, E. A., 1969, Phys. Rev. Letters, 23, 317.

de Swiniarski, R., Conzett, H. E., Lamontagne, C. R., Frois, B., and Slobodrian, R. J., 1973, Can J. Phys., 51, 1293.

Dickens, J. K., Haner, D. A., Waddell, C. J., 1963, Phys. Rev., 132, 2159.

Donovan, P. F., Mollenauer, J. F., and Warburton, E. K., 1964, Phy. Rev., 133, B113.

Eberhard, K. A. and Trombik, W., 1972, Nucl. Phys., A193, 489.

Elliott, R. V. and Spear, R. H., 1966, Nuclear Physics, 84, 209.

Emmerson, J. M., Madden, J. C. W., Johnson, C. M. P., Middlemus, N., Clegg, A. B. and Williams, W. S. C., 1966, Nucl. Phys., 77, 305.

Endt, P. M., and Van der Leun, C., 1973, Nucl. Phys., A214, 1.

Fannon, J. H., Burge, E. J., Smith, D. H. and Ganguly, N. K., 1967, Nucl. Phys., A97, 263.

Fiarman, S., and Meyerhof, W.E. 1973, Nucl. Phys. A206, 1.

Fichtel, C. E., Hartman, R. C., Kniffen, D. A., Thompson, D. J., Bignami, G. F., Ogelman, H., Ozel, M. E., and Tumer, T., 1975, Ap. J. 198, 163.

Foley, K. J., Salmon, G. L. and Clegg, A. G., 1962a, Nucl. Phys. 31, 43.

Foley, K. J., Clegg, A. B., and Salmon, G. L., 1962b, Nucl. Phys. 37, 23.

Friedes, J. L., Palevsky, H., Sutter, R. J., Bennett, G. W., Igo, G. J., Simpson, W. D., and Corley, D. M. 1967, Nucl. Phys. A104, 294.

Furukawa, M., Shizuri, K., Komura, K., Sakamoto, K., and Tanaka, S., 1971, Nucl. Phys. A174, 539.

Garcia, A., Milio, J., and Senent, F. 1970, An. Real Soc. Espan. Fis. Quim., 66, 69.

Garrard, T. L., Stone, E. C. and Vogt, R. E. 1973, High Energy Phenomena On the Sun, p.341, Ed. R. Ramaty and R. G. Stone.

Gibson, B. F. 1972, Nucl. Phys. A195, 449.

Gilman, D., Metzger, A. E., Parker, R. H. and Trombka, J. I. 1978, Gamma Ray Spectroscopy in Astrophysics, ed. T. L. Cline and R. Ramaty, NASA TM 79619, p. 190.

Goldstein, M. L., Fisk, L. A., and Ramaty, R. 1970, Phys. Rev. Letters, 25, 832.

Goldstein, M. L., Ramaty, R. and Fisk, L. A. 1970, Phys. Rev. Letters, 24, 1193.

Goryachev, Yu. M., Kanarets, V. P., Kirpichnikov, I. V., Levintov, I. I., Morozov, B. V., Nikiforov, N. A., and Starostin, A. S. 1973, Sov. J. Nucl. Phys. 17, 476.

Gray, W. S., Kenefick, R. A. and Kraushaar, W. 1965, Nuclear Physics 67, 542.

Guratzsch, H., Hofman, G., Muller, H. and Stiller, G., 1969, Nucl. Phys. A129, 405.

Hall, R. G., Meegan, C. A., Walraven, G. D., Djuth, F. T., Shelton, D. H., and Haymes, R. C. 1976, Ap. J. 210, 593.

Hansen, L. F., Grimes, S. M., Kammerdiener, J. L. and Madsen, V. A. 1973, Phys. Rev. C8, 2072.

Harvey, B. G., Meriwether, J. R., Mahoney, J., Bussier, De Nercy, A., Horen, D. J., 1966, Phys. Rev., 146, 712.

Harvey, B. G., Rivet, E. J-M., Springer, A., Meriwether, J. R., Jones, W. B., Elliott, J. H., and Darriulat, D., 1964, Nucl. Phys. 52, 465.

Harrison, W. D., 1967, Núc. Phys. A92, 260.

Haymes, R. C., Walraven, G. D., Meegan, C. A., Hall, R. D., Djuth, F. T., and Shelton, D. H., 1975, Ap. J. 201, 593.

Higdon, J. C. and Lingenfelter, R. E., 1976, Ap. J. (Letters) 208, L107.

Hoffmann, W.F., Frederick, C.L., and Emery, R.J. 1971, Ap. J. (Letters) 164, L23.

Horowitz, Y.S., Sherman, N.K., and Bell, R.E. 1969, Nucl. Phys. A134, 577.

Horowitz, Y. S. and Bell, R. E., 1970, Cand. J. Phys. 48, 204.

Hendrie, D. L., Glashausser, C., Moss, J. M. and Thirion, J., 1969, Phys. Rev., 189, 1188.

Hornyak, W. F. and Sherr, R., 1955, Phys. Rev. 100, 1409.

Hulubei, H., Neamu, I., Vladuca, G., Scintei, N., Martalogu, N., Teodanescu, C. M., Ivascu, M., and Berinde, A., 1969, Nucl. Phys. A123, 531.

Jackson, J.D. 1962, Classical Electrodynamics (John Wiley & Sons, Inc., New York).

Jacobson, A.S., Ling, J.C., Mahoney, W.A. and Willett, J.B. 1978, Gamma Ray Spectroscopy in Astrophysics, ed. T.L. Cline and R. Ramaty, NASA TM 79619, p. 228.

Janus, R. T., and McCarthy, I. E., 1974, Phys. Rev., C10, 1041.

Jastrzebski, J., Nadasen, A., Rutledge, L., Sadler, M., Segel, R. E., and Singh, P. P., 1976, Bull. Am. Phys. Soc., 21, 979.

Jenkins, I. L. and Wain, A. G., 1970, J. Inorg. Nucl. Chem., 32, 1419.

Johnson, W.N., III, and Haymes, R.C. 1973, Ap. J. 184, 103.

Karban, O., Greaves, P. D., Hnizdo, V., Lowe, J., 1970, Nucl. Phys. A147, 461.

King, C. H., Rossner, H. H., Austin, S. M., Chien, W. S., Mathews, G. J., Viola, V. E. and Clark, R. G., 1975, Phys. Rev. Letters, 35, 988.

Kobayashi, S. 1960, J. Phys. Soc. Japan, 15, 1164.

Kokame, J., Fukunaga, K., Nakamura, H., and Inoue, N. 1965, J. of Phys. Soc. of Japan, 20, 475.

Kolata, J. J., Auble, R., and Galonsky, A. 1967, Phys. Rev. 162, 957.

Korteling, R. G. and Caretto, A. A. 1970a, Phys. Rev. C1, 193.

Korteling, R. G. and Caretto, A. A. 1970b, Phys. Rev. C1, 1960.

Kozlovsky, B. and Ramaty, R. 1974a, Ap. J. (Letters), 191, L43.

Kozlovsky, B and Ramaty, R. 1974b, Astron. Astrophys. 34, 477.

Kozlovsky, B. and Ramaty, R. 1974c, Astron. Astrophys. 36, 307.

Kozlovsky, B. and Ramaty, R. 1977, Astrophysical Letters, 19, 19.

Kuan, H. M. and Risser, J. R. 1964, Nuclear Physics 51, 518.

Leventhal, M., MacCallum, C.J. and Stang, P.D. 1978a, Ap. J. (Letters) 225, L11.

Leventhal, M., MacCallum, C.J. and Stang, P.D. 1978b, Gamma Ray Spectroscopy in Astrophysics, ed. T.L. Cline and R. Ramaty, NASA TM 79619, p. 169.

Lingenfelter, R.E., Higdon, J. and Ramaty, R. 1978, Gamma Ray Spectroscopy in Astrophysics, ed. T.L. Cline and R. Ramaty, NASA TM 79619, p. 252.

Lingenfelter, R. and Ramaty, R.E. 1976, The Structure and Content of the Galaxy and Galactic Gamma Rays, NASA CP002, p. 237.

Lingenfelter, R.E. and Ramaty, R. 1977, Ap. J. (Letters) 211, L19.

Lingenfelter, R.E. and Ramaty, R. 1978 ,Physics Today 31, 40.

Mani, G.S., Freeman, R., Picard, F., Sadeghi, A., and Redon, D. 1964, Nucl. Phys. 60, 588.

Mani, G.S. 1971, Nucl. Phys. A169, 225.

McNeilly, G.S., Thompson, W.J., Van Rij, W.E. and Heydenburg, N.P. 1973, Nucl. Phys. A204, 321.

Mehta, M. K., Hunt, W. E. and Davis, R. H. 1967, Phys. Rev. 160, 791.

Meneguzzi, M. and Reeves, H. 1975, Astron. and Astrophys. 40, 91.

Mitchell, G. E., Carter, E. B. and Davis, R. H. 1964, Phys. Rev. 133, B1434.

Mitler, H. E. 1972, Astrophys. Space Sci. 17, 186.

Morgan, J. F. and Hobbie, R. K. 1970, Phys. Rev. C1, 155.

Nichols, D. B., Arms, R. G., Hausman, H. J. and Seyler, R. G. 1969, Phys. Rev. 183, 945.

Northcliffe, L. C. and Schilling, R. F. 1970, Nuclear Data Tables, A7, 233.

Nuclear Data Group 1973, Nuclear Level Schemes, A = 95 through A = 257 from Nuclear Data Sheets, New York Academic Press, Inc.

Oda, Y., Takeda, M., Hu, C. and Kato, S. 1959, J. Phys. Soc. Japan, 14, 1255.

Oda, Y., Takeda, M., Takano, N., Yamazaki, T., Hu, C., Kikuchi, K., Kobayaski, S., Matsuda, K. and Nagahara, 1960, J. Phys. Soc. Japan, 15, 760.

Oort, J.H. 1977, Ann. Rev. Astron. Astrophys. 15, 295.

Paul, J. A., Bennett, K., Bignami, G. F., Bucheri, R., Caraveo, P., Hermsen, W., Kanbach, G., Mayer-Hasselwander, H. A., Scarsi, L., Seanenburg, B. N., and Wills, R. D., 1978, Astron-Astrophys. 63, L31.

Pelle, R. W. 1957, Phys. Rev. 105, 1311.

Peimbert, M., 1975, Ann. Rev. Astr. Ap., 13, 113.

Peimbert, M., Torres-Peimbert, S., and Rayo, J. F., 1978, Ap. J. 220, 516.

Perey, C. M., Silva, R. J., Dickens, J. K. and Perey, F. G. 1970, Phys. Rev. C2, 468.

Peterson, R. J. 1969, Annals of Phys. 53, 40.

Phillips, G. W., Richard, P., Elliott, D. O., Hopkins, F. F. and Porter, A. C. 1972, Phys. Rev. C5, 297.

Ploughe, W. D. 1961, Phys. Rev. 122, 1232.

Raisbeck, G. M., Yiou, F. 1975, Phys. Rev. C12, 915.

Ramaty, R. and Crannell, C. J. 1976, Ap. J. 203, 766.

Ramaty, R., Kozlovsky, B. and Lingenfelter, R. E. 1975, Space Science Reviews, 18, 341.

Ramaty, R., Kozlovsky, B. and Suri, A.N. 1977, Ap. J. 214, 617.

Ramaty, R. and Lingenfelter, R. E. 1977, Ap. J. (Letters)

Ramaty, R., Reames, D.V. and Lingenfelter, R.E. 1970, Phys. Rev. Letters 24, 913.

Ramaty, R. and Westergaard, N.J. 1976, Astrophys. and Space Sci. 95, 143.

Rao, M.N. 1970, Nuclear Data Sheets B3, No. 3,4, p. 43.

Rebel, H., Schweimer, G.W., Schatz, G., Specht, J., Lohken, R., Hauser, G., Habs, D., and Klewe-Nebenius, H. 1972, Nucl. Phys. A182, 145.

Reeves, H. 1978, Gamma Ray Spectroscopy in Astrophysics, ed. T.L. Cline and R. Ramaty, NASA TM 79619, p. 283.

Reich, C. W., Phillips, G. C. and Russell, J. L. 1956, Phys. Rev. 104, 150.

Roos, P. G., and Wall, N. S., 1965, Phys. Rev. B140, 1237.

Ross, J. E. and Aller, L. H. 1976, Science, 191, 1223.

Rygg, T. A. and Fishman, G. J. 1973, Proc. 13th Intl. Cosmic Ray Conf., Denver, 1, 472.

Ryter, C. E., Cesarsky, C. J., and Audouze, J., 1975, Ap. J. 198, 103.

Satchler, G. R. 1973, Z. Phys. 260, 209.

Sauter, A. H., and Singh, P. P. 1974, Nucl. Phys. A236, 379.

Scherrer, V. E., Theus, R. B. and Faust, W. R. 1953, Phys. Rev. 91, 1476.

Schmidt, F. H., Brown, R. E., Gerhart, J. B. and Kolasinski, W. A., 1964, Nucl. Phys. 52, 353.

Schrank, G., Warburton, E. K. and Daehnick, W. W., 1962, Phys. Rev. 127, 2159.

Searle, L. 1971, Ap. J. 168, 327.

Seidlitz, L., Bleuler, E., and Tendam, D. J. 1958, Phys. Rev. 110, 682.

Seward, F. D. 1959, Phys. Rev. 114, 514.

Shapiro, M. M., Silberberg, R. and Tsao, C. H. 1975, Conf. Papers, 14th Intl. Cosmic Ray Conf., Munich, Germany, 2, p532.

Shields, G. A., 1974, Ap. J., 193, 335.

Shima, Y., and Alsmiller, R. G. 1970, Nucl. Science and Eng. 41, 47.

Shotter, A. C., Fisher, P. S., and Scott, D. K. 1970, Nuclear Physics, A159, 577.

Smith, H. E., 1975, Ap. J., 199, 591.

Smith, S. M., Tibell, G., Cowley, A. A., Goldberg, D. A., Pugh, H. G., Reichart, W., and Wall, N. S. 1973, Nucl. Phys. A207, 273.

Sorokin, P. V., Popov, A. I., Storizhko, V. E., and Takanov, A. Ya., 1963, Sov. Phys. JETP, 16, 529.

Starrfield, S., Truran, J. W., Sparks, W. M. and Kutter, G. S. 1972, Ap. J. 176, 169.

Stecker, F. W. 1976, The Structure and Content of the Galaxy and Galactic Gamma Rays, NASA CP002, p.315.

Stecker, F. W., Solomon, P. M., Scoville, N. F. and Ryter, C. E. 1975, Ap. J. 201, 90.

Stoval, T., and Hintz, M. 1964, Phys. Rev. 135, B330.

Strauch, K. and Titus, F. 1956, Phys. Rev., 103, 200.

Sturrock, P. A. 1971, Ap. J. 164, 529.

Sundberg, O., and Tibell, G. 1969, Arkiv for Fysik, 39, 397.

Thompson, W.J., Crawford, G.E. and Davis, R.H. 1967, Nucl. Phys. A98, 228.

Tucker, W., Kellogg, E., Gurski, H., Giacconi, R. and Tananbaum, H. 1973, Ap. J. 180, 715.

Tinsley, B.M. and Larson, R.B. 1978, Ap. J. 221, 554.

Tyren, H. and Maris, T. A. J., 1957, Nucl. Phys. 4, 637.

Willis, A., Geoffrion, B., Marty, N., Morlet, M., Rolland, C. and Tatischeff, B. 1968, Nuclear Physics, A112, 417.

Winterbon, K. B. 1975, Ion Implantation Range and Energy Deposition Distributions (New York:IFI/Plenum), 341.

Wong, C., Anderson, J. D., McClure, J. W., and Pohl, B. 1967, Phys. Rev. 156, 1266.

Yagi, K., Ejiri, H., Furukawa, M., Ishizaki, Y., Koike, M., Matsudo, K., Nakajima, Y., Nonaka, I., Saji, Y., Tanaka, E., and Satchler, G., 1964, Phys. Lett. 10, 186.

Yavin, A. I., and Farwell, G. W. 1959, Nucl. Phys. 12, 1.

Zobel, W., Maienschein, F. C., Todd, J. H. and Chapman, G. T. 1968, Nucl. Sci and Eng. 32, 392.

TABLE 1

ORIGINAL PAGE IS
OF POOR QUALITY

Photon Energy (MeV)	Emission Mechanism	Production Processes	Mean Life (sec)
0.092	$^{55}Fe^{*}1.408\rightarrow^{55}Fe^{*}1.316$	$^{56}Fe(p,pn)^{55}Fe^{*}$	--
0.110	$^{19}F^{*}0.110\rightarrow g.s.$	$^{20}Ne(p,2p)^{19}F^{*}$	8.5×10^{-10}
0.158	$^{56}Co^{*}0.158\rightarrow g.s.$	$^{56}Fe(p,n)^{56}Co^{*}$	$<10^{-10}$
0.197	$^{19}F^{*}0.197\rightarrow g.s.$	$^{20}Ne(p,2p)^{19}F^{*}$	1.3×10^{-7}
0.238	$^{19}Ne^{*}0.238\rightarrow g.s.$	$^{20}Ne(p,pn)^{19}Ne^{*}$	2.6×10^{-8}
0.275	$^{19}Ne^{*}0\ 275\rightarrow g.s.$	$^{20}Ne(p,pn)^{19}Ne^{*}$	6.1×10^{-11}
0.412	$^{55}Fe^{*}0.412\rightarrow g.s.$	$^{56}Fe(p,pn)^{55}Fe^{*}$	--
0.431	$^{7}Be^{*}0.431\rightarrow g.s.$	$^{4}He(\alpha,n)^{7}Be^{*}$	$2\ 7\times10^{-13}$
0.440	$^{23}Na^{*}0.440\rightarrow g.s$	$^{24}Mg(p,2p)^{23}Na^{*}$	1.6×10^{-12}
0.451	$^{23}Mg^{*}0.451\rightarrow g.s.$	$^{24}Mg(p,pn)^{23}Mg^{*}$	1.8×10^{-12}
0.477	$^{55}Fe^{*}1.408\rightarrow^{55}Fe^{*}0.931$	$^{56}Fe(p,pn)^{55}Fe^{*}$	--
		$^{56}Fe(p,2n)^{55}Co(e^{+};\varepsilon)^{55}Fe^{*}$(16%)	9.5×10^{4}
0.478	$^{7}Li^{*}0.478\rightarrow g.s.$	$^{4}He(\alpha,p)^{7}Li^{*}$	10^{-16}
		$^{4}He(\alpha,n)^{7}Be(\varepsilon)^{7}Li^{*}$(10%)	6.6×10^{6}
0 717	$^{10}B^{*}0.717\rightarrow g.s.$	$^{12}C(p,x)^{10}B^{*}$	1.0×10^{-9}
		$^{16}O(p,x)^{10}B^{*}$	1.0×10^{-9}
		$^{12}C(p,x)^{10}C^{*}(e^{+})^{10}B^{*}$(100%)	28
		$^{16}O(p,x)^{10}C^{*}(e^{+})^{10}B^{*}$(100%)	28
0.744	$^{52}Cr^{*}3.114\rightarrow^{52}Cr^{*}2.370$	$^{56}Fe(p,x)^{52}Cr^{*}$	--
		$^{56}Fe(p,x)^{52}Mn(e^{+};\varepsilon)^{52}Cr^{*}$(88%)	7.1×10^{5}
0.780	$^{27}Si^{*}0.780\rightarrow g.s.$	$^{28}Si(p,pn)^{27}Si^{*}$	5×10^{-11}
0.812	$^{56}Co^{*}0.970\rightarrow^{56}Co^{*}0.158$	$^{56}Fe(p,n)^{56}Co^{*}$	$<10^{-10}$
0.835	$^{54}Cr^{*}0.835\rightarrow g.s.$	$^{56}Fe(p,x)^{54}Mn(\varepsilon)^{54}Cr^{*}$(100%)	3.9×10^{7}
0.844	$^{27}Al^{*}0.844\rightarrow g.s.$	$^{28}Si(p,2p)^{27}Al^{*}$	5.3×10^{-11}
0.847	$^{56}Fe^{*}0.847\rightarrow g.s.$	$^{56}Fe(p,p')^{56}Fe^{*}$	9.7×10^{-12}
		$^{56}Fe(p,n)^{56}Co(e^{+};\varepsilon)^{56}Fe^{*}$(100%)	9.6×10^{6}
0.891	$^{22}Na^{*}0.891\rightarrow g.s.$	$^{24}Mg(p,x)^{22}Na^{*}$	1.4×10^{-11}
0.931	$^{55}Fe^{*}0.931\rightarrow g.s.$	$^{56}Fe(p,pn)^{55}Fe^{*}$	--
		$^{56}Fe(p,2n)^{55}Co\ (e^{+};\varepsilon)^{55}Fe^{*}$(73%)	9.5×10^{4}
0.936	$^{52}Cr^{*}2.370\rightarrow^{52}Cr^{*}1.434$	$^{56}Fe(p,x)^{52}Mn(e^{+};\varepsilon)^{52}Cr^{*}$(94%)	7.1×10^{5}
0.957	$^{27}Si^{*}0.957\rightarrow g.s.$	$^{28}Si(p,pn)^{27}Si^{*}$	1.8×10^{-12}
1.014	$^{27}Al^{*}1.014\ g.s.$	$^{27}Al(p,p')^{27}Al^{*}$	1.9×10^{-12}
		$^{28}Si(p,2p)^{27}Al^{*}$	1.9×10^{-12}
1.023	$^{10}B^{*}1.740\rightarrow^{10}B^{*}0.717$	$^{12}C(p,x)^{10}B^{*}$	1.5×10^{-13}
		$^{16}O(p,x)^{10}B^{*}$	1.5×10^{-13}
1.038	$^{56}Fe^{*}3.123\rightarrow^{56}Fe^{*}2.085$	$^{56}Fe(p,n)^{56}Co\ (e^{+},\varepsilon)^{56}Fe^{*}$(14%)	9.6×10^{6}
1.238	$^{56}Fe^{*}2.085\rightarrow^{56}Fe^{*}0.847$	$^{56}Fe(p,p')^{56}Fe^{*}$	1.0×10^{-12}
		$^{56}Fe\ (p,n)^{56}Co(e^{+},\varepsilon)^{56}Fe^{*}$(67%)	9.6×10^{6}
1 249	$^{31}S^{*}1.249\rightarrow g.s.$	$^{32}S(p,pn)^{31}S^{*}$	7.2×10^{-13}
1.266	$^{31}P^{*}1.266\rightarrow g.s.$	$^{32}S(p,2p)^{31}P^{*}$	7.4×10^{-13}
1.275	$^{22}Ne^{*}1.275\rightarrow g.s.$	$^{22}Ne(p,p')^{22}Ne^{*}$	4.9×10^{-12}
		$^{22}Ne(\alpha,\alpha')^{22}Ne^{*}$	4.9×10^{-12}
		$^{22}Ne(p,n)^{22}Na(e^{+};\varepsilon)^{22}Ne^{*}$(100%)	1.2×10^{8}
		$^{23}Mg(p,x)^{22}Na(e^{+},\varepsilon)^{22}Ne^{*}$(100%)	1.2×10^{8}
		$^{24}Mg(p,x)^{22}Na(e^{+};\varepsilon)^{22}Ne^{*}$(100%)	1.2×10^{8}
		$^{28}Si(p,x)^{22}Na(e^{+},\varepsilon)^{22}Ne^{*}$(100%)	1.2×10^{8}

Photon Energy (MeV)	Emission Mechanism	Production Processes	Mean Life (sec)
1.334	$^{52}Cr^{*}2.763\rightarrow^{52}Cr^{*}1.434$	$^{56}Fe(p,x)^{52}Cr^{*}$	--
1 369	$^{24}Mg^{*}1.369\rightarrow g.s.$	$^{24}Mg(p,p')^{24}Mg^{*}$	1.75×10^{-12}
		$^{24}Mg(\alpha,\alpha')^{24}Mg^{*}$	1.75×10^{-12}
		$^{28}Si(p,x)^{24}Mg^{*}$	1.75×10^{-12}
1.370	$^{55}Fe^{*}2.301\rightarrow^{55}Fe^{*}0.931$	$^{56}Fe(p,pn)^{55}Fe^{*}$	--
1.408	$^{54}Fe^{*}1\ 408\rightarrow g.s.$	$^{56}Fe(p,x)^{54}Fe^{*}$	1.3×10^{-12}
1.408	$^{55}Fe^{*}1.408\rightarrow g.s.$	$^{56}Fe(p,pn)^{55}Fe^{*}$	--
		$^{56}Fe(p,2n)^{55}Co(e^{+};\varepsilon)^{55}Fe^{*}$(18%)	9.5×10^{4}
1.434	$^{52}Cr^{*}1.434\rightarrow g.s.$	$^{56}Fe(p,x)^{52}Cr^{*}$	1.3×10^{-12}
		$^{56}Fe(p,x)^{52}Mn^{*}(e^{+};\varepsilon)^{52}Cr^{*}$(100%)	1.8×10^{3}
		$^{56}Fe(p,x)^{52}Mn(e^{+},\varepsilon)^{52}Cr^{*}$(100%)	7.1×10^{5}
1.600	$^{23}Mg^{*}2.051\rightarrow^{23}Mg^{*}0.451$	$^{24}Mg(p,pn)^{23}Mg^{*}$	8×10^{-14}
1.632	$^{14}N^{*}3.945\rightarrow^{14}N^{*}2.313$	$^{14}N(p,p')^{14}N^{*}$	4.5×10^{-15}
		$^{14}N(\alpha,\alpha')^{14}N^{*}$	4.5×10^{-15}
		$^{16}O(p,x)^{14}N^{*}$	4.5×10^{-15}
1.634	$^{20}Ne^{*}1.634\rightarrow g.s.$	$^{20}Ne(p,p')^{20}Ne^{*}$	1.2×10^{-12}
		$^{20}Ne(\alpha,\alpha')^{20}Ne^{*}$	1.2×10^{-12}
		$^{20}Ne(p,n)^{20}Na(e^{+})^{20}Ne^{*}$(80%)	6.4×10^{-1}
		$^{24}Mg(p,x)^{20}Ne^{*}$	1.2×10^{-12}
		$^{28}Si(p,x)^{20}Ne^{*}$	1.2×10^{-12}
1.636	$^{23}Na^{*}2.076\rightarrow^{23}Na^{*}0.440$	$^{24}Mg(p,2p)^{23}Na^{*}$	4×10^{-14}
1.772	$^{56}Fe^{*}3.857\rightarrow^{56}Fe^{*}2.085$	$^{56}Fe(p,p')^{56}Fe^{*}$	3.3×10^{-14}
		$^{56}Fe(p,n)^{56}Co(e^{+};\varepsilon)^{56}Fe^{*}$(16%)	9.6×10^{6}
1.779	$^{28}Si^{*}1.779\rightarrow g.s.$	$^{28}Si(p,p')^{28}Si^{*}$	6.8×10^{-13}
		$^{28}Si(\alpha,\alpha')^{28}Si^{*}$	6.8×10^{-13}
		$^{32}S(p,x)^{28}Si^{*}$	6.8×10^{-13}
1.809	$^{26}Mg^{*}1.809\rightarrow g.s.$	$^{26}Mg(p,p')^{26}Mg^{*}$	4×10^{-13}
		$^{26}Mg(\alpha,\alpha')^{26}Mg^{*}$	4×10^{-13}
		$^{26}Mg(p,n)^{26}Al(e^{+},\varepsilon)^{26}Mg^{*}$(100%)	3.4×10^{13}
		$^{27}Al(p,pn)^{26}Al(e^{+};\varepsilon)^{26}Mg^{*}$(100%)	3.4×10^{13}
		$^{28}Si(p,x)^{26}Al(e^{+};\varepsilon)^{26}Mg^{*}$(100%)	3.4×10^{13}
1.811	$^{56}Fe^{*}2.658\rightarrow^{56}Fe^{*}0.847$	$^{56}Fe(p,p')^{56}Fe^{*}$	4×10^{-14}
1.995	$^{11}C^{*}1.995\rightarrow g.s.$	$^{12}C(p,pn)^{11}C^{*}$	--
2.029	$^{31}P^{*}3.295\rightarrow^{31}P^{*}1.266$	$^{32}S(p,2p)^{31}P^{*}$	1.4×10^{-13}
2.034	$^{31}S^{*}3.283\rightarrow^{31}S^{*}1.249$	$^{32}S(p,pn)^{31}S^{*}$	--
2.094	$^{56}Fe^{*}2.941\rightarrow^{56}Fe^{*}0.847$	$^{56}Fe(p,p')^{56}Fe^{*}$	2.2×10^{-13}
2.113	$^{56}Fe^{*}2.960\rightarrow^{56}Fe^{*}0.847$	$^{56}Fe(p,p')^{56}Fe^{*}$	3.9×10^{-14}
2.124	$^{11}B^{*}2.124\rightarrow g.s.$	$^{12}C(p,2p)^{11}B^{*}$	5.4×10^{-15}
2.230	$^{32}S^{*}2.230\rightarrow g.s.$	$^{32}S(p,p')^{32}S^{*}$	2.4×10^{-13}
		$^{32}S(\alpha,\alpha')^{32}S^{*}$	2.4×10^{-13}
2 232	$^{31}S^{*}2.232\rightarrow g.s.$	$^{32}S(p,pn)^{31}S^{*}$	3.2×10^{-13}
2.234	$^{31}P^{*}2.234\rightarrow g.s.$	$^{32}S(p,2p)^{31}P^{*}$	4.0×10^{-13}
2.313	$^{14}N^{*}2.313\rightarrow g.s.$	$^{14}N(p,p')^{14}N^{*}$	8.5×10^{-14}
		$^{14}N(\alpha,\alpha')^{14}N^{*}$	8.5×10^{-14}
		$^{14}N(p,n)^{14}O(e^{+})^{14}N^{*}$(100%)	102
		$^{16}O(p,x)^{14}N^{*}$	8.5×10^{-14}
		$^{16}O(p,x)^{14}O(e^{+})^{14}N^{*}$(100%)	102

Photon Energy (Mev)	Emission Mechanism	Production Processes	Mean-Life (sec)
2.599	$^{56}Fe^{*}3.446 \rightarrow {}^{56}Fe^{*}0.847$	$^{56}Fe(p,n)^{56}Co(e^{+};c)^{56}Fe(17\%)$	9.6×10^{6}
2.613	$^{20}Ne^{*}4.247 \rightarrow {}^{20}Ne^{*}1.634$	$^{20}Ne(p,p')^{20}Ne^{*}$	9.3×10^{-14}
		$^{20}Ne(\alpha,\alpha')^{20}Ne^{*}$	9.3×10^{-14}
		$^{24}Mg(p,x)^{20}Ne^{*}$	9.3×10^{-14}
		$^{28}Si(p,x)^{20}Ne^{*}$	9.3×10^{-14}
2.640	$^{23}Na^{*}2.640 \rightarrow g.s.$	$^{24}Mg(p,2p)^{23}Na^{*}$	1.1×10^{-13}
2.741	$^{16}O^{*}8.872 \rightarrow {}^{16}O^{*}6.131$	$^{16}O(p,p')^{16}O^{*}$	1.8×10^{-13}
2.754	$^{24}Mg^{*}4.123 \rightarrow {}^{24}Mg^{*}1.369$	$^{24}Mg(p,p')^{24}Mg^{*}$	5.4×10^{-14}
		$^{24}Mg(\alpha,\alpha')^{24}Mg^{*}$	5.4×10^{-14}
3.334	$^{20}Ne^{*}4.968 \rightarrow {}^{20}Ne^{*}1.634$	$^{20}Ne(p,p')^{20}Ne^{*}$	4.8×10^{-12}
		$^{20}Ne(\alpha,\alpha')^{20}Ne^{*}$	4.8×10^{-12}
3.561	$^{6}Li^{*}3.562 \rightarrow g.s.$	$^{4}He(\alpha,pn)^{6}Li^{*}$	$>1.3\times10^{-19}$
3.684	$^{13}C^{*}3.684 \rightarrow g.s.$	$^{13}C(p,p')^{13}C^{*}$	1.5×10^{-15}
		$^{13}C(\alpha,\alpha')^{13}C^{*}$	1.5×10^{-15}
		$^{16}O(p,x)^{13}C^{*}$	1.5×10^{-15}
3.736	$^{40}Ca^{*}3.736 \rightarrow g.s.$	$^{40}Ca(p,p')^{40}Ca^{*}$	6.1×10^{-11}
		$^{40}Ca(\alpha,\alpha')^{40}Ca^{*}$	6.1×10^{-11}
3.853	$^{13}C^{*}3.684 \rightarrow g.s.$	$^{13}C(p,p')^{13}C^{*}$	1.1×10^{-11}
		$^{13}C(\alpha,\alpha')^{13}C^{*}$	1.1×10^{-11}
		$^{16}O(p,x)^{13}C^{*}$	1.1×10^{-11}
4.438	$^{12}C^{*}4.439 \rightarrow g.s.$	$^{12}C(p,p')^{12}C^{*}$	5.62×10^{-14}
		$^{12}C(\alpha,\alpha')^{12}C^{*}$	5.62×10^{-14}
		$^{14}N(p,x)^{12}C^{*}$	5.62×10^{-14}
		$^{14}N(\alpha,x)^{12}C^{*}$	5.62×10^{-14}
		$^{16}O(p,x)^{12}C^{*}$	5.62×10^{-14}
		$^{16}O(\alpha,x)^{12}C^{*}$	5.62×10^{-14}
4.443	$^{11}B^{*}4.444 \rightarrow g.s.$	$^{12}C(p,2p)^{11}B^{*}$	1.2×10^{-15}
		$^{12}C(\alpha,x)^{11}B^{*}$	1.2×10^{-15}
5.099	$^{28}Si^{*}6.879 \rightarrow {}^{28}Si^{*}1.779$	$^{28}Si(p,p')^{28}Si^{*}$	2.5×10^{-12}
		$^{28}Si(\alpha,\alpha')^{28}Si^{*}$	2.5×10^{-12}
5.105	$^{14}N^{*}5.106 \rightarrow g.s.$	$^{14}N(p,p')^{14}N^{*}$	1.2×10^{-11}
		$^{14}N(\alpha,\alpha')^{14}N^{*}$	1.2×10^{-11}
		$^{16}O(p,x)^{14}N^{*}$	1.2×10^{-11}
		$^{16}O(\alpha,x)^{14}N^{*}$	1.2×10^{-11}
5.180	$^{15}O^{*}5.181 \rightarrow g.s.$	$^{16}O(p,pn)^{15}O^{*}$	$<10^{-13}$
		$^{16}O(\alpha,x)^{15}O^{*}$	$<10^{-13}$
5.241	$^{15}O^{*}5.242 \rightarrow g.s.$	$^{16}O(p,pn)^{15}O^{*}$	3.2×10^{-12}
		$^{16}O(\alpha,x)^{15}O^{*}$	3.2×10^{-12}
5.270	$^{15}N^{*}5.271 \rightarrow g.s.$	$^{16}O(p,2p)^{15}N^{*}$	2.9×10^{-12}
		$^{16}O(\alpha,x)^{15}N^{*}$	2.9×10^{-12}
5.298	$^{15}N^{*}5.299 \rightarrow g.s.$	$^{16}O(p,2p)^{15}N^{*}$	$<10^{-14}$
		$^{16}O(\alpha,x)^{15}N^{*}$	$<10^{-14}$
6.129	$^{16}O^{*}6.131 \rightarrow g.s.$	$^{16}O(p,p')^{16}O^{*}$	2.4×10^{-11}
		$^{16}O(\alpha,\alpha')^{16}O^{*}$	2.4×10^{-11}
		$^{20}Ne(p,x)^{16}O^{*}$	2.4×10^{-11}
6.176	$^{15}O^{*}6.177 \rightarrow g.s.$	$^{16}O(p,pn)^{15}O^{*}$	$<4\ 7\times10^{-14}$
		$^{16}O(\alpha,x)^{15}O^{*}$	$<4.7\times10^{-14}$
6.322	$^{15}N^{*}6.324 \rightarrow g.s.$	$^{16}O(p,2p)^{15}N^{*}$	$<4\times10^{-14}$
		$^{16}O(\alpha,x)^{15}N^{*}$	$<4\times10^{-14}$
6.337	$^{11}C^{*}6.339 \rightarrow g.s.$	$^{12}C(p,pn)^{11}C^{*}$	$<1.1\times10^{-13}$
6.478	$^{11}C^{*}6.480 \rightarrow g.s.$	$^{12}C(p,pn)^{11}C^{*}$	$<2.5\times10^{-13}$
6.741	$^{11}B^{*}6.743 \rightarrow g.s.$	$^{12}C(p,2p)^{11}B^{*}$	$<3\times10^{-13}$
6.791	$^{11}B^{*}6.793 \rightarrow g.s.$	$^{12}C(p,2p)^{11}B^{*}$	$<5\times10^{-14}$
6.878	$^{28}Si^{*}6.879 \rightarrow g.s.$	$^{28}Si(p,p')^{28}Si^{*}$	2.5×10^{-12}
		$^{28}Si(\alpha,\alpha')^{28}Si^{*}$	2.5×10^{-12}
6.917	$^{16}O^{*}6.919 \rightarrow g.s.$	$^{16}O(p,p')^{16}O^{*}$	6.8×10^{-15}
		$^{16}O(\alpha,\alpha')^{16}O^{*}$	6.8×10^{-15}
7.117	$^{16}O^{*}7.119 \rightarrow g.s.$	$^{16}O(p,p')^{16}O^{*}$	1.1×10^{-14}
		$^{16}O(\alpha,\alpha')^{16}O^{*}$	1.1×10^{-14}
7.299	$^{15}N^{*}7.301 \rightarrow g.s.$	$^{16}O(p,2p)^{15}N^{*}$	$<2.5\times10^{-14}$

C - 2

TABLE 2

NUCLEUS	ABUNDANCE	DIRECT DEEXCITATION LINES (MeV)	SECONDARY NUCLEI AND THEIR GAMMA RAY LINES (MeV)
^{1}H	1	----	----
^{4}He	10^{-1}	----	$^{6}Li(3.561)$, $^{7}Li(0.478)$, $^{7}Be(0.431;0.478)$
^{12}C	4.2×10^{-4}	4.438,15.11	$^{10}B(0.717;1.023)$, $^{10}C(0.717)$, $^{11}B(2.124;4.443;6.741;6.791)$, $^{11}C(1.995;6.337;6.478)$
^{13}C	4.7×10^{-6}	3.684,3.853	----
^{14}N	8.7×10^{-5}	1.632,2.313,5.105	$^{12}C(4.438;15.11)$, $^{14}O(2.313)$
^{16}O	6.9×10^{-4}	2.741,6.129,6.917,7.117	$^{10}B(0.717)$, $^{10}C(0.717)$, $^{12}C(4.438;15.11)$, $^{13}C(3.684;3.854)$, $^{14}N(1.632;2.313;5.105)$, $^{14}O(2.313)$, $^{15}N(5.270;5.298;6.322;7.299)$, $^{15}O(5.180;5.241;6.176)$
^{20}Ne	3.3×10^{-5}	1.634,2.613,3.334	$^{16}O(6.129)$, $^{19}F(0.110;0.197)$, $^{19}Ne(0.238;0.275)$, $^{20}Na(1.634)$
^{22}Ne	4.1×10^{-6}	1.275	$^{22}Na(1.275)$
^{24}Mg	3.2×10^{-5}	1.369,2.754	$^{20}Ne(1.634,2.613)$, $^{22}Na(0.891;1.275)$, $^{23}Na(0.440;1.636;2.640)$, $^{23}Mg(0.451;1.600)$
^{25}Mg	4.0×10^{-6}	----	$^{22}Na(1.275)$
^{26}Mg	4.4×10^{-6}	1.809	$^{26}Al(1.809)$
^{27}Al	3.3×10^{-6}	1.014	$^{26}Al(1.809)$
^{28}Si	4.5×10^{-5}	1.779,5.099,6.878	$^{20}Ne(1.634;2.613)$, $^{22}Na(1.275)$, $^{24}Mg(1.369)$, $^{26}Al(1.809)$, $^{27}Al(0.844;1.014)$; $^{27}Si(0.780;0.957$
^{32}S	1.6×10^{-5}	2.230	$^{28}Si(1.779)$, $^{31}P(1.266;2.029;2.234)$, $^{31}S(1.249;2.034;2.232)$
^{40}Ca	2.2×10^{-6}	3.736	----
^{56}Fe	3.2×10^{-5}	0.847,1.238,1.772, 1.811,2.094,2.113	$^{52}Cr(0.744;1.334;1.434)$ $^{52}Mn(0.744;0.936;1.434)$ $^{54}Mn(0.835)$, $^{54}Fe(1.408)$ $^{55}Fe(0.092;0.412;0.477;0.931;1.370;1.408)$, $^{55}Co(0.477;0.931;1.408)$, $^{56}Co(0.158;0.812;0.847;1.038;1.238;1.772;2.599)$

TABLE 3

ABUNDANCES

Element	Solar System	Local Cosmic Ray Source	5kpc Ambient	5kpc Cosmic Ray Source
H	1	1	1	1
He	10^{-1}	0.1	0.1	0.1
C	4.2×10^{-4}	3.8×10^{-3}	2.1×10^{-3}	1.9×10^{-2}
N	8.7×10^{-5}	5.6×10^{-4}	1.3×10^{-3}	8.4×10^{-3}
O	6.9×10^{-4}	4.3×10^{-3}	3.5×10^{-3}	2.2×10^{-2}
Ne	3.7×10^{-5}	5.8×10^{-4}	1.9×10^{-4}	2.9×10^{-3}
Mg	4.0×10^{-5}	9.2×10^{-4}	2.0×10^{-4}	4.6×10^{-3}
Aℓ	3.3×10^{-6}	5.9×10^{-5}	1.7×10^{-5}	3.0×10^{-4}
Si	4.5×10^{-5}	8.1×10^{-4}	2.3×10^{-4}	4.1×10^{-3}
S	1.6×10^{-5}	1.2×10^{-4}	8.0×10^{-5}	6.0×10^{-4}
Ca	2.2×10^{-6}	9.0×10^{-5}	1.1×10^{-5}	4.5×10^{-4}
Fe	3.2×10^{-5}	8.5×10^{-4}	1.6×10^{-4}	4.3×10^{-3}

TABLE 4

4.44 MeV Gamma Ray Line and Relative Positron Emissivities Per Unit Energy Content and Deposition Rate of the Energetic Particles for s=4 and E_c=30 MeV/nucleon

CASE	$\langle q(4.44)/W \rangle$ [Photons/(sec Hatom eVcm^{-3})] Narrow Line	Broad Line	$\langle q(4.44)/W \rangle$ [Photons/erg] Narrow Line	Broad Line	$\frac{q_+}{q_{narrow}(4.44) + q_{broad}(4.44)}$ (positrons/photon)
(1)	2.6×10^{-26}	2.6×10^{-26}	0.29	0.29	0.63
(2)	2.3×10^{-26}	1.7×10^{-25}	0.15	1.1	0.83
(3)	1.5×10^{-25}	1.5×10^{-25}	1.3	1.3	0.63
(4)	8.4×10^{-26}	6.4×10^{-25}	0.30	2.3	0.77

Table 5

Gamma Ray Line Fluxes from the Direction of the Galactic Center for s=4 and E_c=20 MeV/nucleon (in photons/cm^{2}sec rad)

CASE	$I_{4.44}$(narrow)	$I_{6.129}$(narrow) + $I_{6.129}$(very narrow)	$I_{0.847}$(narrow) + $I_{0.847}$(very narrow)	$I_{0.511}$
1	1.3×10^{-5}	6.4×10^{-6}	2.0×10^{-6}	1×10^{-5}
2	1.2×10^{-5}	5.9×10^{-6}	1.9×10^{-6}	5×10^{-5}
3	7.2×10^{-5}	3.0×10^{-5}	9.2×10^{-6}	6×10^{-5}
4	4.2×10^{-5}	1.8×10^{-5}	5.4×10^{-6}	1.7×10^{-4}

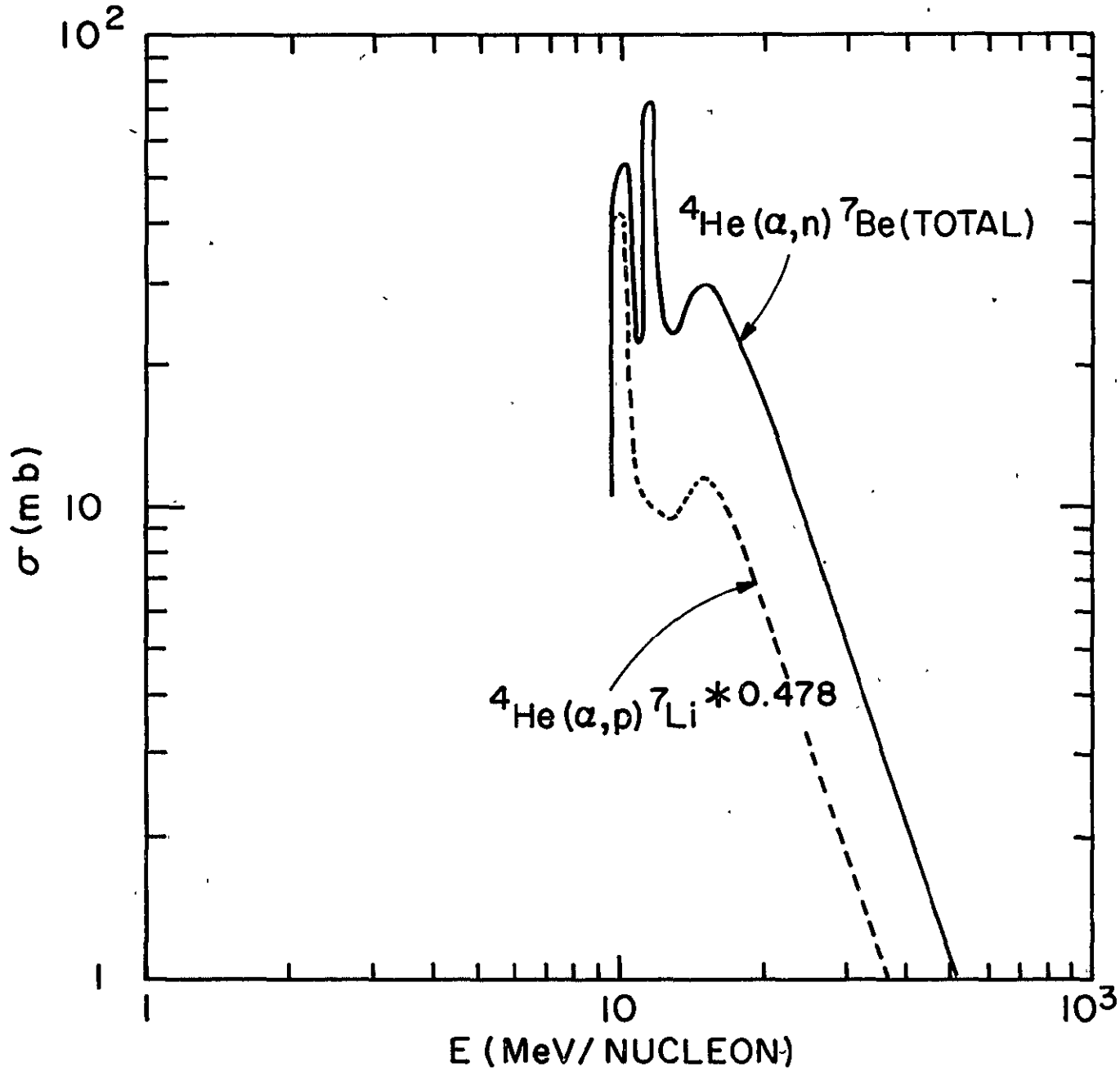
10^2
10
1
σ (mb)
^{4}He (α,n) ^{7}Be(TOTAL)
^{4}He (α,p) ^{7}Li * 0.478
1
10
10^3
E (MeV/ NUCLEON)

Fig. 1

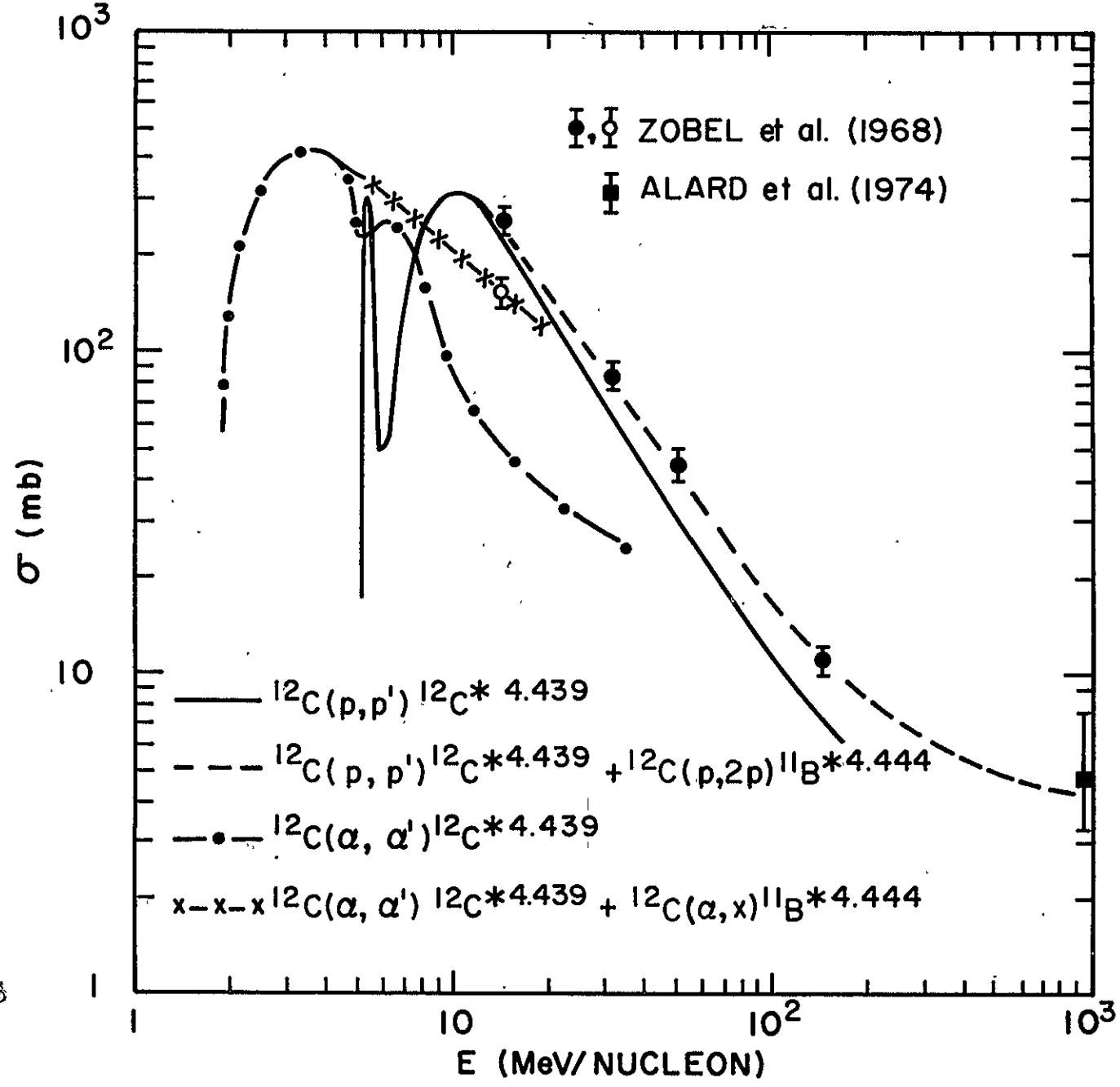

Fig. 2

ORIGINAL PAGE IS
OF POOR QUALITY

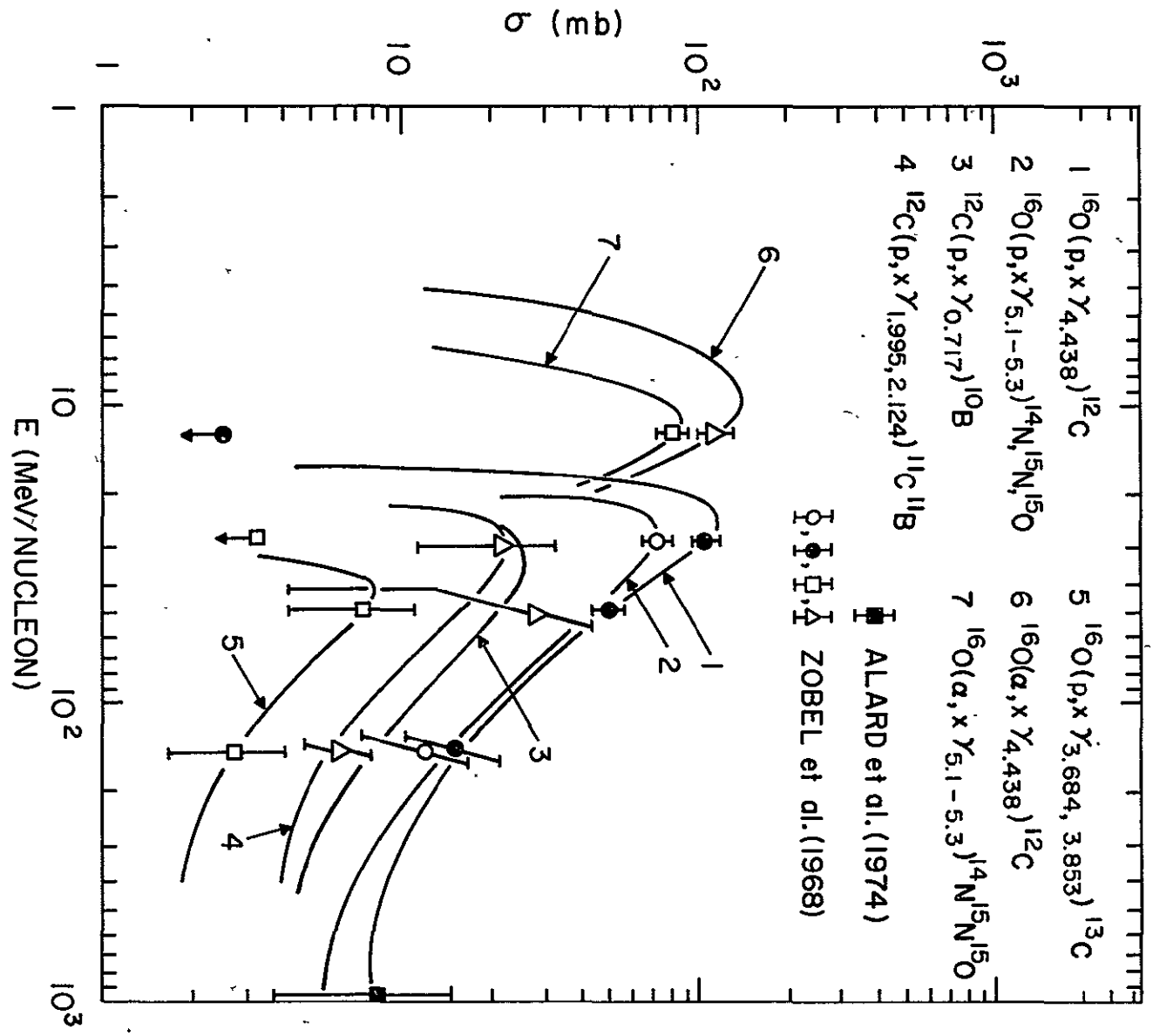

Fig.3

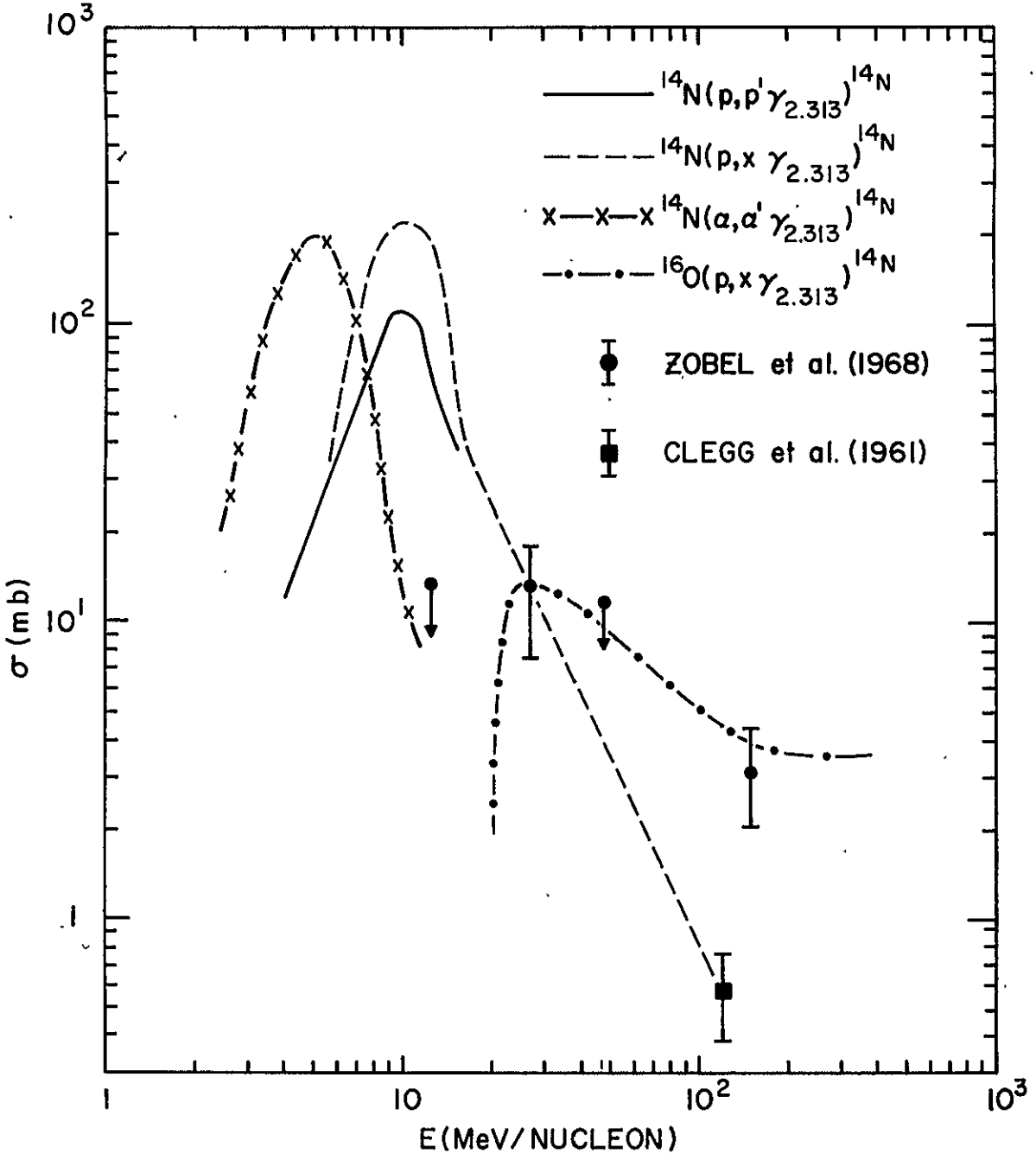
$^{14}N(p,p'\gamma_{2.313})^{14}N$
$^{14}N(p,x\,\gamma_{2.313})^{14}N$
$^{14}N(\alpha,\alpha'\gamma_{2.313})^{14}N$
$^{16}O(p,x\,\gamma_{2.313})^{14}N$
ZOBEL et al. (1968)
CLEGG et al. (1961)
σ (mb)
E(MeV/NUCLEON)
10^3
10^2
10^1
1
10
10^2
10^3

Fig. 4

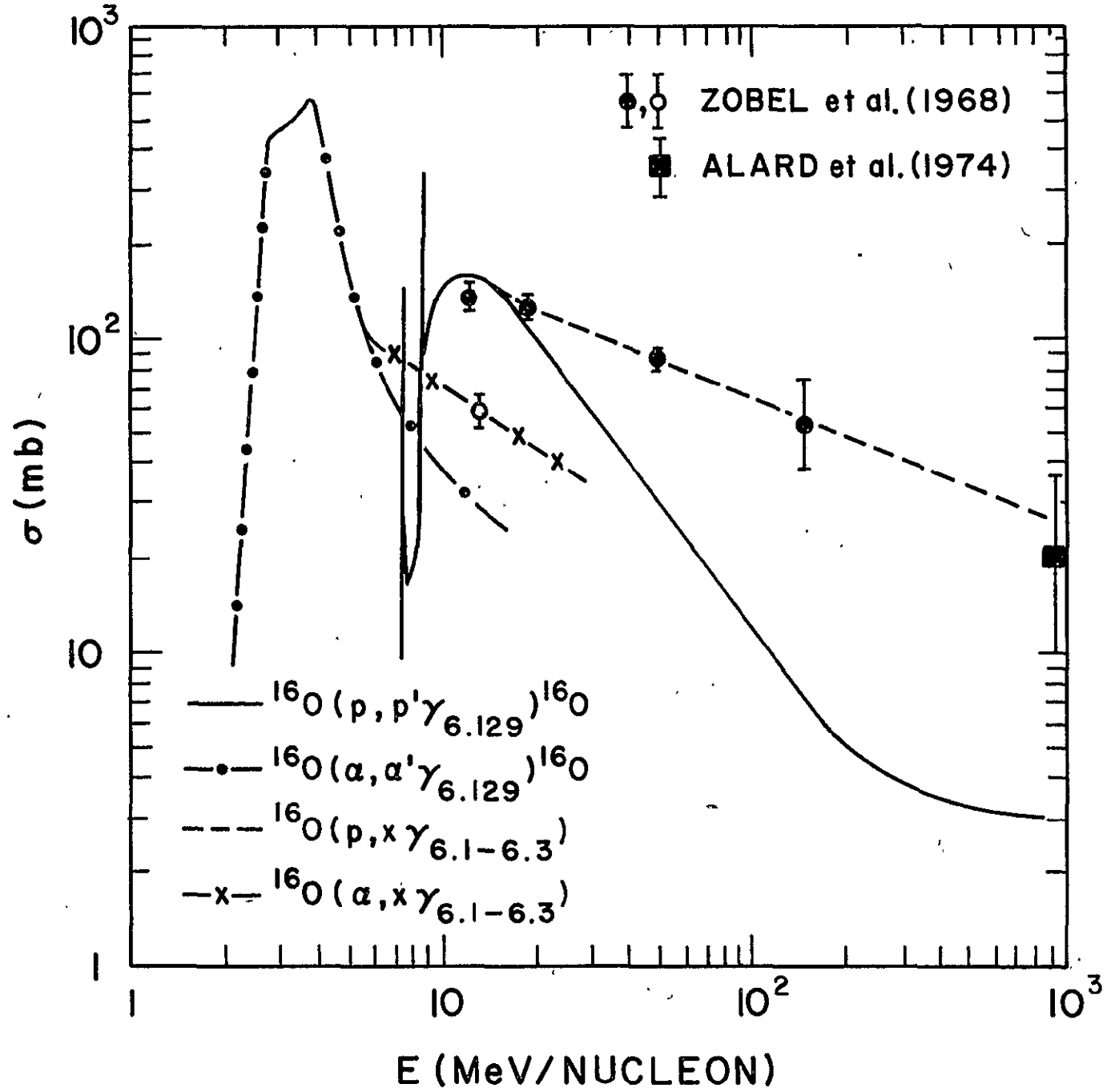

Fig. 5

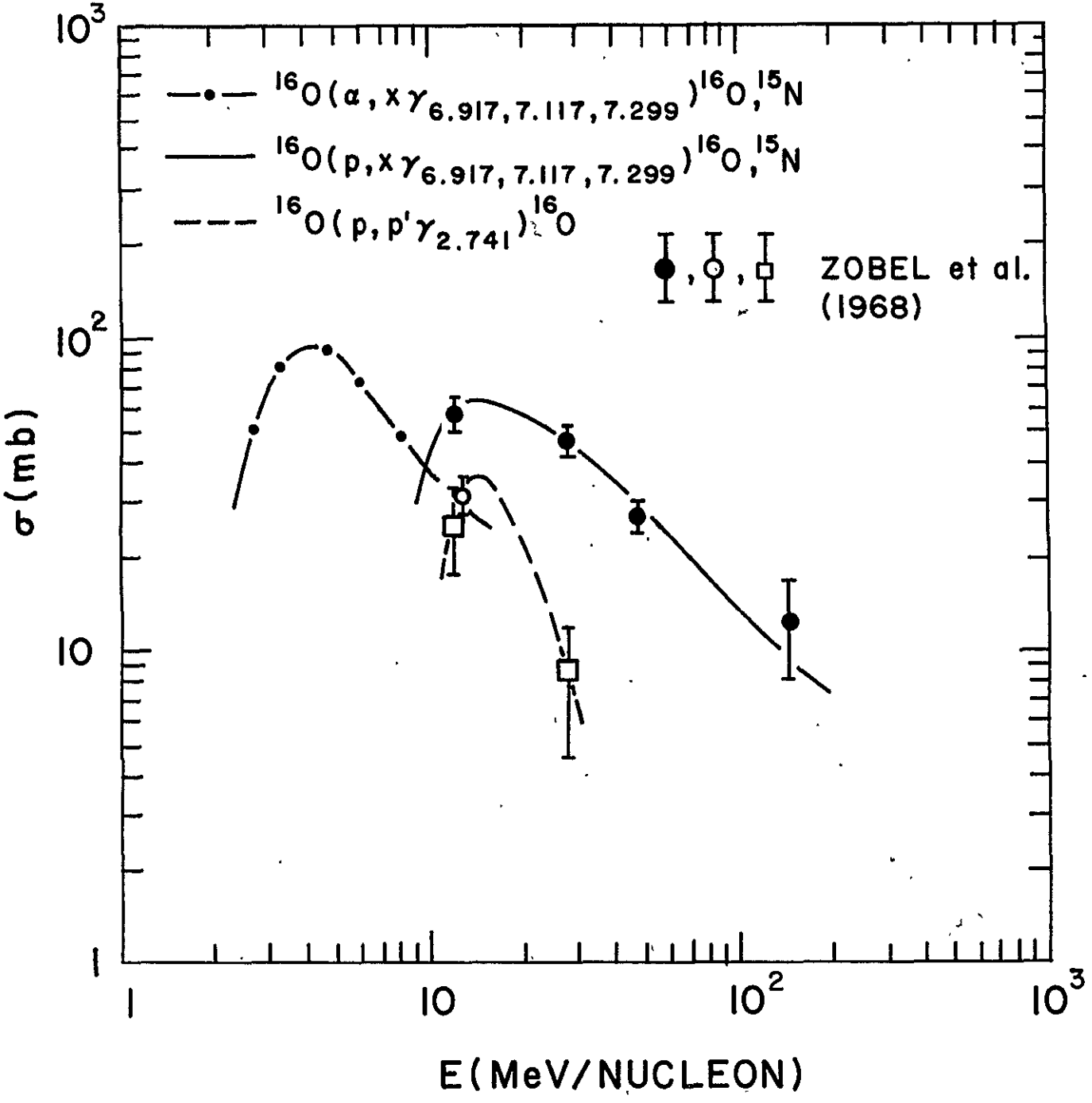
$^{16}O(\alpha, x\gamma_{6.917, 7.117, 7.299})^{16}O, ^{15}N$
$^{16}O(p, x\gamma_{6.917, 7.117, 7.299})^{16}O, ^{15}N$
$^{16}O(p, p'\gamma_{2.741})^{16}O$
ZOBEL et al. (1968)
σ(mb)
E(MeV/NUCLEON)
10^3
10^2
10
1
1
10
10^2
10^3

Fig. 6

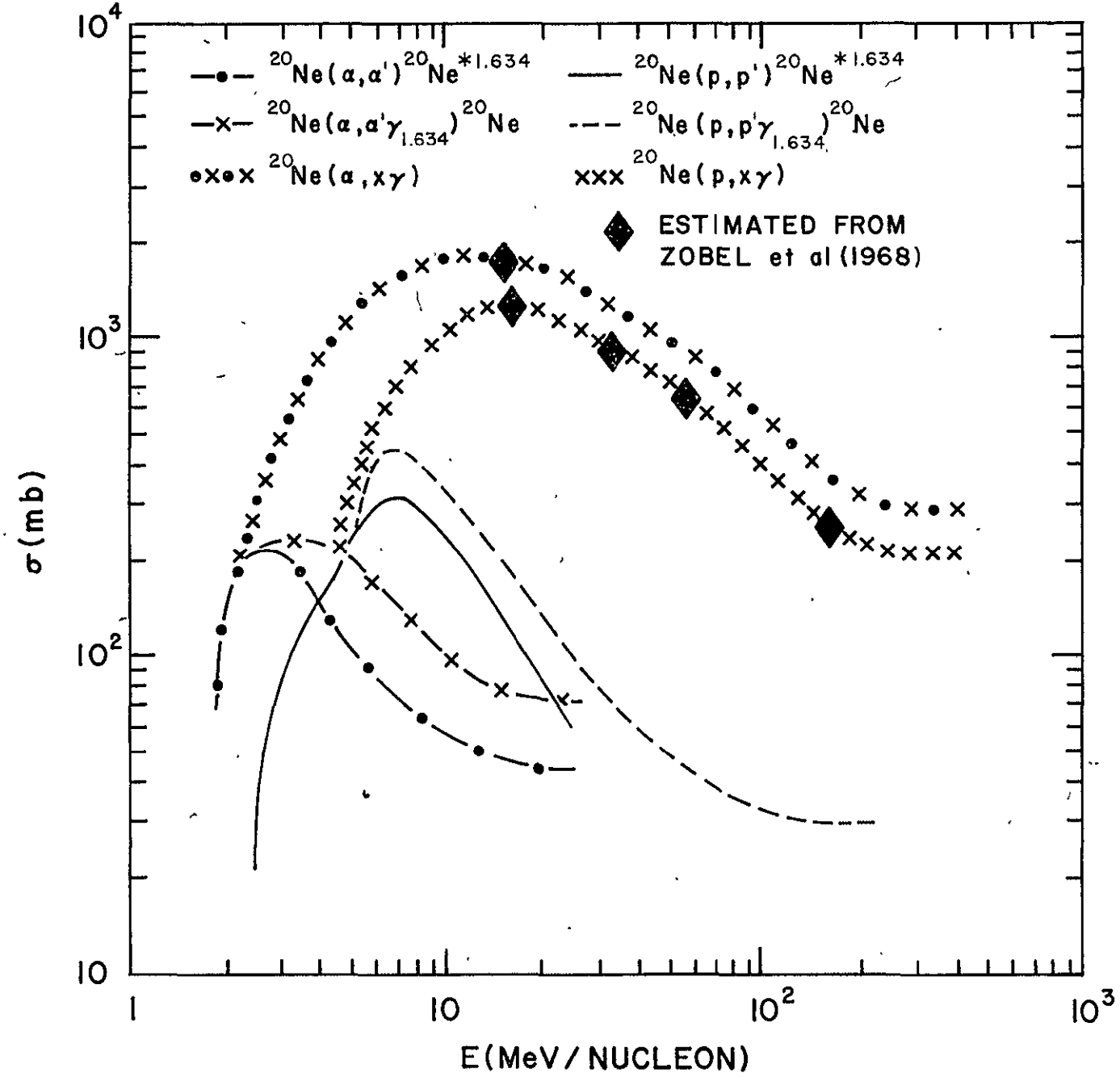

Fig. 7

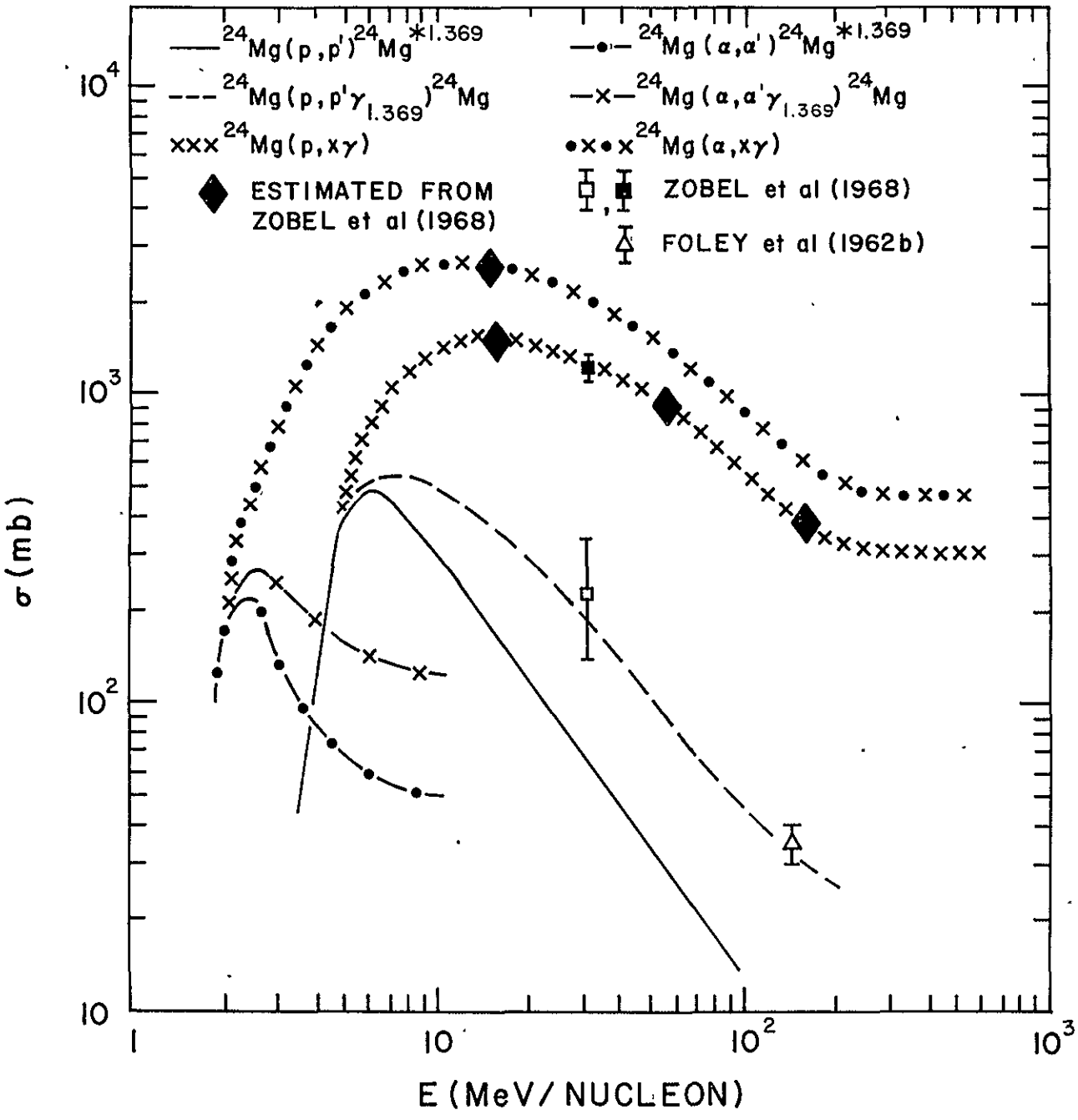
$^{24}Mg(p,p')^{24}Mg^{*1.369}$
$^{24}Mg(p,p'\gamma_{1.369})^{24}Mg$
$^{24}Mg(p,x\gamma)$
$^{24}Mg(\alpha,\alpha')^{24}Mg^{*1.369}$
$^{24}Mg(\alpha,\alpha'\gamma_{1.369})^{24}Mg$
$^{24}Mg(\alpha,x\gamma)$
ESTIMATED FROM ZOBEL et al (1968)
ZOBEL et al (1968)
FOLEY et al (1962b)
σ (mb)
E (MeV/ NUCLEON)
10
10^2
10^3
10^4
1

Fig. 8

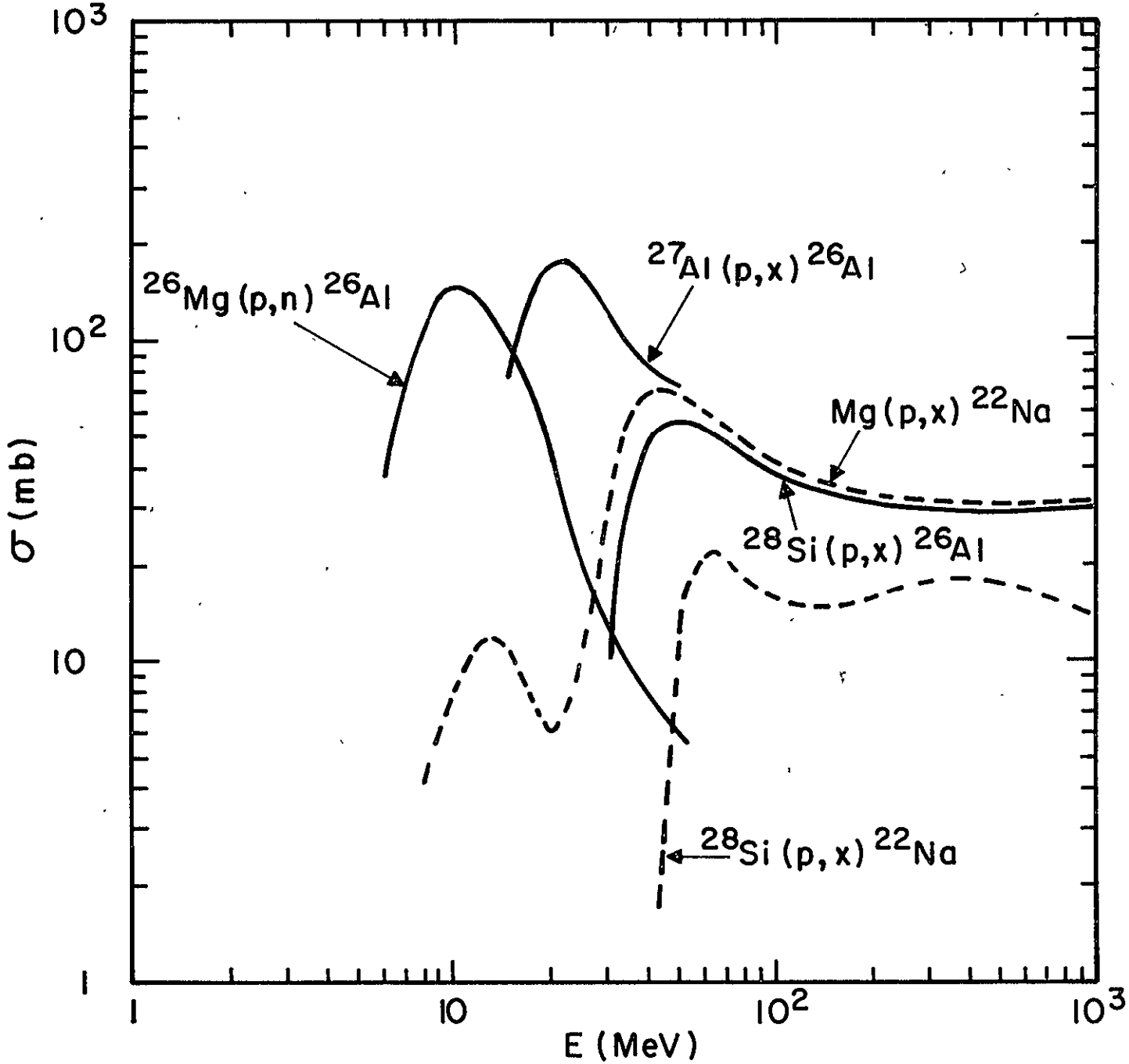
10^3
10^2
10
1
σ (mb)
1
10
10^2
10^3
E (MeV)
$^{26}Mg(p,n)^{26}Al$
$^{27}Al(p,x)^{26}Al$
$Mg(p,x)^{22}Na$
$^{28}Si(p,x)^{26}Al$
$^{28}Si(p,x)^{22}Na$

Fig. 9

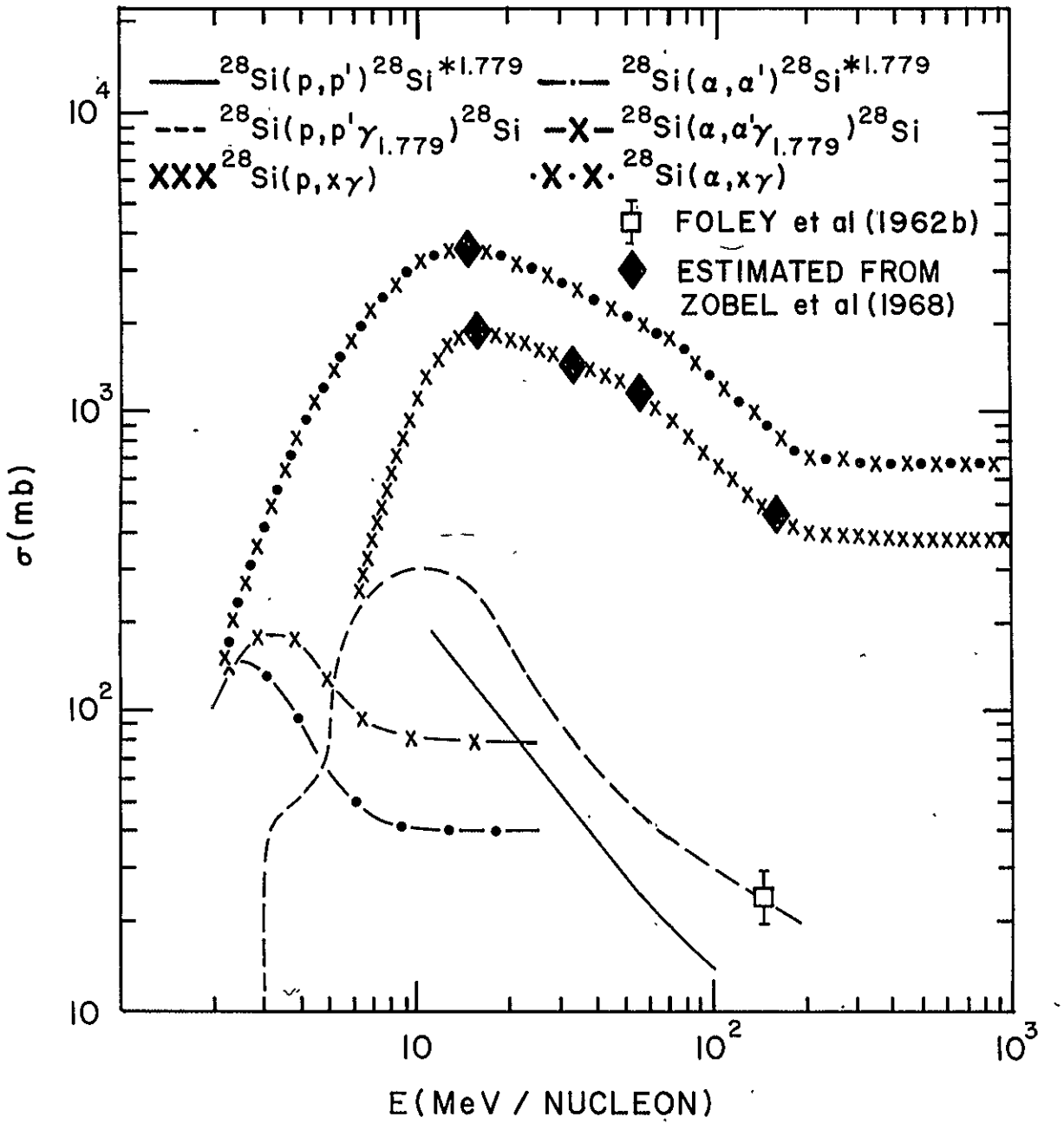
$^{28}Si(p,p')^{28}Si^{*1.779}$
$^{28}Si(\alpha,\alpha')^{28}Si^{*1.779}$
$^{28}Si(p,p'\gamma_{1.779})^{28}Si$
$^{28}Si(\alpha,\alpha'\gamma_{1.779})^{28}Si$
$^{28}Si(p,x\gamma)$
$^{28}Si(\alpha,x\gamma)$
FOLEY et al (1962b)
ESTIMATED FROM ZOBEL et al (1968)
σ (mb)
E (MeV / NUCLEON)
10
10^2
10^3
10^4

Fig. 10

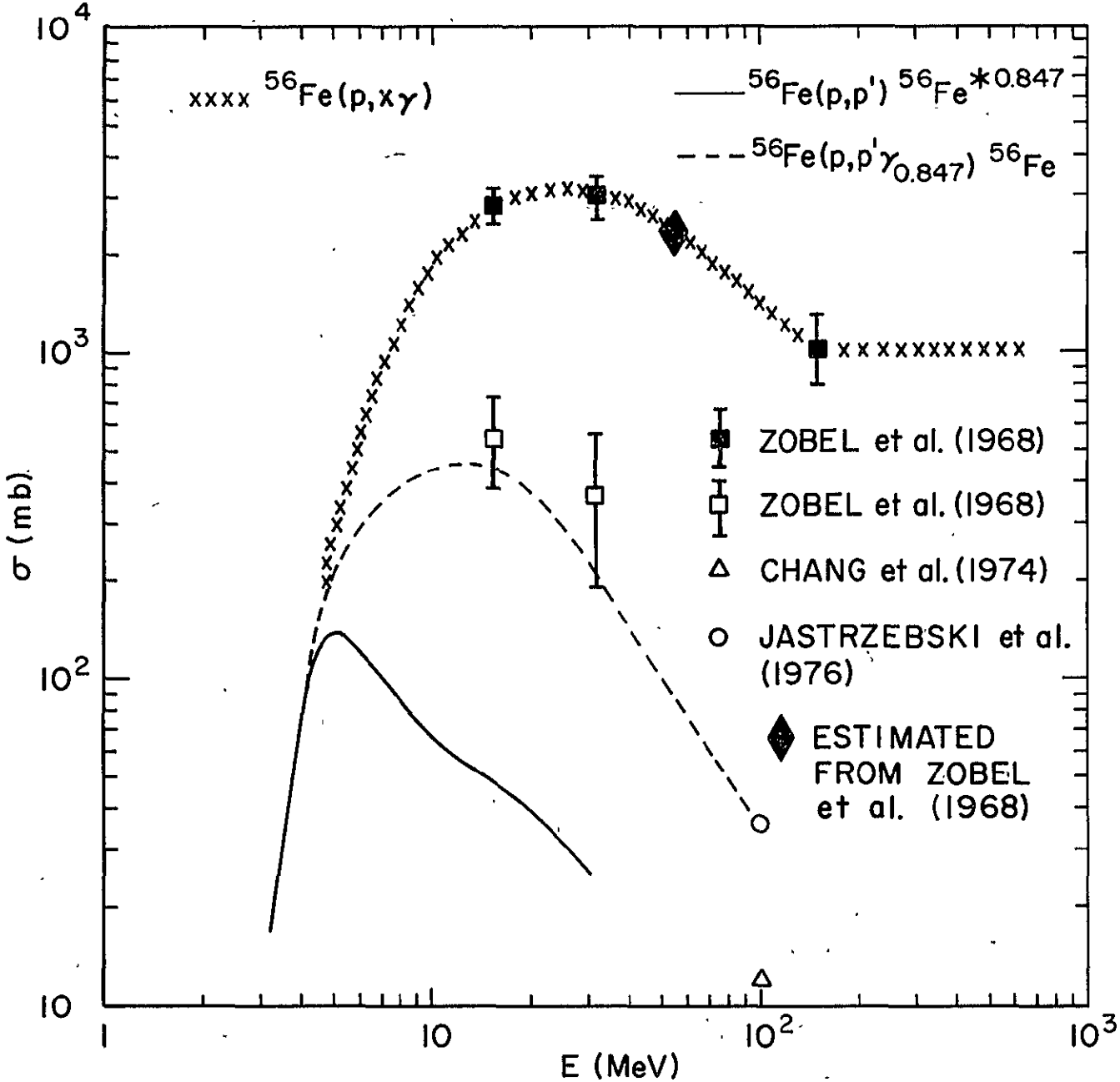
xxxx ^{56}Fe(p,xγ)
^{56}Fe(p,p') ^{56}Fe*0.847
^{56}Fe(p,p'γ$_{0.847}$) ^{56}Fe
ZOBEL et al. (1968)
ZOBEL et al. (1968)
CHANG et al. (1974)
JASTRZEBSKI et al. (1976)
ESTIMATED FROM ZOBEL et al. (1968)
σ (mb)
E (MeV)
10^4
10^3
10^2
10
1
10
10^2
10^3

Fig. 11

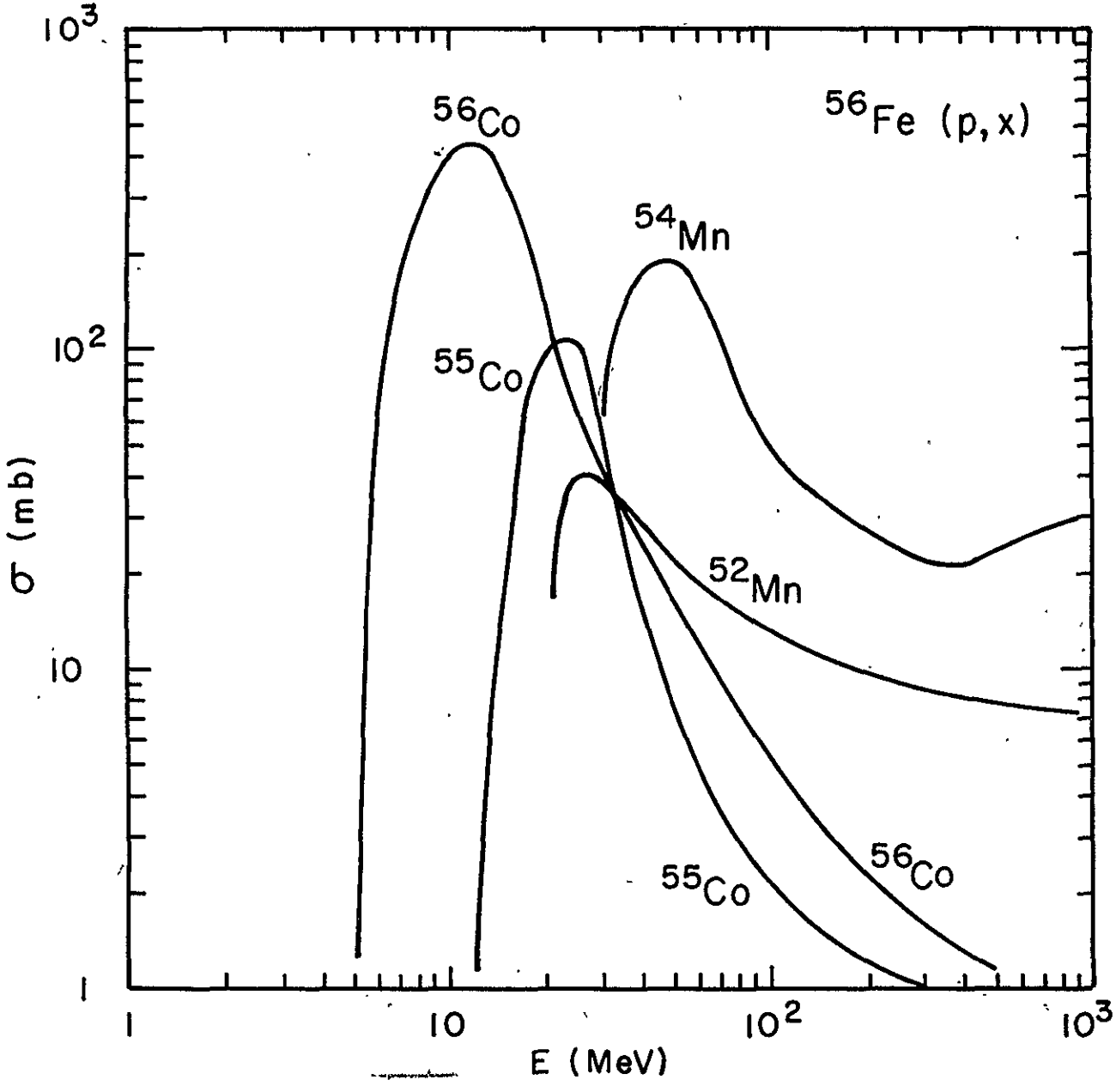
10^3
10^2
10
1
σ (mb)
^{56}Co
^{56}Fe (p, x)
^{54}Mn
^{55}Co
^{52}Mn
^{55}Co
^{56}Co
1
10
10^2
10^3
E (MeV)

Fig. 12

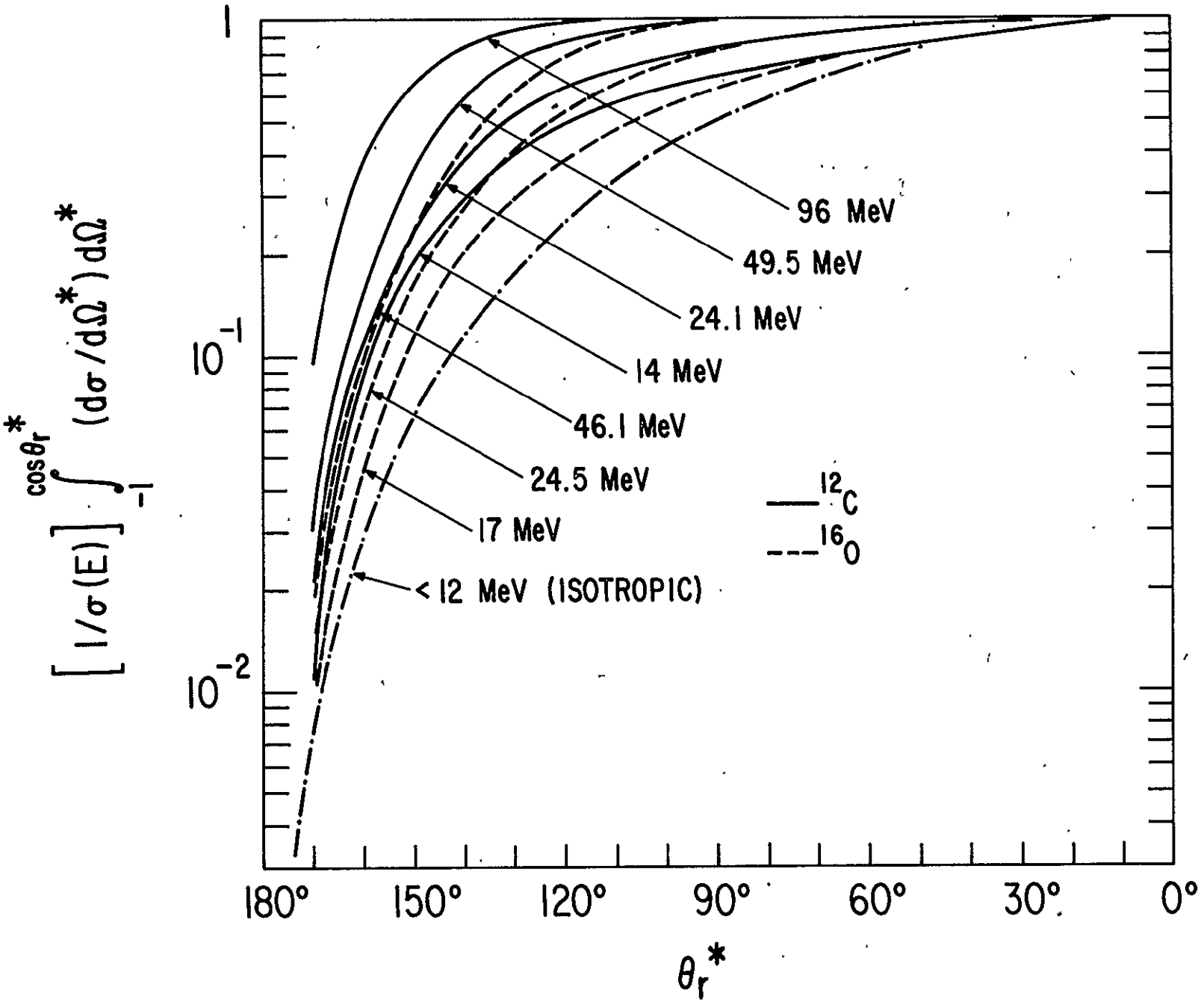
1
10^{-1}
10^{-2}
$\left[1/\sigma(E)\right]\int_{-1}^{\cos\theta_r^*}(d\sigma/d\Omega^*)\,d\Omega^*$
96 MeV
49.5 MeV
24.1 MeV
14 MeV
46.1 MeV
24.5 MeV
17 MeV
< 12 MeV (ISOTROPIC)
^{12}C
^{16}O
180°
150°
120°
90°
60°
30°
0°
θ_r^*

Fig. 13

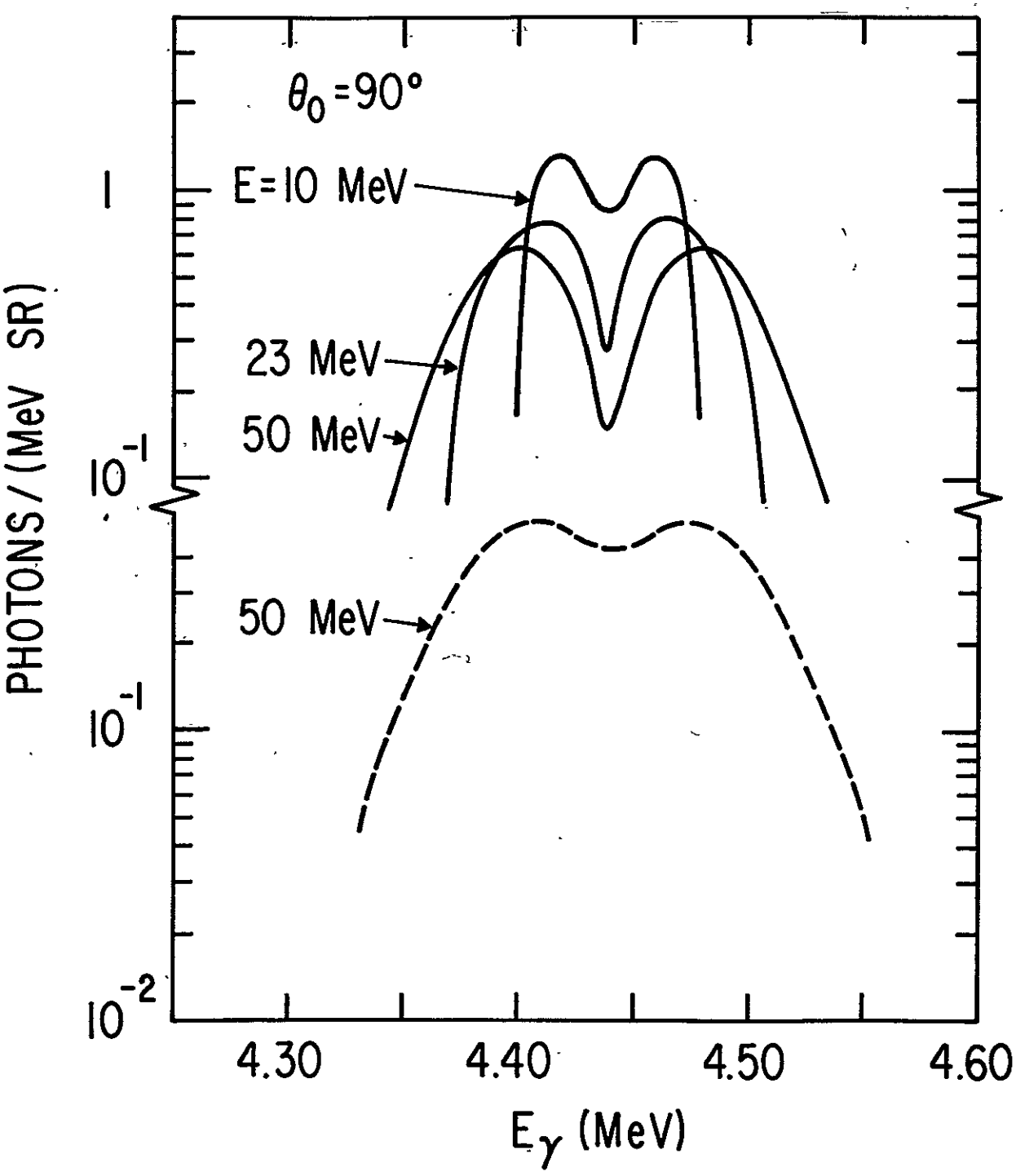
$\theta_0 = 90°$
E=10 MeV
23 MeV
50 MeV
50 MeV
1
10^{-1}
10^{-1}
10^{-2}
PHOTONS/(MeV SR)
4.30
4.40
4.50
4.60
E_γ (MeV)

Fig. 14

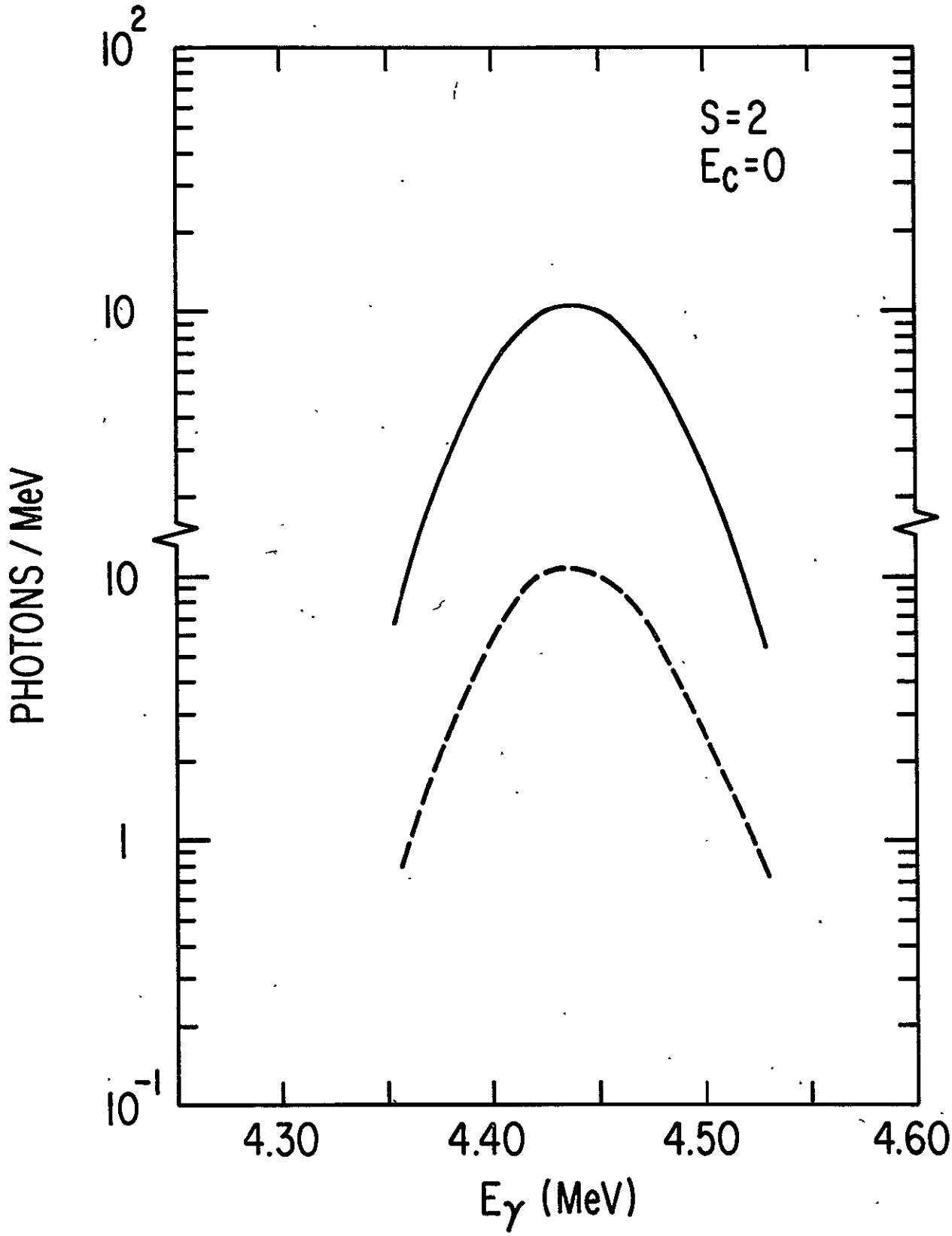

Fig.15

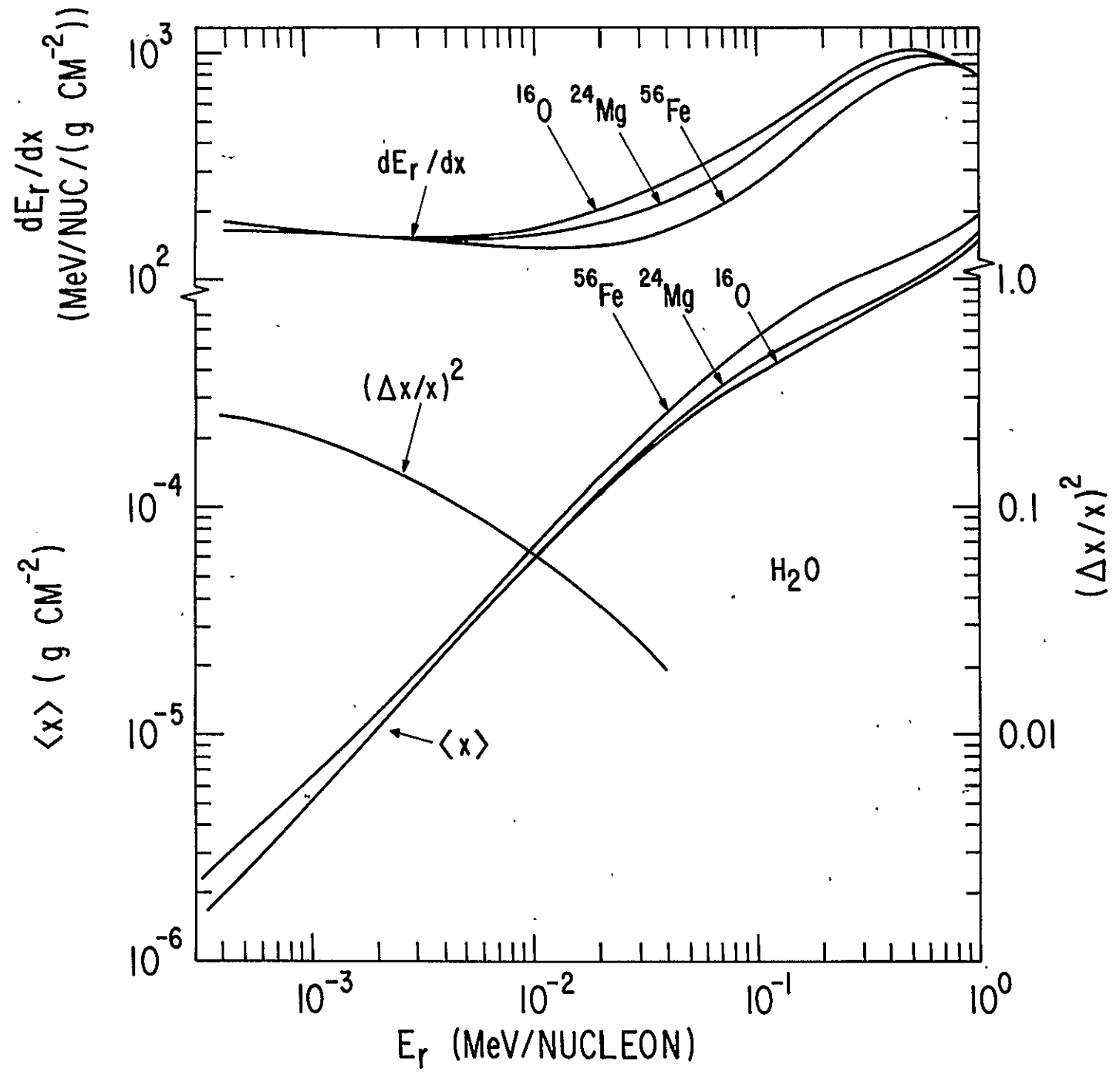
dE_r/dx (MeV/NUC/(g CM^-2))
10^3
10^2
10^-4
10^-5
10^-6
dE_r/dx
16O 24Mg 56Fe
56Fe 24Mg 16O
(Δx/x)^2
H2O
⟨x⟩
⟨x⟩ (g CM^-2)
1.0
0.1
0.01
(Δx/x)^2
10^-3
10^-2
10^-1
10^0
E_r (MeV/NUCLEON)

Fig. 16

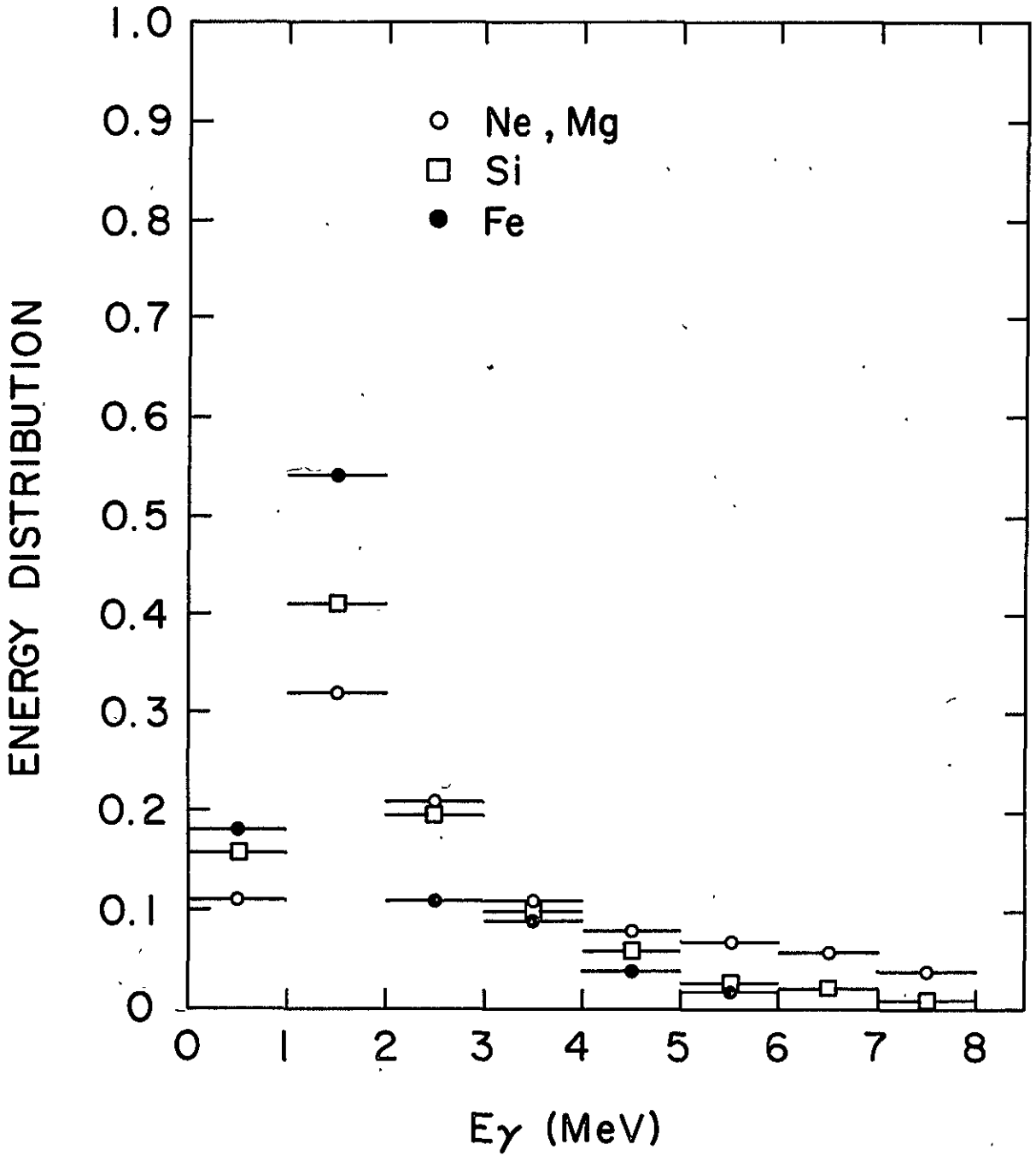
ENERGY DISTRIBUTION
1.0
0.9
0.8
0.7
0.6
0.5
0.4
0.3
0.2
0.1
0
Ne , Mg
Si
Fe
0
1
2
3
4
5
6
7
8
Eγ (MeV)

Fig. 17

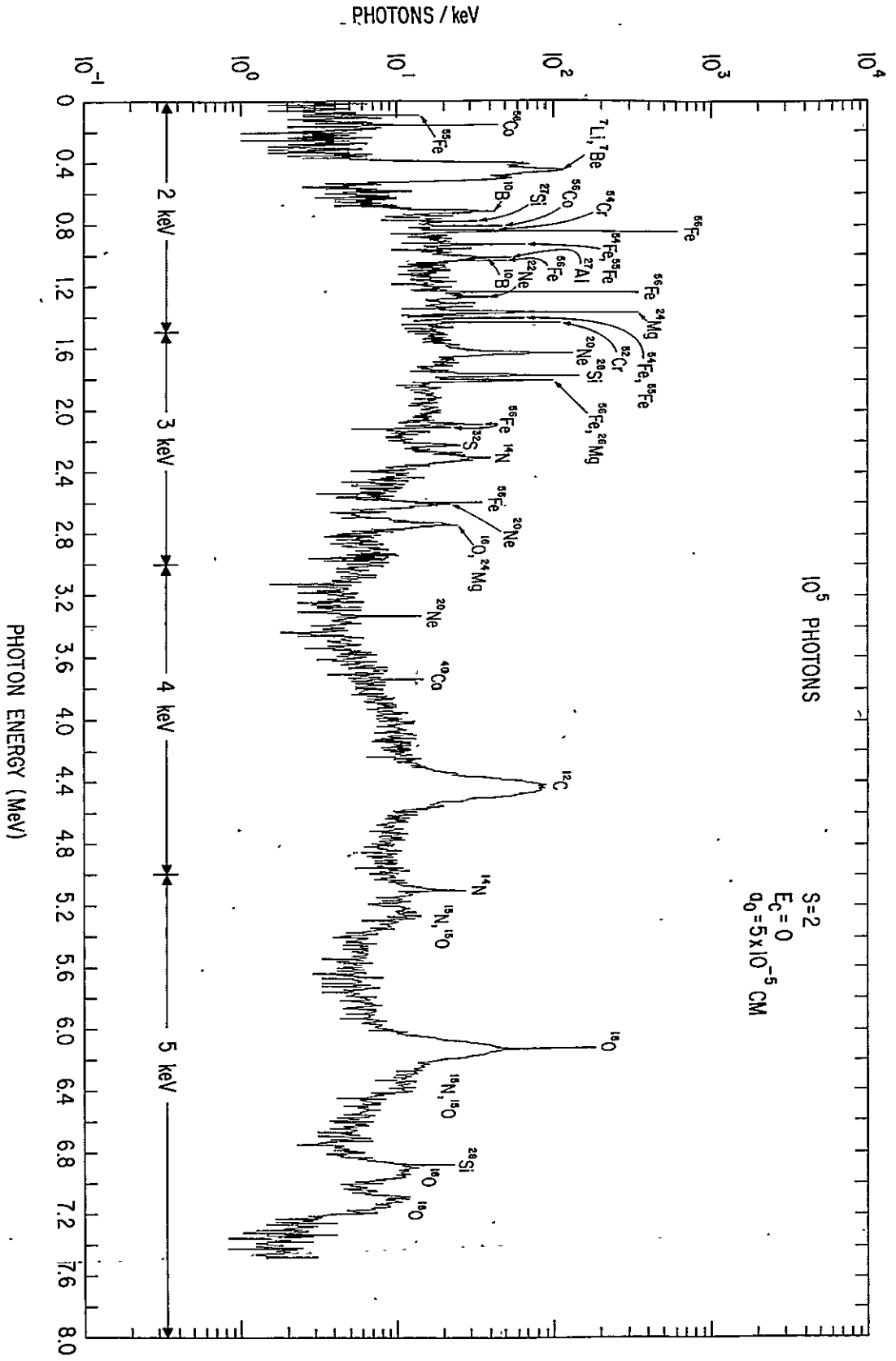

Fig. 18

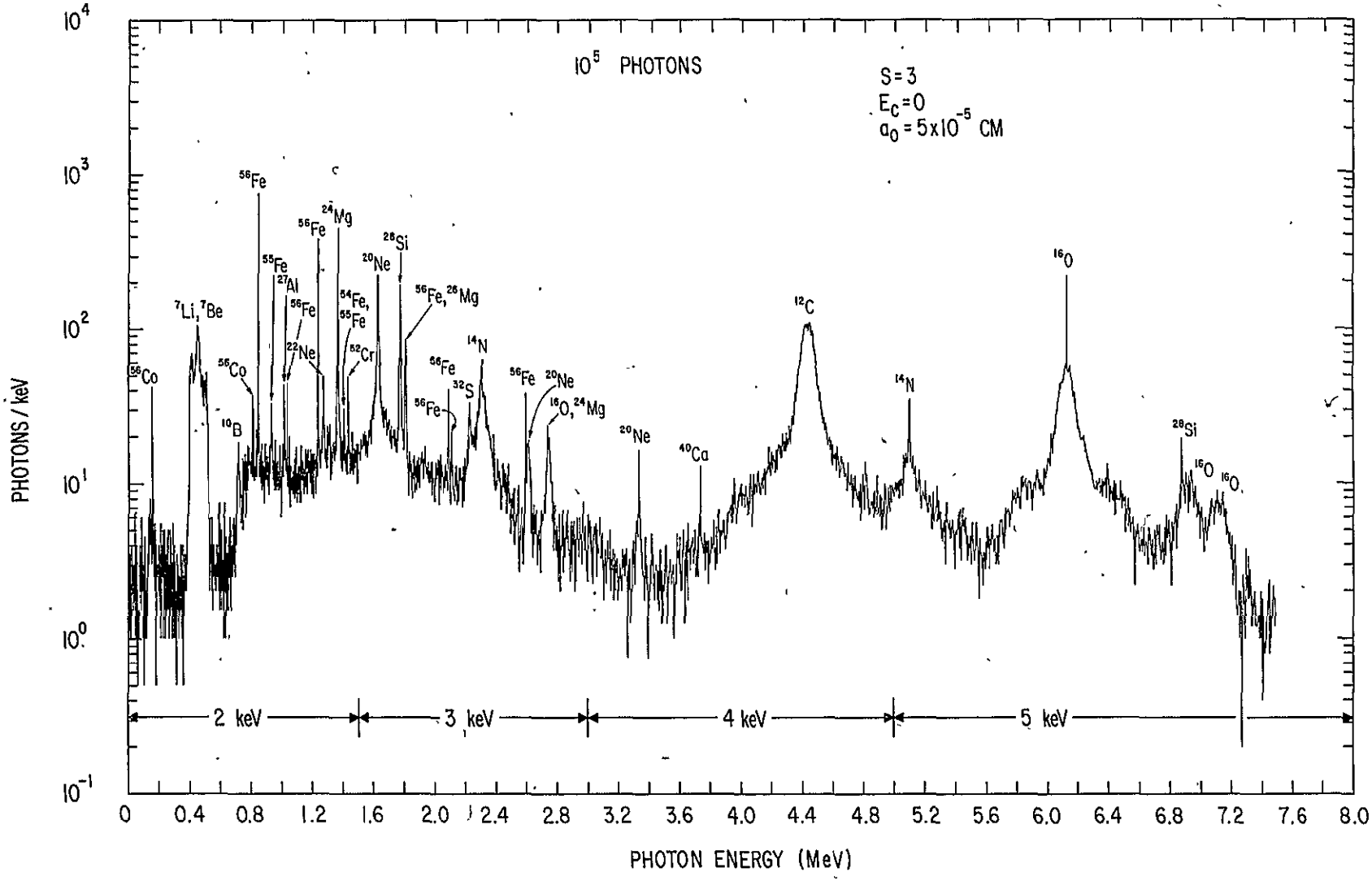

Fig.19

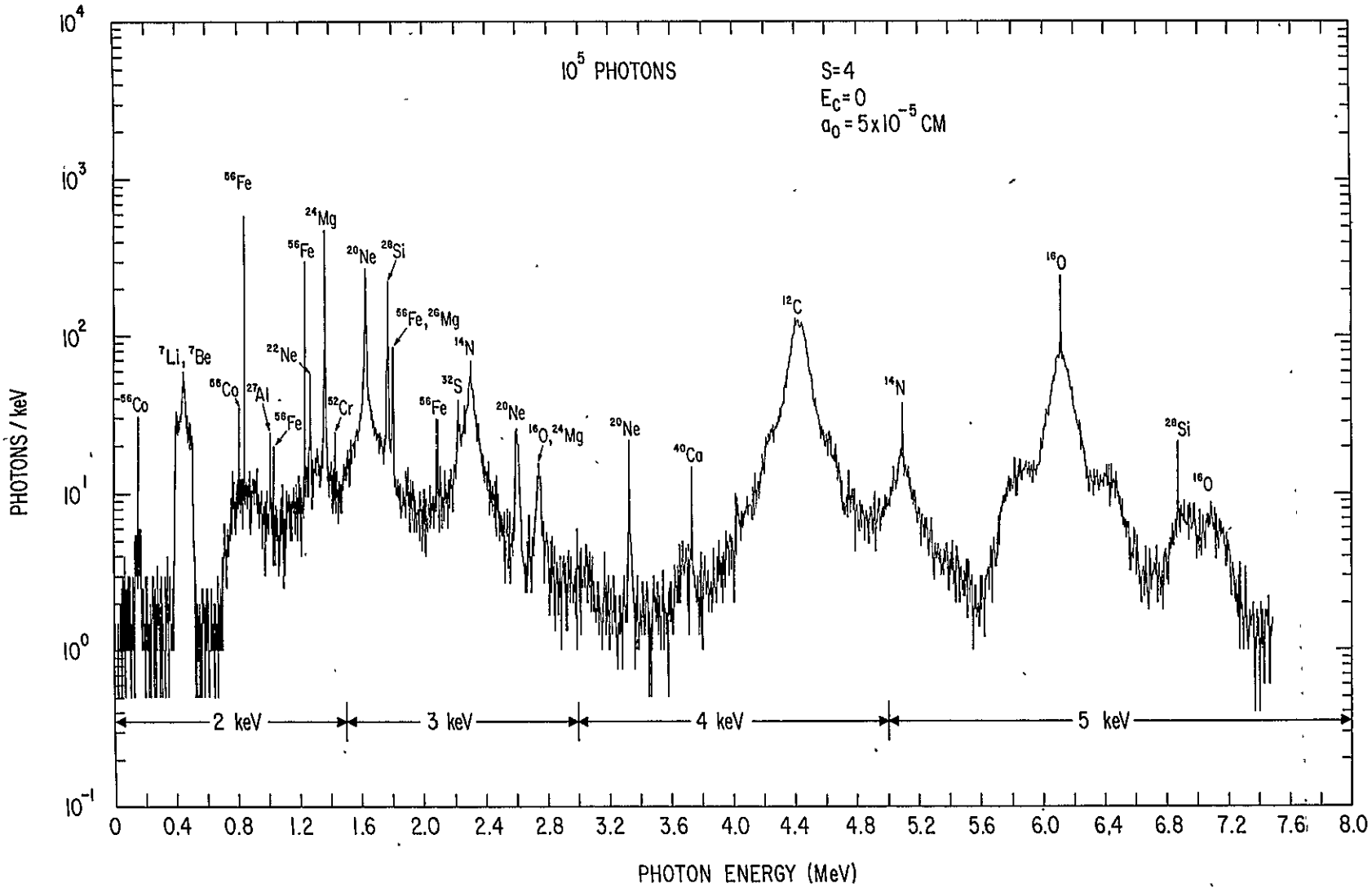
10^5 PHOTONS
S=4
E_c=0
a_0=5x10^{-5} CM
PHOTONS / keV
PHOTON ENERGY (MeV)
10^4
10^3
10^2
10^1
10^0
10^{-1}
0
0.4
0.8
1.2
1.6
2.0
2.4
2.8
3.2
3.6
4.0
4.4
4.8
5.2
5.6
6.0
6.4
6.8
7.2
7.6
8.0
^{56}Co
^{7}Li, ^{7}Be
^{55}Co
^{27}Al
^{56}Fe
^{22}Ne
^{56}Fe
^{24}Mg
^{52}Cr
^{56}Fe
^{20}Ne
^{28}Si
^{56}Fe, ^{26}Mg
^{14}N
^{32}S
^{56}Fe
^{20}Ne
^{16}O, ^{24}Mg
^{20}Ne
^{40}Ca
^{12}C
^{14}N
^{16}O
^{28}Si
^{16}O
2 keV
3 keV
4 keV
5 keV

Fig. 20

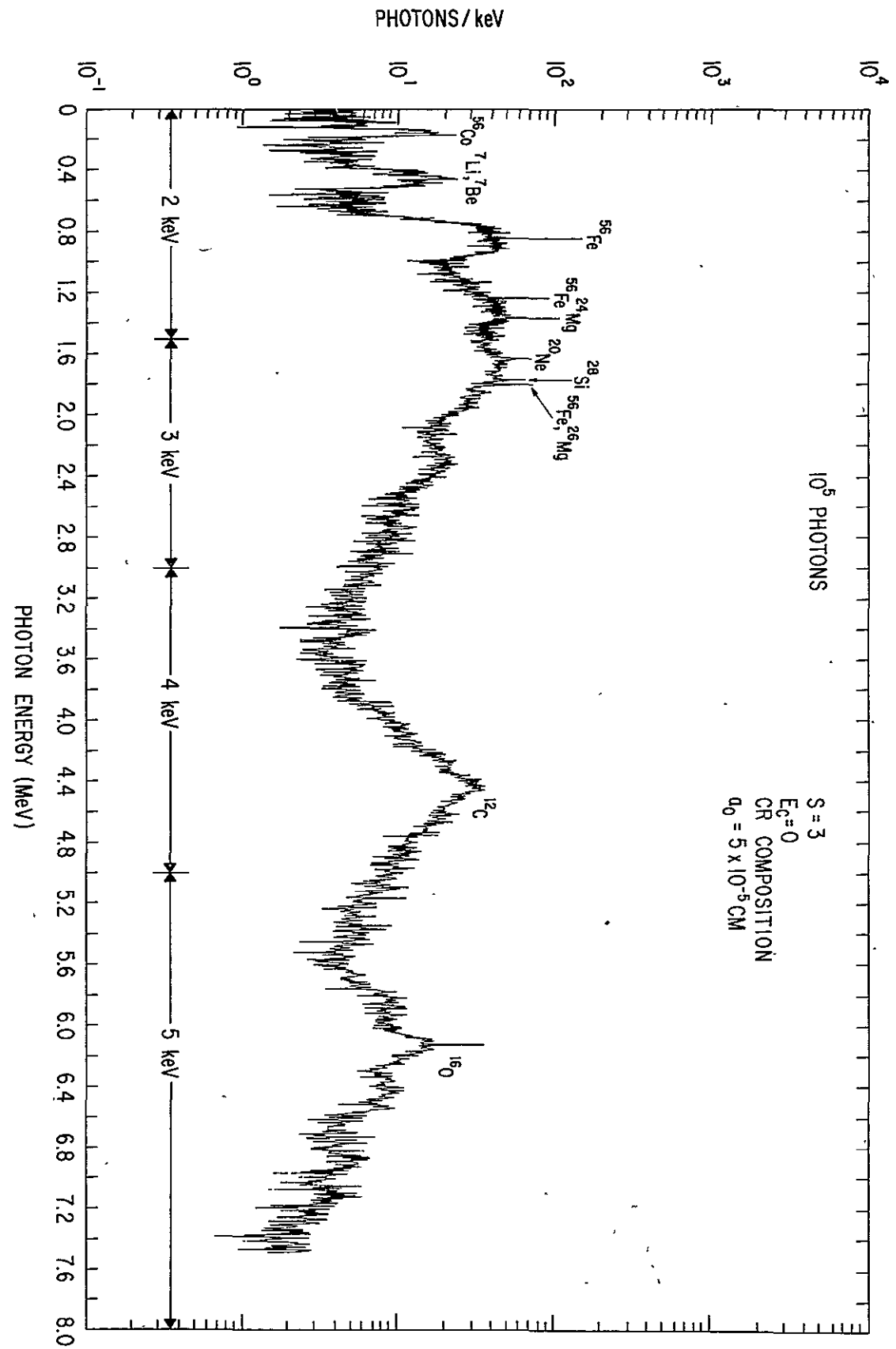

Fig. 21

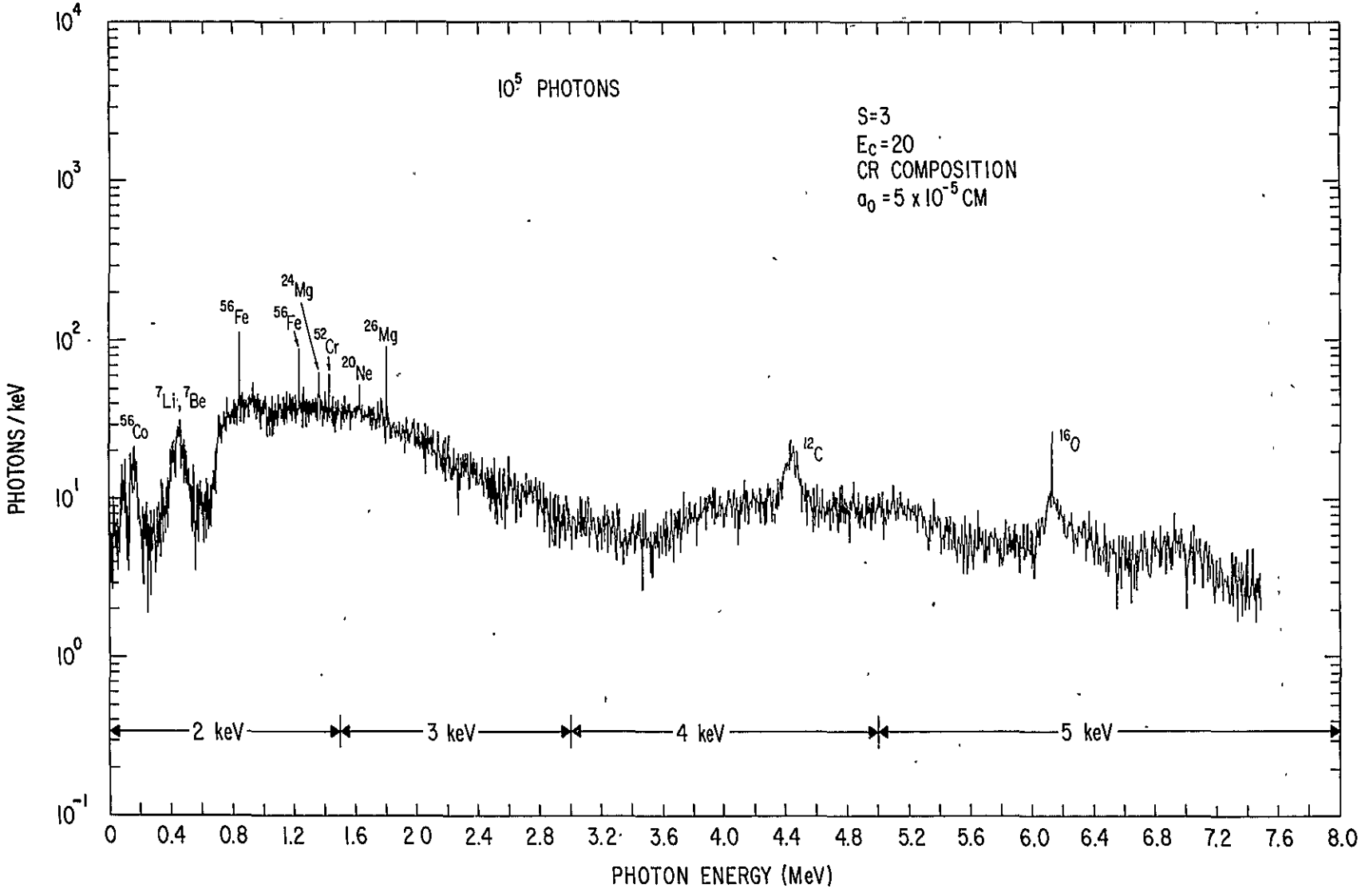
10^5 PHOTONS
S=3
E_c=20
CR COMPOSITION
$a_0 = 5 \times 10^{-5}$ CM
PHOTONS / keV
PHOTON ENERGY (MeV)
^{56}Co
^{7}Li, ^{7}Be
^{56}Fe
^{24}Mg
^{56}Fe
^{52}Cr
^{20}Ne
^{26}Mg
^{12}C
^{16}O
2 keV
3 keV
4 keV
5 keV

Fig. 22

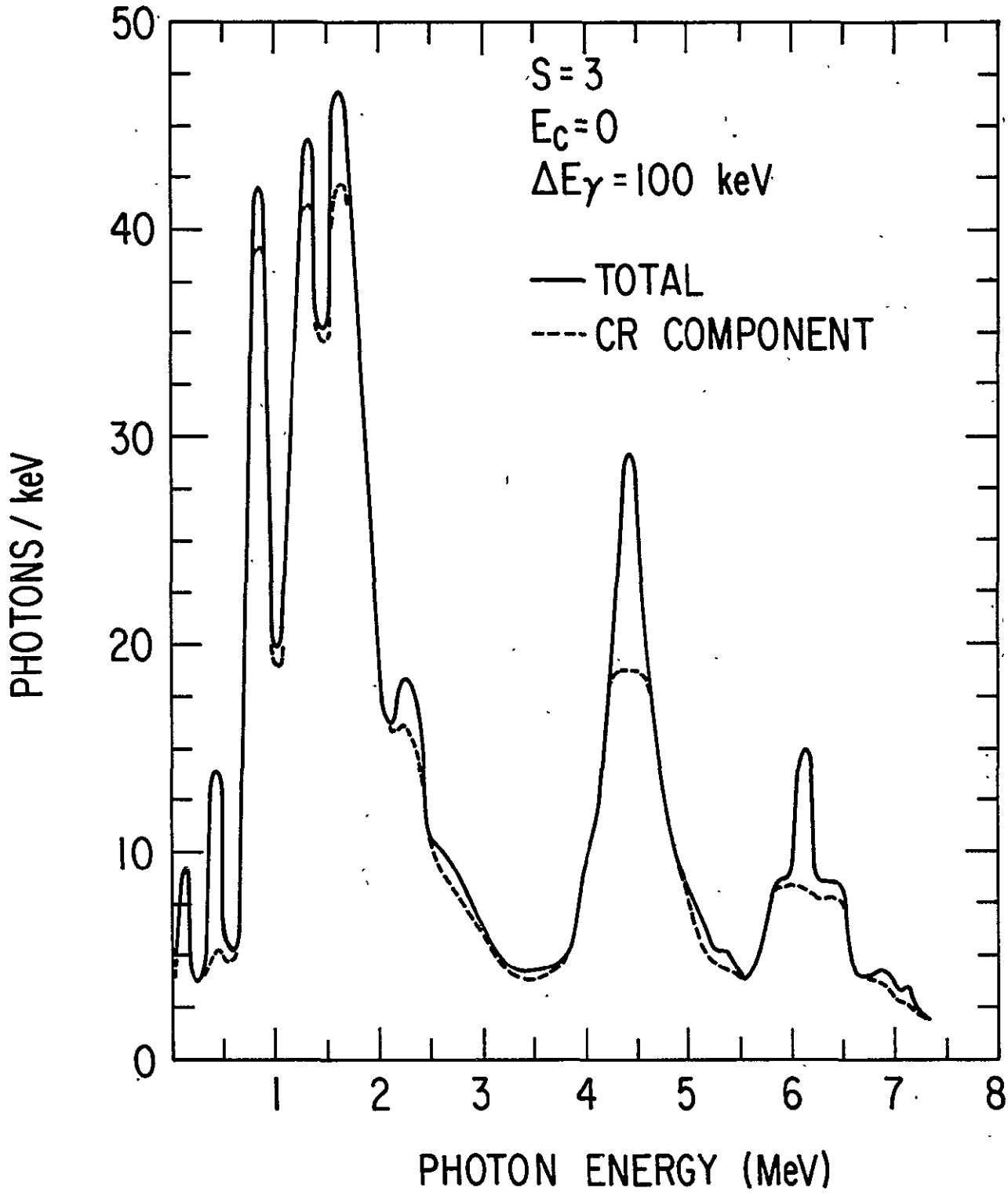
S = 3
E_C = 0
ΔE_γ = 100 keV
TOTAL
CR COMPONENT
PHOTONS / keV
PHOTON ENERGY (MeV)
0
10
20
30
40
50
1
2
3
4
5
6
7
8

Fig. 23

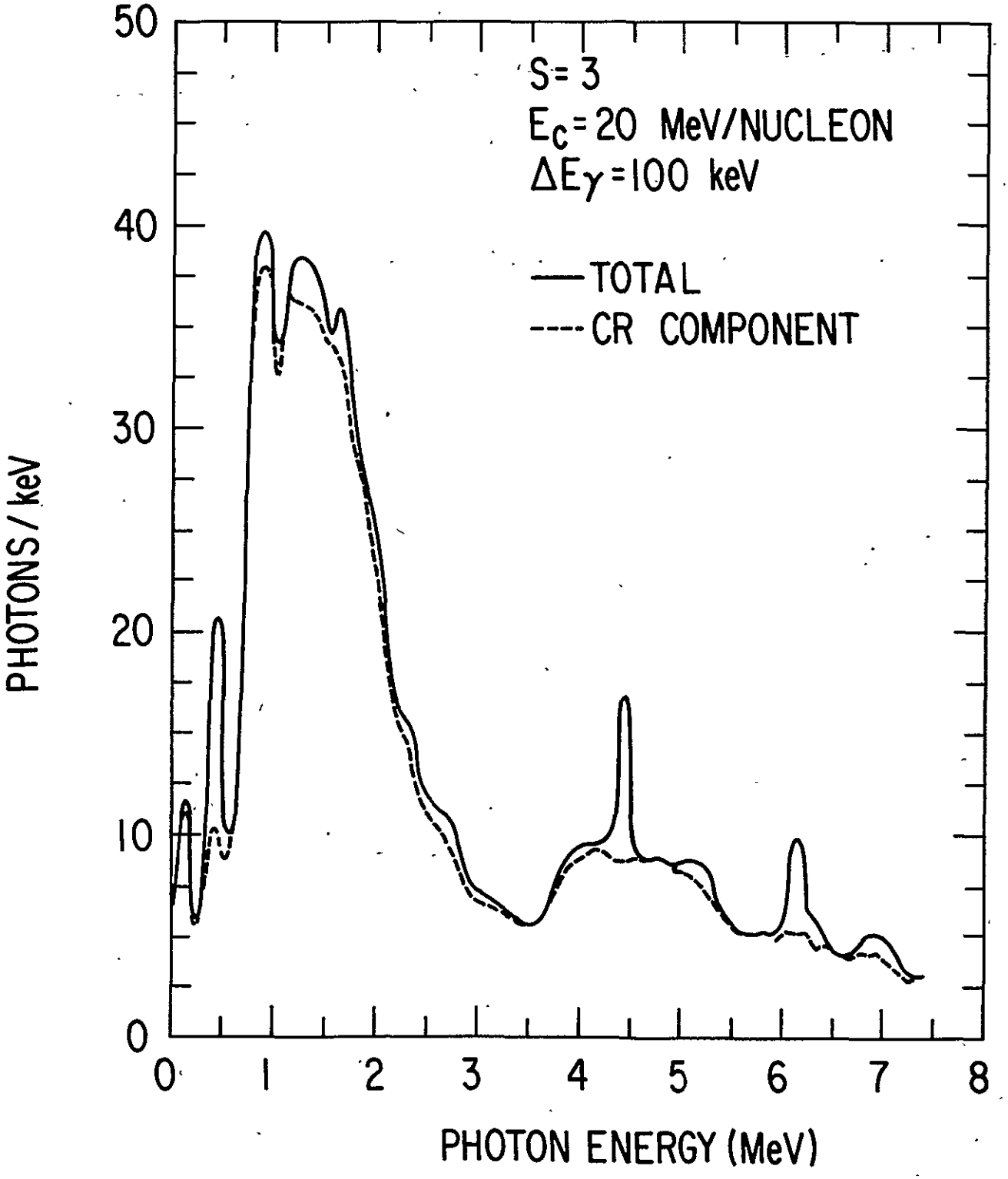
S= 3
E_c= 20 MeV/NUCLEON
ΔE_γ = 100 keV
—TOTAL
----CR COMPONENT
PHOTONS / keV
PHOTON ENERGY (MeV)
0
10
20
30
40
50
0
1
2
3
4
5
6
7
8

Fig. 24

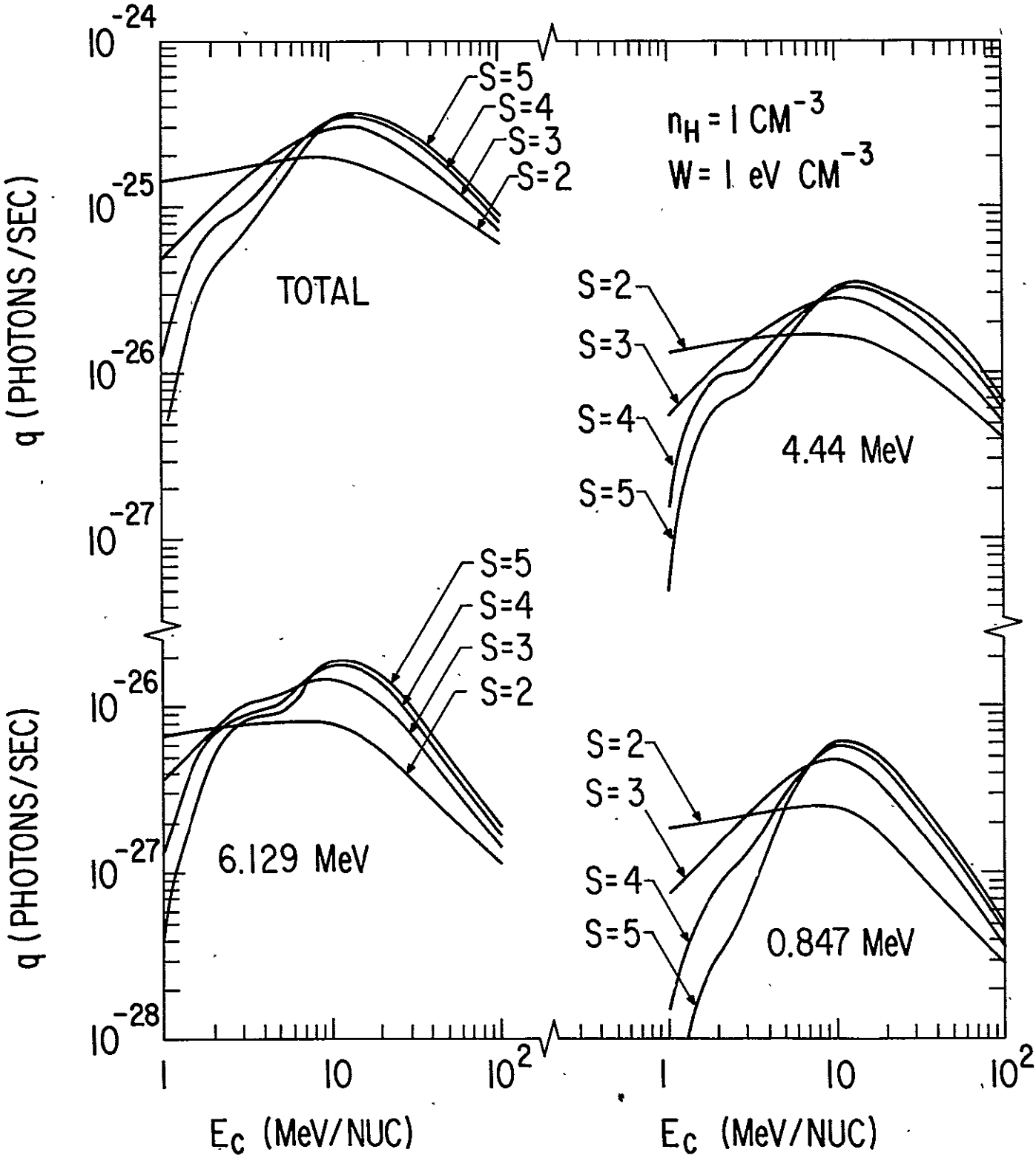
10^{-24}
10^{-25}
10^{-26}
10^{-27}
10^{-26}
10^{-27}
10^{-28}
q (PHOTONS/SEC)
q (PHOTONS/SEC)
S=5
S=4
S=3
S=2
TOTAL
$n_H = 1\ CM^{-3}$
$W = 1\ eV\ CM^{-3}$
S=2
S=3
S=4
S=5
4.44 MeV
S=5
S=4
S=3
S=2
6.129 MeV
S=2
S=3
S=4
S=5
0.847 MeV
1
10
10^2
1
10
10^2
E_C (MeV/NUC)
E_C (MeV/NUC)

Fig. 25

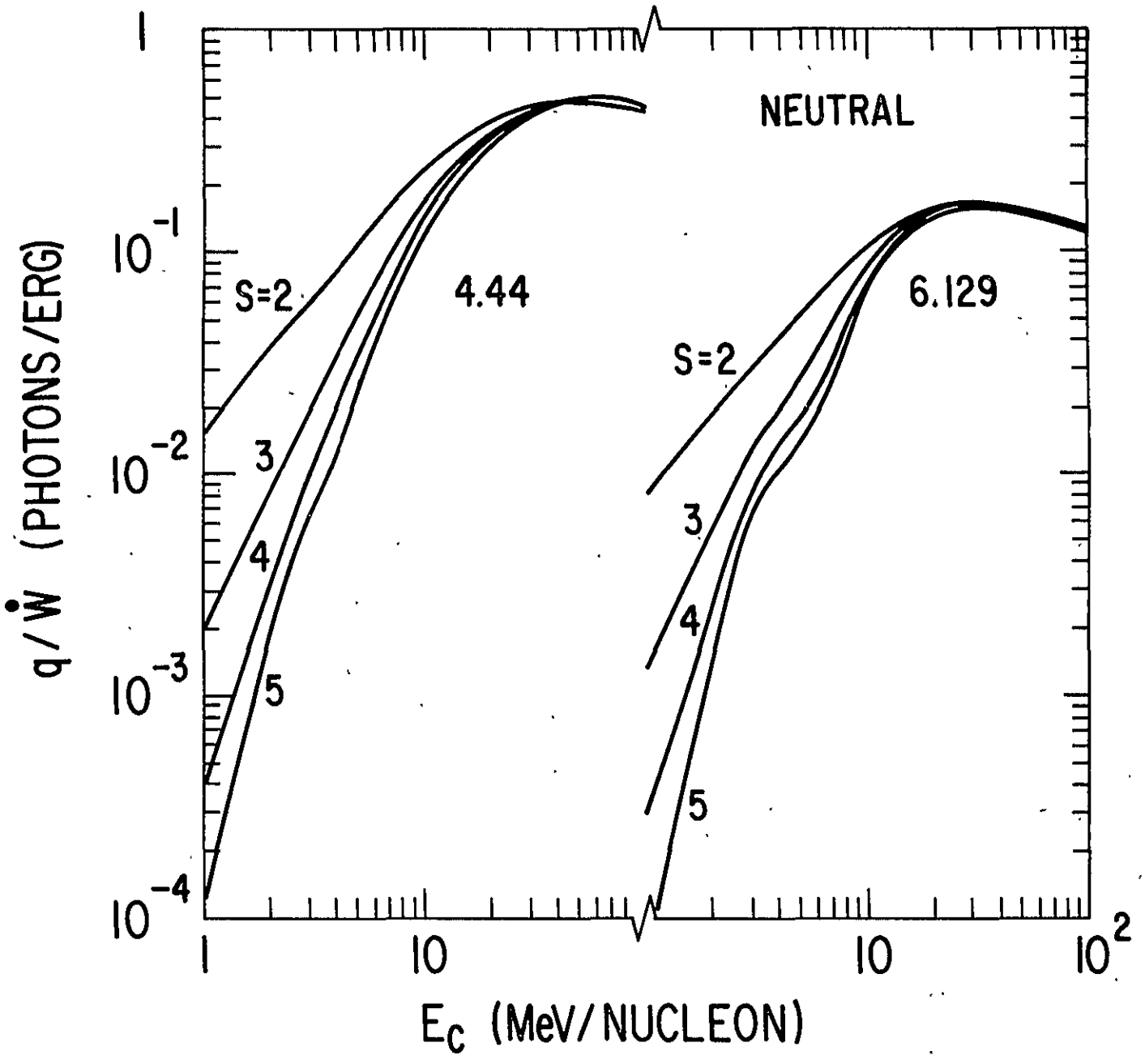
NEUTRAL
4.44
6.129
S=2
3
4
5
S=2
3
4
5
$q/\dot{W}$ (PHOTONS/ERG)
E_c (MeV/NUCLEON)
1
10^{-1}
10^{-2}
10^{-3}
10^{-4}
1
10
10
10^2

Fig. 26

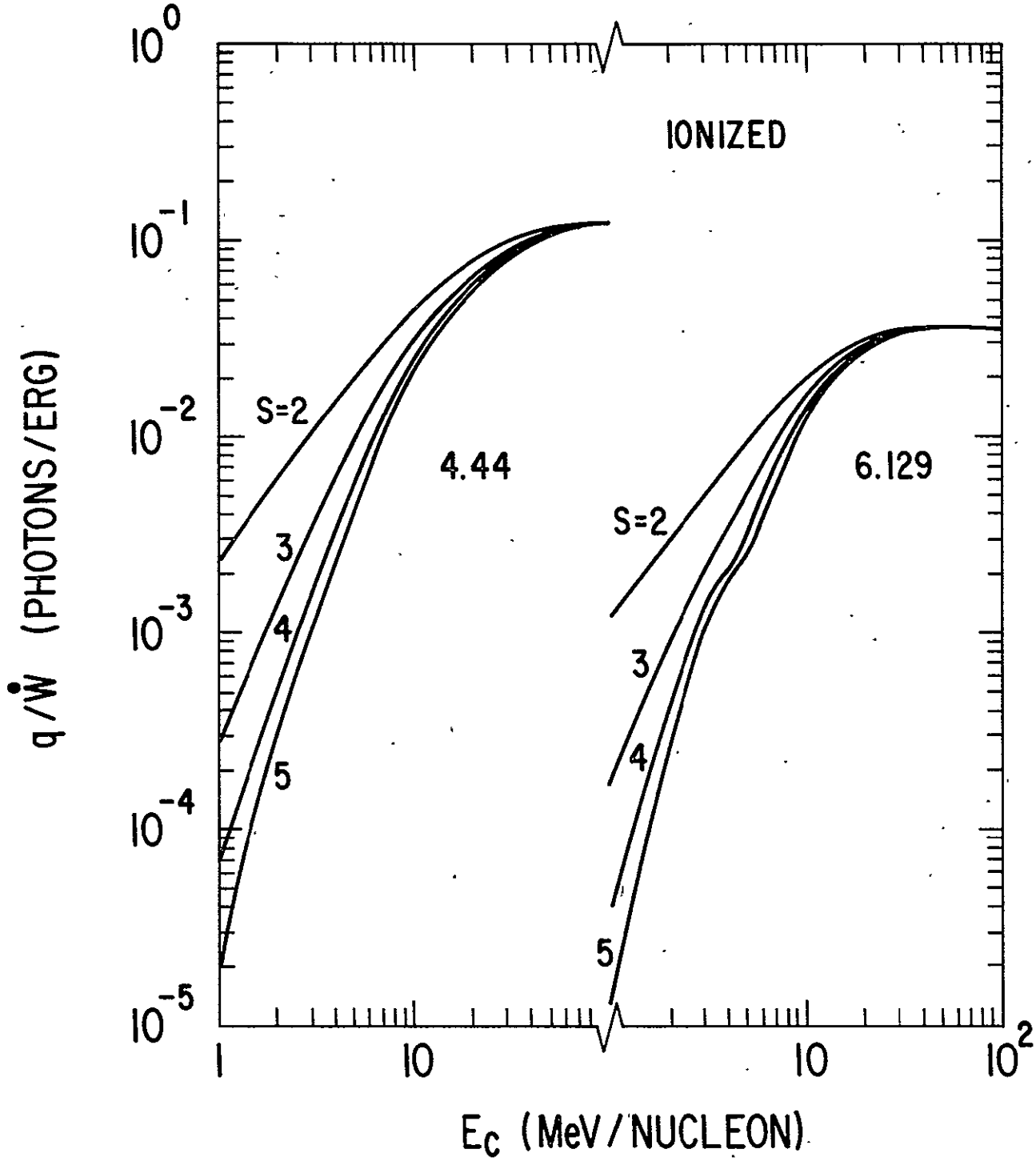
IONIZED
4.44
6.129
S=2
3
4
5
S=2
3
4
5
10^0
10^{-1}
10^{-2}
10^{-3}
10^{-4}
10^{-5}
1
10
10
10^2
$\dot{q}/\dot{W}$ (PHOTONS/ERG)
E_C (MeV/NUCLEON)

Fig. 27

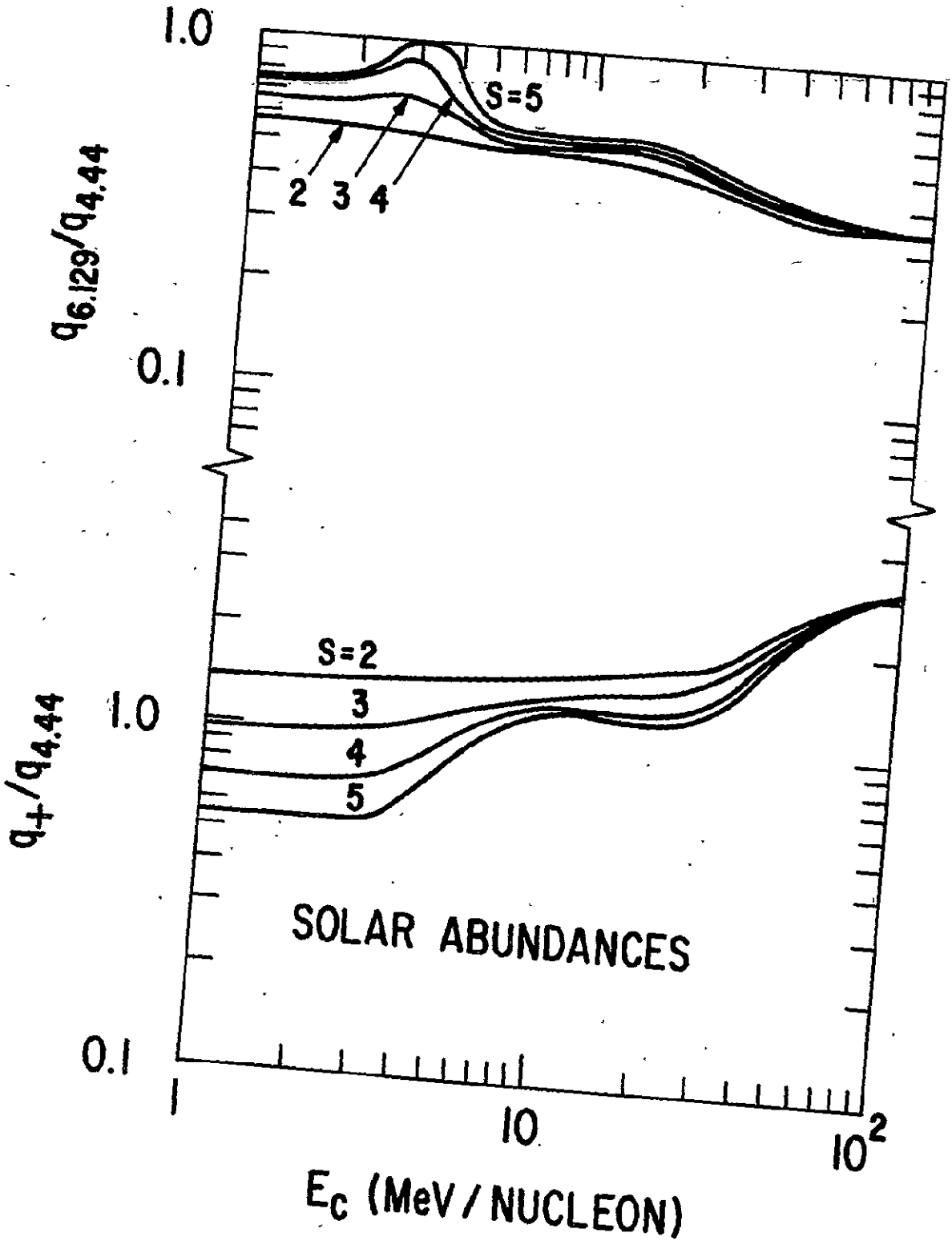

Fig. 28

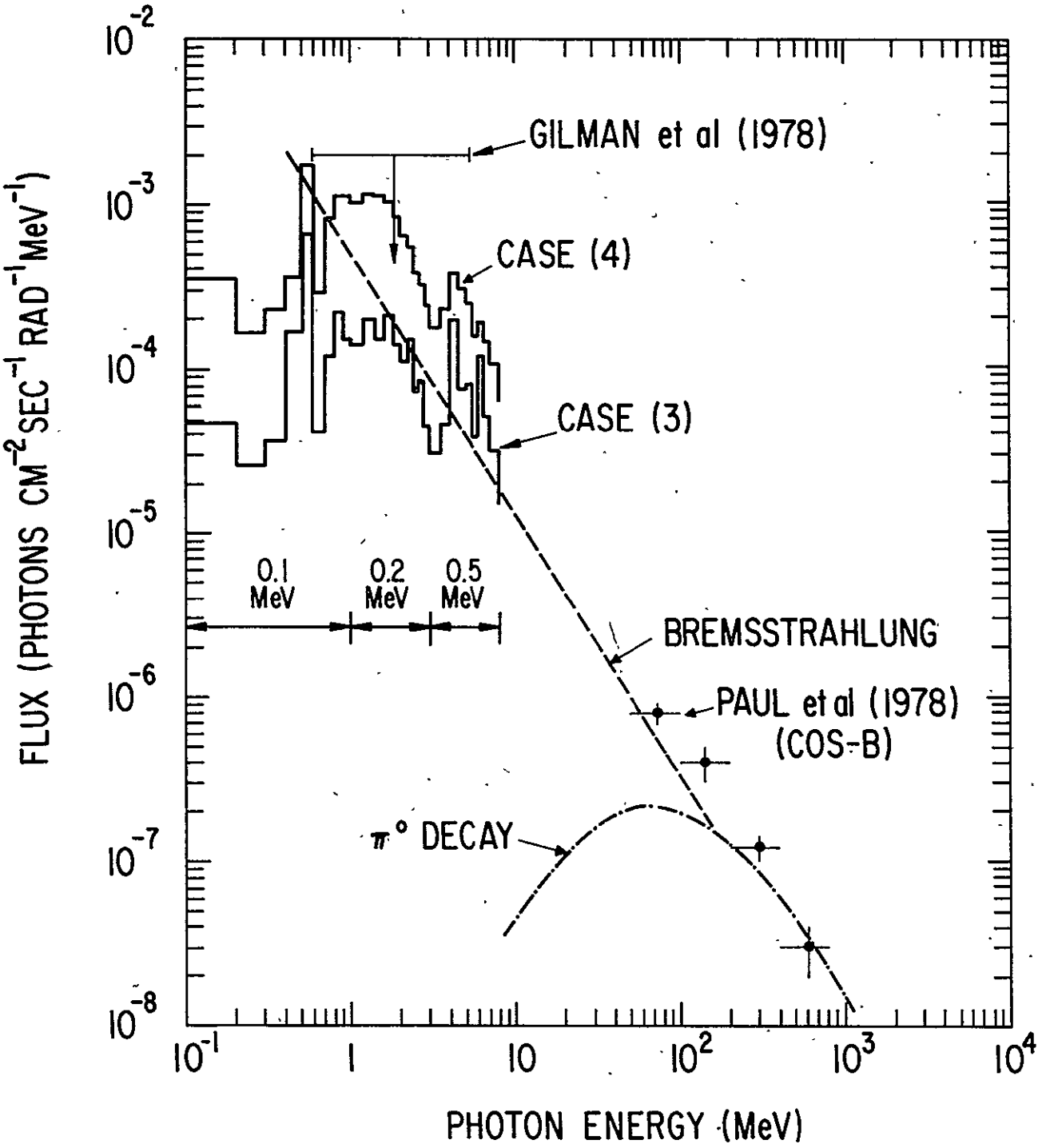
GILMAN et al (1978)
CASE (4)
CASE (3)
0.1 MeV
0.2 MeV
0.5 MeV
BREMSSTRAHLUNG
PAUL et al (1978) (COS-B)
π° DECAY
FLUX (PHOTONS CM⁻²SEC⁻¹RAD⁻¹MeV⁻¹)
PHOTON ENERGY (MeV)
10⁻²
10⁻³
10⁻⁴
10⁻⁵
10⁻⁶
10⁻⁷
10⁻⁸
10⁻¹
1
10
10²
10³
10⁴

Fig. 29

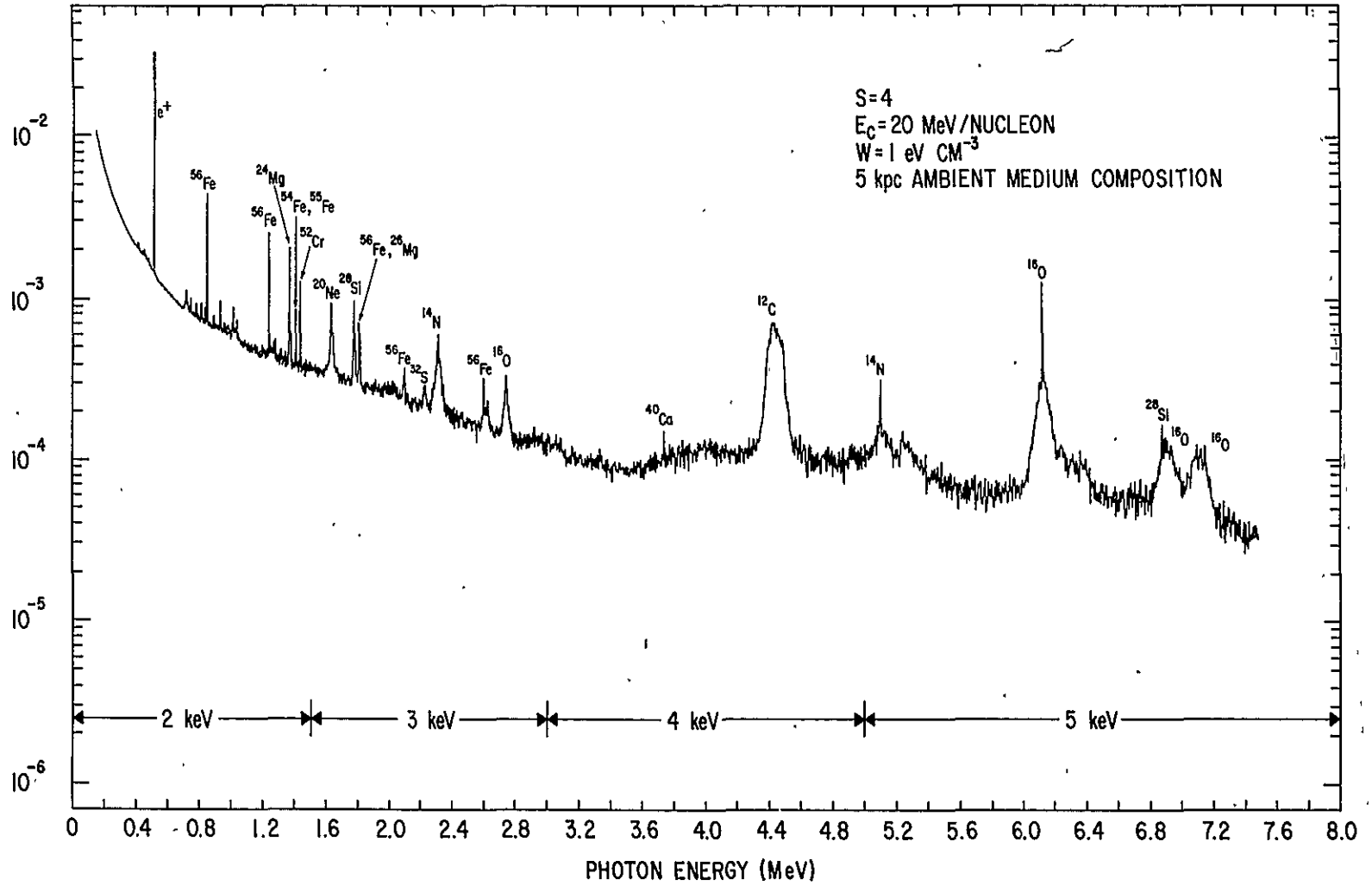
S=4
E_C=20 MeV/NUCLEON
W=1 eV CM^{-3}
5 kpc AMBIENT MEDIUM COMPOSITION
10^{-2}
10^{-3}
10^{-4}
10^{-5}
10^{-6}
e^+
^{56}Fe
^{24}Mg
^{54}Fe, ^{55}Fe
^{52}Cr
^{20}Ne
^{28}Si
^{56}Fe, ^{26}Mg
^{14}N
^{56}Fe
^{32}S
^{16}O
^{40}Ca
^{12}C
^{14}N
^{16}O
^{28}Si
^{16}O
^{16}O
2 keV
3 keV
4 keV
5 keV
0 0.4 0.8 1.2 1.6 2.0 2.4 2.8 3.2 3.6 4.0 4.4 4.8 5.2 5.6 6.0 6.4 6.8 7.2 7.6 8.0
PHOTON ENERGY (MeV)

Fig. 30

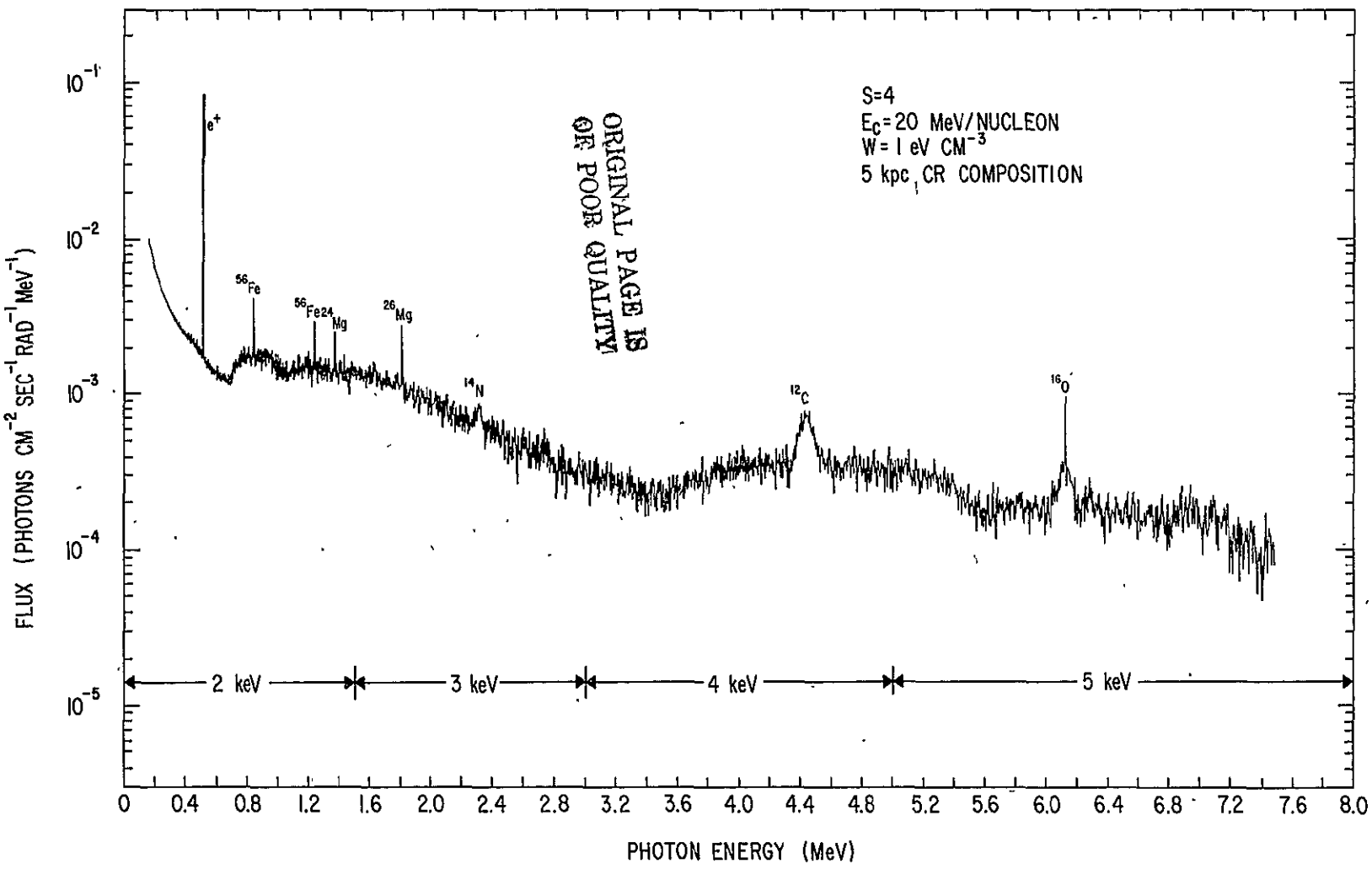
S=4
E_C=20 MeV/NUCLEON
W=1 eV CM^{-3}
5 kpc$_1$ CR COMPOSITION
ORIGINAL PAGE IS
OF POOR QUALITY
FLUX (PHOTONS CM^{-2} SEC^{-1} RAD^{-1} MeV^{-1})
PHOTON ENERGY (MeV)
e^+
^{56}Fe
^{56}Fe$_{24}$Mg
^{26}Mg
^{14}N
^{12}C
^{16}O
2 keV
3 keV
4 keV
5 keV

Fig. 31

BIBLIOGRAPHIC DATA SHEET

1. Report No.	2. Government Accession No.	3. Recipient's Catalog No.
TM-79654		

4. Title and Subtitle	5. Report Date
Nuclear Gamma Rays From Energetic Particle Interactions	November 1978
	6. Performing Organization Code 660
7. Author(s) R. Ramaty, Benzion Kozlovsky, R. Lingenfelter	8. Performing Organization Report No.
9. Performing Organization Name and Address Laboratory for High Energy Astrophysics Theoretical Group	10. Work Unit No.
	11. Contract or Grant No.
	13. Type of Report and Period Covered
12. Sponsoring Agency Name and Address	
	14. Sponsoring Agency Code

15. Supplementary Notes

To be published in Astrophysical Journal Supplement (1979)

16. Abstract

Gamma ray line emission from nuclear deexcitation following energetic particle reactions is evaluated. The compiled nuclear data and the calculated gamma ray spectra and intensities can be used for the study of astrophysical sites which contain large fluxes of energetic protons and nuclei. A detailed evaluation of gamma ray line production in the interstellar medium is made in the present paper.

17. Key Words (Selected by Author(s))	18. Distribution Statement
Gamma ray lines, nuclear reactions, interstellar medium, galactic center	

19. Security Classif. (of this report)	20. Security Classif. (of this page)	21. No. of Pages	22. Price*
UN	UN		

*For sale by the National Technical Information Service, Springfield, Virginia 22151.

GSFC 25-44 (10/77)